

APPENDIX C

**NON-WORK PLAN SPECIFIC WORK
AND ASSOCIATED RESULTS**

This page intentionally left blank.

CONTENTS

| | | |
|---------|--|------|
| C.1.0 | INTRODUCTION | C-1 |
| C.2.0 | TANK FARM HISTORY | C-2 |
| C.3.0 | LEAK INVENTORY ESTIMATES | C-3 |
| C.3.1 | WASTE COMPOSITION ESTIMATES | C-3 |
| C.3.2 | GAMMA LOGGING DATA | C-9 |
| C.3.3 | KRIGING ANALYSIS | C-10 |
| C.3.4 | INVENTORY ESTIMATES FOR WASTE MANAGEMENT AREA S-SX TANK LEAKS | C-23 |
| C.3.5 | SPECIATION ANALYSIS | C-28 |
| C.3.5.1 | Aluminum Solubility in Reduction-Oxidation Wastes | C-29 |
| C.3.5.2 | Los Alamos National Laboratory Speciation Results for Tank SX-108 | C-34 |
| C.3.5.3 | Technetium-99 Speciation | C-34 |
| C.4.0 | GEOLOGY | C-36 |
| C.4.1 | REGIONAL GEOLOGIC SETTING | C-36 |
| C.4.2 | GEOLOGY OF THE S AND SX TANK FARMS | C-36 |
| C.4.2.1 | Columbia River Basalt Group | C-41 |
| C.4.2.2 | Ringold Formation | C-41 |
| C.4.2.3 | Plio-Pleistocene Unit | C-43 |
| C.4.2.4 | Hanford Formation | C-47 |
| C.4.2.5 | Backfill | C-52 |
| C.4.2.6 | Clastic Dikes | C-52 |
| C.5.0 | MOISTURE CONTENT AND MATRIC POTENTIAL MEASUREMENTS | C-55 |
| C.5.1 | MOISTURE CONTENT FOR DRYWELL SEDIMENTS | C-55 |
| C.5.2 | MEASUREMENTS FOR BOREHOLES 299-W23-19, 299-W22-48, AND 299-W22-50 | C-58 |
| C.5.3 | MEASUREMENTS FOR BOREHOLE 41-09-39 | C-59 |
| C.6.0 | GEOCHEMISTRY | C-63 |
| C.7.0 | GROUNDWATER CONTAMINATION | C-64 |
| C.8.0 | REFERENCES | C-73 |

FIGURES

| | | |
|-------|--|------|
| C.1. | Three-Dimensional Perspective of Cesium-137 Contaminated Soil Above 5×10^1 pCi/g | C-13 |
| C.2. | Three-Dimensional Perspective of Cesium-137 Contaminated Soil Above 5×10^2 pCi/g | C-14 |
| C.3. | Three-Dimensional Perspective of Cesium-137 Contaminated Soil Above 5×10^3 pCi/g | C-15 |
| C.4. | Three-Dimensional Perspective of Cesium-137 Contaminated Soil Above 5×10^4 pCi/g | C-16 |
| C.5. | Three-Dimensional Perspective of Cesium-137 Contaminated Soil Above 5×10^5 pCi/g | C-17 |
| C.6. | Three-Dimensional Perspective of Cesium-137 Contaminated Soil Above 5×10^6 pCi/g | C-18 |
| C.7. | Three-Dimensional Perspective of Cesium-137 Contaminated Soil Above 5×10^7 pCi/g | C-19 |
| C.8. | Total Pico-Curies of Cesium-137 Inventory by Tank..... | C-20 |
| C.9. | Estimated Activity Levels and Estimated Contaminated Soil Volume Using Max, Mean, and Geometric Mean Sample Data Filtering for Tank SX-107 | C-20 |
| C.10. | Solubility of Aluminum in Tank SX-108 Waste at 100 °C (212 °F) | C-31 |
| C.11. | Solubility of Aluminum in Tank SX-108 Waste at 50 °C (122 °F) | C-32 |
| C.12. | REDOX Waste Chemistry During Water Removal..... | C-33 |
| C.13. | Generalized, Composite Stratigraphy for the Late Cenozoic Sediments Overlying the Columbia River Basalt Group on the Hanford Site | C-37 |
| C.14. | SX Tank Farm and Vicinity Showing Location of Borehole 299-W23-19 | C-39 |
| C.15. | Hydrogeologic Cross-Section of the Vadose Zone Beneath the SX Tank Farm..... | C-40 |
| C.16. | Lithofacies Distribution for the Lower Plio-Pleistocene Subunit PPlc | C-45 |
| C.17. | Digital Elevation Model Map of a Portion of the Pasco Basin Showing Routes and Facies Distributions for the Last Pleistocene Cataclysmic Floods | C-49 |
| C.18. | Clastic Dike in the SY Tank Farm Excavation..... | C-53 |
| C.19. | Projection of a Hypothetical Network of Clastic Dikes onto Waste Management Area S-SX | C-54 |
| C.20. | Measured Moisture Contents for the Drywell Sediments Beneath SX Tank Farm..... | C-56 |
| C.21. | Moisture Content Distribution for the Drywell Sediments for Three Cross-Sections.. | C-57 |
| C.22. | Gravimetric Moisture Content Distribution for the Sediment Profile at Borehole 299-W23-19 | C-58 |
| C.23. | Soil Suction Profiles for 299-W22-48, 299-W22-50 and 299-W23-19 Borehole Samples | C-60 |
| C.24. | Matric Suction Profile for Samples from Borehole 41-09-39 | C-61 |
| C.25. | Technetium-99/Nitrate Ratios for Waste Management Area S-SX Network Wells | C-67 |
| C.26. | Tritium/Technetium-99 Ratios for Waste Management Area S-SX Network Wells ... | C-68 |
| C.27. | Theoretical Groundwater Plume Dispersion Pattern from a Tank Leak Source in the SX Tank Farm Monitoring Efficiency Model..... | C-70 |
| C.28. | Technetium-99 for Waste Management Area S-SX Network Wells..... | C-71 |

TABLES

| | | |
|-------|---|------|
| C.1. | Summary of Chemical Tank Supernate/Salt Concentrations at Time of Leak | C-4 |
| C.2. | Summary of Radionuclide Tank Supernate/Salt Concentrations at Time of Leak | C-6 |
| C.3. | SX Tank Farm Cesium-137 Inventory Estimates from Kriging Analyses | C-11 |
| C.4. | Summary of Activity and Volume Estimates by Tank and Activity Threshold with Geometric Mean Filtering | C-21 |
| C.5. | Summary of Activity and Volume Estimates by Tank and Activity Threshold with Maximum Value Filtering | C-22 |
| C.6. | Estimated Inventory Lost to Vadose Zone in the S and SX Tank Farms | C-24 |
| C.7. | Estimated Inventory Lost to Vadose Zone in the S and SX Tank Farms (Radionuclides) | C-26 |
| C.8. | REDOX High-Level Waste Components During Volume Reduction (with Constant OH) | C-32 |
| C.9. | REDOX High-Level Waste Components Assuming Water Removal Only | C-33 |
| C.10. | Stratigraphic Terminology Used in this Report for the Vadose Zone Beneath the SX Tank Farm | C-42 |
| C.11. | Example of Granulometric and Calcium Carbonate Data from Drive-Barrel Samples of Subunit PPlz Encountered Beneath the SX Tank Farm | C-47 |
| C.12. | Data from Drive Barrel and Split-Spoon Samples of the Hanford Formation Beneath SX Tank Farm located in Figure C.14 | C-51 |
| C.13. | Water Content and Matric Suction Values for Samples from Borehole 41-09-39 | C-61 |
| C.14. | Observed Contaminant Concentrations in Shallow and Extended Well 299-W23-19 Completions Near Tank SX-115 | C-65 |
| C.15. | Depth Distribution of Key Contaminants at SX Tank Farm Wells | C-65 |
| C.16. | Hydrochemical Parameters at SX Tank Farm Wells | C-66 |
| C.17. | Maximum Contaminant Concentrations for Groundwater Samples Collected from Waste Management Area S-SX Network Wells (November 1997 to April 2000) | C-72 |

LIST OF TERMS

| | |
|-------|---|
| bgs | below ground surface |
| ESP | Environmental Simulation Program |
| HDW | Hanford defined waste (model) |
| HGL | HydroGeologic, Inc. |
| HLW | high-level waste |
| MSU | Montana State University |
| RCRA | <i>Resource Conservation and Recovery Act of 1976</i> |
| REDOX | reduction-oxidation |
| SST | single-shell tank |
| WMA | waste management area |

C.1.0 INTRODUCTION

The work plan addenda associated with waste management area (WMA) S-SX were developed for the primary purpose of directing field work (Myers 1997; Henderson 1999; Rogers and Knepp 2000). During the course of conducting the identified field work, other activities were identified that would either complement or supplement that field work. Some 'projects-of-opportunity' that fit within the general scope of the Tank Farm Vadose Zone Project were undertaken. Included in this category were sampling and geological mapping associated with *Resource Conservation and Recovery Act of 1976* (RCRA) groundwater monitoring wells that were drilled to enhance or maintain the WMA S-SX groundwater monitoring program. Included are the data derived from the monitoring of well 299-W23-19 that was drilled to characterize the vadose zone but converted to a groundwater monitoring well due to the technetium-99 activity of the single sample identified in the work plan (Henderson 1999). Efforts to fully document the history of S and SX tank farm activities continued even though the majority of the information had been garnered for the subsurface conditions description report (Johnson et al. 1999).

As noted in Jones et al. (1998), determination of the contaminant inventory that was lost to the vadose zone is the most pressing need. This inventory was estimated using historical data and then revised based on the data gathered during the drilling of the characterization boreholes called out in the work plan addenda.

An effort to characterize the distribution of moisture in the southern portion of the SX tank farm was undertaken in an attempt to determine if pressurized water lines in that portion of the farm were a possible source of recharge. Those measurements added to the drive to cut-off unnecessary pressurized water lines leading to the tank farm. These measurements also added to the database used by the Science and Technology Program modeling effort reported in Appendix D.

Geochemical characterization of sediments collected from cores during construction of the RCRA groundwater monitoring wells provide a basis against which to judge the impact of tank waste lost to the environment.

Finally, data and analysis of the groundwater provide additional insight into the overall conceptual model of contaminant flow and transport through the vadose zone and into the unconfined aquifer.

C.2.0 TANK FARM HISTORY

Operating history of the S and SX tank farms was compiled and documented in Johnson et al. (1999). As work proceeded in conjunction with the various work plan addenda, that history was correlated with the new field data and the interpretations of that data. No additional incidents in the history of actual tank farm operations were identified.

Adjacent facilities and operations have been scrutinized in an attempt to further define the potential impact; some potentially important historic records could not be located. The most important of those records concern the inventory of technetium-99 disposed to the 216-S-25 trench during the U-1, U-2 pump-and-treat era. This pump-and-treat system used ion exchange columns to remove uranium from groundwater. The resins were used until uranium breakthrough occurred; this mode of operation ensured that technetium-99 was returned to the environment through the trench. The Hanford Environmental Information System was interrogated to ascertain the levels of technetium-99 in wells surrounding the 200-UP-1 and 200-UP-2 pump and treat operation. The values contained in Hanford Environmental Information System show technetium-99 to have been in the range of 3,000 to 4,000 pCi/L maximum.

C.3.0 LEAK INVENTORY ESTIMATES

The development of credible inventory estimates of chemicals and radionuclides lost to the WMA S-SX vadose zone represents a major component of the characterization activities. This inventory estimate provides both quantitative data for transport modeling and constrains the range of components that need be considered in the risk evaluation. The development of these estimates was based on an extensive review of historical records, previously developed methods for estimating tank waste compositions, extensive field investigation data, and statistical modeling of certain data sets. Highlights of these activities are discussed in Section 3.0 of the main text of this report. More extensive data tables are included in this section.

C.3.1 WASTE COMPOSITION ESTIMATES

There has long been an interest in using flowsheet data from various Hanford Site chemical processes coupled with waste transfer records to develop tank waste inventory estimates (Jungfleish 1984). Researchers at Los Alamos National Laboratory, supported by many individuals associated with the Hanford tank waste characterization program (Agnew 1997) brought the approach developed by Jungfleish to fruition. The Los Alamos National Laboratory task involved two major activities.

- The extensive waste transfer records were centralized into a single document, *Waste Status and Transfer Record Summary (WSTRS Rev. 4)* (Agnew et al. 1997).
- Flowsheet information was coupled with an understanding of the chemistry of each waste stream to develop estimates of solid and liquid compositions for each waste stream.

The composition of each major waste stream was coupled with the waste volumes for each of the transfers into and out of each Hanford Site waste tank. Using simple waste mixing rules for the sum of waste transfers through individual tanks, current waste compositions and total inventories were calculated for each Hanford Site waste tank. This approach is termed the Hanford defined waste (HDW) model (Agnew 1997). The HDW model develops two waste composition estimates:

- Sludge composition, estimated by the tank layering model
- Supernatant composition, estimated by the supernatant mixing model.

The waste composition estimates from the supernatant mixing model module are a combination of liquid and salt cake (Agnew 1997).

Although the driver for the HDW model was to develop ‘current’ tank inventory estimates, the HDW model provides the capability for developing inventory estimates at any point in time in each tank. As noted above, the HDW model results for selected SX tank farm high-heat tanks are used in Agnew and Corbin (1998) to develop the ‘Hanford leak model,’ which projects preliminary leak volume estimates for tanks SX-108, SX-109, SX-111, and SX-112. The Agnew and Corbin (1998) approach for developing tank composition estimates at specific points in time was used in estimating tank leak events in WMA S-SX (Jones et al. 2000a). Tables C.1 and C.2 list the waste composition estimates at the times tanks were suspected to have leaked for 10 tanks in the S and SX tank farms (for more details in the development of these tables see discussion in Jones et al. 2000a).

Table C.1. Summary of Chemical Tank Supernate/Salt Concentrations at Time of Leak (2 Sheets)

| Tank | S-104 | SX-107 | SX-108 | SX-109 | SX-110 | SX-111 | SX-112 | SX-113 | SX-114 | SX-115 |
|----------------------|-----------------|-----------------------|-----------------------|-----------------------|-----------------|-----------------|-----------------|-----------------|-----------------|-----------------|
| Assumed Leak Date | 1965 (mol/L) | Ave. 64-67 (mol/L) | Ave. 65-66 (mol/L) | Ave. 64-67 (mol/L) | 1974 (mol/L) | 1973 (mol/L) | 1969 (mol/L) | 1962 (mol/L) | 1972 (mol/L) | 1964 (mol/L) |
| Chemicals | | | | | | | | | | |
| Na | 8.671E+00 | 1.873E+01 | 1.960E+01 | 1.519E+01 | 6.068E+00 | 5.310E+00 | 1.319E+01 | 7.982E+00 | 8.852E+00 | 3.593E+00 |
| Al | 1.556E+00 | 3.273E+00 | 3.361E+00 | 2.560E+00 | 7.336E-01 | 5.270E-01 | 2.167E+00 | 1.267E+00 | 9.692E-01 | 8.258E-01 |
| Total Fe | 3.543E-03 | 6.878E-03 | 7.209E-03 | 5.598E-03 | 4.216E-03 | 5.323E-03 | 3.542E-03 | 2.967E-03 | 7.436E-03 | 2.111E-03 |
| Cr | 1.647E-01 | 3.919E-01 | 4.128E-01 | 3.211E-01 | 6.793E-02 | 5.862E-02 | 2.065E-01 | 1.712E-01 | 1.015E-01 | 5.088E-02 |
| Bi | 8.951E-09 | 0.000E+00 | 0.000E+00 | 0.000E+00 | 1.139E-04 | 1.179E-04 | 6.395E-06 | 0.000E+00 | 1.475E-04 | 6.627E-08 |
| La | 2.205E-14 | 0.000E+00 | 0.000E+00 | 0.000E+00 | 8.532E-10 | 1.326E-09 | 1.575E-11 | 0.000E+00 | 1.720E-09 | 1.632E-13 |
| Hg | 3.541E-06 | 1.154E-07 | 1.966E-09 | 0.000E+00 | 1.518E-06 | 1.586E-06 | 1.006E-06 | 0.000E+00 | 1.864E-06 | 6.293E-06 |
| Zr (as ZrO(OH)2) | 8.935E-10 | 0.000E+00 | 0.000E+00 | 0.000E+00 | 1.953E-05 | 1.614E-05 | 6.383E-07 | 0.000E+00 | 1.959E-05 | 6.615E-09 |
| Pb | 5.666E-04 | 1.846E-05 | 3.146E-07 | 0.000E+00 | 2.093E-04 | 2.206E-04 | 1.596E-04 | 0.000E+00 | 2.569E-04 | 1.007E-03 |
| Ni | 3.101E-03 | 6.187E-03 | 6.488E-03 | 5.038E-03 | 2.012E-03 | 1.942E-03 | 3.187E-03 | 2.671E-03 | 3.005E-03 | 1.732E-03 |
| Sr | 0.000E+00 | 0.000E+00 | 0.000E+00 | 0.000E+00 | 0.000E+00 | 0.000E+00 | 0.000E+00 | 0.000E+00 | 0.000E+00 | 0.000E+00 |
| Mn | 6.515E-08 | 0.000E+00 | 0.000E+00 | 0.000E+00 | 2.254E-03 | 3.538E-03 | 4.655E-05 | 0.000E+00 | 4.565E-03 | 4.824E-07 |
| Ca | 1.595E-02 | 3.096E-02 | 3.245E-02 | 2.520E-02 | 1.012E-02 | 9.760E-03 | 1.594E-02 | 1.336E-02 | 1.505E-02 | 9.502E-03 |
| K | 3.069E-02 | 6.989E-02 | 7.386E-02 | 5.763E-02 | 2.632E-02 | 2.451E-02 | 5.094E-02 | 3.106E-02 | 3.951E-02 | 1.105E-02 |
| Density (g/cc) | 1.397E+00 | 1.840E+00 | 1.874E+00 | 1.674E+00 | 1.255E+00 | 1.218E+00 | 1.583E+00 | 1.349E+00 | 1.366E+00 | 1.181E+00 |
| Void Frac. | 0.000E+00 | 0.000E+00 | 0.000E+00 | 0.000E+00 | 0.000E+00 | 0.000E+00 | 0.000E+00 | 0.000E+00 | 0.000E+00 | 0.000E+00 |
| wt.% H2O | 5.153E+01 | 2.325E+01 | 2.089E+01 | 3.139E+01 | 6.465E+01 | 6.807E+01 | 3.815E+01 | 5.480E+01 | 5.276E+01 | 7.507E+01 |
| TOC wt% C | 8.391E-06 | 0.000E+00 | 0.000E+00 | 0.000E+00 | 2.959E-01 | 3.911E-01 | 5.289E-03 | 0.000E+00 | 4.950E-01 | 7.345E-05 |
| free OH | 0.000E+00 | 0.000E+00 | 0.000E+00 | 0.000E+00 | 0.000E+00 | 0.000E+00 | 0.000E+00 | 0.000E+00 | 0.000E+00 | 0.000E+00 |
| OH | 9.009E+00 | 1.980E+01 | 2.049E+01 | 1.571E+01 | 4.745E+00 | 3.510E+00 | 1.331E+01 | 7.968E+00 | 6.429E+00 | 4.171E+00 |
| NO3 | 3.006E+00 | 4.891E+00 | 5.464E+00 | 4.485E+00 | 1.714E+00 | 1.534E+00 | 3.486E+00 | 2.818E+00 | 2.476E+00 | 1.197E+00 |
| NO2 | 1.638E+00 | 4.485E+00 | 4.418E+00 | 3.225E+00 | 1.256E+00 | 1.131E+00 | 3.132E+00 | 1.336E+00 | 1.864E+00 | 7.840E-01 |
| CO3 | 1.596E-02 | 3.096E-02 | 3.245E-02 | 2.520E-02 | 1.802E-01 | 2.263E-01 | 2.055E-02 | 1.336E-02 | 3.169E-01 | 9.550E-03 |

Table C.1. Summary of Chemical Tank Supernate/Salt Concentrations at Time of Leak (2 Sheets)

| Tank | S-104 | SX-107 | SX-108 | SX-109 | SX-110 | SX-111 | SX-112 | SX-113 | SX-114 | SX-115 |
|----------------------|-----------------|-----------------------|-----------------------|-----------------------|-----------------|-----------------|-----------------|-----------------|-----------------|-----------------|
| Assumed Leak Date | 1965 (mol/L) | Ave. 64-67 (mol/L) | Ave. 65-66 (mol/L) | Ave. 64-67 (mol/L) | 1974 (mol/L) | 1973 (mol/L) | 1969 (mol/L) | 1962 (mol/L) | 1972 (mol/L) | 1964 (mol/L) |
| Chemicals | | | | | | | | | | |
| PO4 | 5.792E-07 | 0.000E+00 | 0.000E+00 | 0.000E+00 | 1.140E-02 | 1.317E-02 | 4.138E-04 | 0.000E+00 | 1.791E-02 | 4.288E-06 |
| SO4 | 3.206E-02 | 9.299E-02 | 9.229E-02 | 6.775E-02 | 9.641E-02 | 1.226E-01 | 6.646E-02 | 2.879E-02 | 1.714E-01 | 1.920E-02 |
| Si (as SiO32-) | 2.806E-02 | 9.803E-02 | 9.334E-02 | 6.561E-02 | 3.481E-02 | 3.425E-02 | 5.563E-02 | 2.229E-02 | 5.508E-02 | 1.279E-02 |
| F | 4.617E-07 | 0.000E+00 | 0.000E+00 | 0.000E+00 | 5.400E-03 | 5.272E-03 | 3.299E-04 | 0.000E+00 | 6.534E-03 | 3.418E-06 |
| Cl | 1.412E-01 | 3.215E-01 | 3.397E-01 | 2.651E-01 | 1.017E-01 | 8.848E-02 | 2.215E-01 | 1.429E-01 | 1.488E-01 | 5.071E-02 |
| C6H5O7 | 4.771E-07 | 0.000E+00 | 0.000E+00 | 0.000E+00 | 1.810E-02 | 2.602E-02 | 3.408E-04 | 0.000E+00 | 3.548E-02 | 3.532E-06 |
| EDTA | 1.858E-08 | 0.000E+00 | 0.000E+00 | 0.000E+00 | 3.213E-04 | 4.655E-04 | 1.328E-05 | 0.000E+00 | 5.988E-04 | 1.376E-07 |
| HEDTA | 1.543E-08 | 0.000E+00 | 0.000E+00 | 0.000E+00 | 5.799E-04 | 9.256E-04 | 1.102E-05 | 0.000E+00 | 1.202E-03 | 1.142E-07 |
| glycolate | 6.734E-07 | 0.000E+00 | 0.000E+00 | 0.000E+00 | 3.077E-02 | 1.215E-02 | 4.811E-04 | 0.000E+00 | 3.811E-02 | 4.985E-06 |
| acetate | 6.989E-08 | 0.000E+00 | 0.000E+00 | 0.000E+00 | 2.233E-04 | 5.419E-05 | 4.993E-05 | 0.000E+00 | 3.255E-05 | 5.175E-07 |
| oxalate | 2.888E-14 | 0.000E+00 | 0.000E+00 | 0.000E+00 | 1.118E-09 | 1.738E-09 | 2.063E-11 | 0.000E+00 | 2.253E-09 | 2.138E-13 |
| DBP | 4.231E-07 | 0.000E+00 | 0.000E+00 | 0.000E+00 | 1.082E-02 | 1.686E-02 | 3.023E-04 | 0.000E+00 | 2.136E-02 | 3.133E-06 |
| butanol | 4.231E-07 | 0.000E+00 | 0.000E+00 | 0.000E+00 | 1.082E-02 | 1.686E-02 | 3.023E-04 | 0.000E+00 | 2.136E-02 | 3.133E-06 |
| NH3 | 2.051E-02 | 1.122E-01 | 1.051E-01 | 7.226E-02 | 3.248E-02 | 3.205E-02 | 6.916E-02 | 2.123E-02 | 5.011E-02 | 1.305E-02 |
| Fe(CN)6 | 0.000E+00 | 0.000E+00 | 0.000E+00 | 0.000E+00 | 0.000E+00 | 0.000E+00 | 0.000E+00 | 0.000E+00 | 0.000E+00 | 0.000E+00 |

Source: Jones et al. (2000a).

Note: This chart selects a single waste composition (from a single selected year or average of a range of years) for each tank that leaked. The objective is to provide the Tank Farm Vadose Zone Project with an unambiguous set of leak composition values. Data source is HDW model-SMM concentrations for selected tanks and for each year.

HDW = Hanford defined waste (model).

SMM = supernatant mixing model.

TOC = total organic compound.

Table C.2. Summary of Radionuclide Tank Supernate/Salt Concentrations at Time of Leak (3 Sheets)

| Tank | S-104 | SX-107 | SX-108 | SX-109 | SX-110 | SX-111 | SX-112 | SX-113 | SX-114 | SX-115 |
|-------------------|-------------|-------------------|-------------------|-------------------|-------------|-------------|-------------|-------------|-------------|-------------|
| Assumed Leak Date | 1965 (Ci/L) | Ave. 64-67 (Ci/L) | Ave. 65-66 (Ci/L) | Ave. 64-67 (Ci/L) | 1974 (Ci/L) | 1973 (Ci/L) | 1969 (Ci/L) | 1962 (Ci/L) | 1972 (Ci/L) | 1964 (Ci/L) |
| Radionuclides | | | | | | | | | | |
| H-3 | 7.812E-05 | 6.640E-04 | 6.013E-04 | 3.960E-04 | 1.661E-04 | 1.531E-04 | 4.208E-04 | 8.092E-05 | 2.548E-04 | 7.551E-05 |
| C-14 | 6.059E-06 | 3.044E-05 | 2.876E-05 | 1.996E-05 | 2.218E-05 | 2.942E-05 | 2.028E-05 | 6.264E-06 | 4.091E-05 | 3.657E-06 |
| Ni-59 | 7.660E-07 | 3.543E-06 | 3.373E-06 | 2.361E-06 | 1.201E-06 | 1.418E-06 | 1.712E-06 | 7.828E-07 | 2.078E-06 | 4.413E-07 |
| Ni-63 | 7.157E-05 | 3.475E-04 | 3.291E-04 | 2.290E-04 | 1.186E-04 | 1.403E-04 | 1.675E-04 | 7.309E-05 | 2.053E-04 | 4.315E-05 |
| Co-60 | 2.420E-06 | 3.097E-05 | 2.744E-05 | 1.755E-05 | 2.491E-05 | 3.360E-05 | 1.961E-05 | 2.473E-06 | 4.646E-05 | 3.550E-06 |
| Se-79 | 1.287E-06 | 5.756E-06 | 5.507E-06 | 3.878E-06 | 1.904E-06 | 1.984E-06 | 3.275E-06 | 1.330E-06 | 3.107E-06 | 7.007E-07 |
| Sr-90 | 4.961E-02 | 1.166E-01 | 1.225E-01 | 9.516E-02 | 5.514E-02 | 6.636E-02 | 6.020E-02 | 5.044E-02 | 9.720E-02 | 1.777E-02 |
| Y-90 | 4.962E-02 | 1.166E-01 | 1.226E-01 | 9.519E-02 | 5.515E-02 | 6.638E-02 | 6.022E-02 | 5.046E-02 | 9.722E-02 | 1.777E-02 |
| Zr-93 | 6.075E-06 | 2.853E-05 | 2.715E-05 | 1.900E-05 | 9.435E-06 | 9.899E-06 | 1.631E-05 | 6.278E-06 | 1.544E-05 | 3.455E-06 |
| Nb-93m | 4.963E-06 | 2.047E-05 | 1.977E-05 | 1.407E-05 | 6.690E-06 | 6.949E-06 | 1.154E-05 | 5.133E-06 | 1.090E-05 | 2.510E-06 |
| Tc-99 | 4.247E-05 | 2.435E-04 | 2.272E-04 | 1.553E-04 | 1.593E-04 | 2.080E-04 | 1.602E-04 | 4.385E-05 | 2.912E-04 | 2.904E-05 |
| Ru-106 | 1.820E-11 | 7.971E-09 | 6.766E-09 | 4.071E-09 | 4.222E-09 | 4.573E-09 | 4.831E-09 | 6.907E-12 | 7.089E-09 | 8.857E-10 |
| Cd-113m | 1.878E-05 | 1.334E-04 | 1.223E-04 | 8.175E-05 | 5.331E-05 | 5.863E-05 | 8.581E-05 | 1.935E-05 | 8.880E-05 | 1.570E-05 |
| Sb-125 | 3.669E-06 | 1.158E-04 | 9.998E-05 | 6.166E-05 | 1.065E-04 | 1.452E-04 | 7.206E-05 | 3.631E-06 | 2.000E-04 | 1.307E-05 |
| Sn-126 | 1.976E-06 | 8.667E-06 | 8.312E-06 | 5.868E-06 | 2.869E-06 | 2.979E-06 | 4.920E-06 | 2.044E-06 | 4.675E-06 | 1.054E-06 |
| I-129 | 8.158E-08 | 4.604E-07 | 4.302E-07 | 2.945E-07 | 3.066E-07 | 4.016E-07 | 3.033E-07 | 8.423E-08 | 5.616E-07 | 5.496E-08 |
| Cs-134 | 6.935E-08 | 7.004E-06 | 5.972E-06 | 3.617E-06 | 9.609E-07 | 4.299E-07 | 4.180E-06 | 6.248E-08 | 1.077E-06 | 7.764E-07 |
| Cs-137 | 1.249E-01 | 8.378E-01 | 7.712E-01 | 5.185E-01 | 1.272E-01 | 5.765E-02 | 5.329E-01 | 1.288E-01 | 1.415E-01 | 9.885E-02 |
| Ba-137m | 1.182E-01 | 7.925E-01 | 7.296E-01 | 4.905E-01 | 1.204E-01 | 5.454E-02 | 5.042E-01 | 1.218E-01 | 1.339E-01 | 9.351E-02 |
| Sm-151 | 4.591E-03 | 2.021E-02 | 1.937E-02 | 1.367E-02 | 6.685E-03 | 6.948E-03 | 1.148E-02 | 4.746E-03 | 1.090E-02 | 2.465E-03 |
| Eu-152 | 4.539E-07 | 5.471E-06 | 4.860E-06 | 3.121E-06 | 2.014E-06 | 2.388E-06 | 2.600E-06 | 4.657E-07 | 3.527E-06 | 6.185E-07 |
| Eu-154 | 5.843E-05 | 7.543E-04 | 6.680E-04 | 4.271E-04 | 3.916E-04 | 4.777E-04 | 4.733E-04 | 5.974E-05 | 6.919E-04 | 8.618E-05 |
| Eu-155 | 2.150E-05 | 2.785E-04 | 2.466E-04 | 1.576E-04 | 1.160E-04 | 1.412E-04 | 1.323E-04 | 2.198E-05 | 2.057E-04 | 3.158E-05 |

Table C.2. Summary of Radionuclide Tank Supernate/Salt Concentrations at Time of Leak (3 Sheets)

| Tank | S-104 | SX-107 | SX-108 | SX-109 | SX-110 | SX-111 | SX-112 | SX-113 | SX-114 | SX-115 |
|-------------------|-------------|-------------------|-------------------|-------------------|-------------|-------------|-------------|-------------|-------------|-------------|
| Assumed Leak Date | 1965 (Ci/L) | Ave. 64-67 (Ci/L) | Ave. 65-66 (Ci/L) | Ave. 64-67 (Ci/L) | 1974 (Ci/L) | 1973 (Ci/L) | 1969 (Ci/L) | 1962 (Ci/L) | 1972 (Ci/L) | 1964 (Ci/L) |
| Radionuclides | | | | | | | | | | |
| Ra-226 | 8.936E-11 | 2.125E-10 | 2.235E-10 | 1.735E-10 | 6.432E-11 | 6.273E-11 | 1.098E-10 | 9.199E-11 | 1.017E-10 | 2.893E-11 |
| Ra-228 | 2.064E-12 | 9.465E-15 | 8.319E-15 | 5.265E-15 | 1.060E-08 | 4.447E-09 | 1.474E-09 | 6.165E-16 | 3.049E-09 | 1.528E-11 |
| Ac-227 | 5.177E-10 | 1.234E-09 | 1.298E-09 | 1.008E-09 | 3.845E-10 | 3.764E-10 | 6.374E-10 | 5.341E-10 | 5.958E-10 | 1.657E-10 |
| Pa-231 | 1.917E-09 | 6.197E-09 | 6.190E-09 | 4.567E-09 | 1.971E-09 | 2.053E-09 | 3.381E-09 | 1.986E-09 | 3.134E-09 | 7.760E-10 |
| Th-229 | 1.631E-13 | 6.367E-13 | 5.954E-13 | 4.081E-13 | 2.714E-10 | 1.442E-10 | 3.554E-11 | 1.176E-13 | 1.075E-10 | 4.400E-13 |
| Th-232 | 2.767E-13 | 2.681E-14 | 2.351E-14 | 1.483E-14 | 9.589E-10 | 7.156E-10 | 1.965E-10 | 1.635E-15 | 6.976E-10 | 2.039E-12 |
| U-232 | 4.198E-11 | 6.790E-11 | 6.427E-11 | 4.481E-11 | 1.125E-07 | 1.272E-07 | 1.496E-08 | 1.449E-11 | 1.092E-07 | 1.808E-10 |
| U-233 | 8.080E-11 | 1.721E-12 | 1.715E-12 | 1.266E-12 | 4.326E-07 | 4.899E-07 | 5.718E-08 | 5.523E-13 | 4.218E-07 | 5.933E-10 |
| U-234 | 4.484E-07 | 8.120E-07 | 8.406E-07 | 6.458E-07 | 3.239E-07 | 3.572E-07 | 5.165E-07 | 3.297E-07 | 5.050E-07 | 3.818E-07 |
| U-235 | 1.894E-08 | 3.188E-08 | 3.357E-08 | 2.623E-08 | 1.314E-08 | 1.460E-08 | 2.051E-08 | 1.419E-08 | 2.065E-08 | 1.473E-08 |
| U-236 | 1.063E-08 | 4.325E-08 | 3.908E-08 | 2.572E-08 | 1.186E-08 | 1.202E-08 | 2.506E-08 | 5.216E-09 | 1.755E-08 | 2.257E-08 |
| U-238 | 4.340E-07 | 6.400E-07 | 6.979E-07 | 5.629E-07 | 3.227E-07 | 3.424E-07 | 4.263E-07 | 3.365E-07 | 4.740E-07 | 2.823E-07 |
| U-Total (M) | 5.463E-03 | 8.064E-03 | 8.792E-03 | 7.089E-03 | 3.662E-03 | 4.149E-03 | 5.314E-03 | 4.234E-03 | 5.818E-03 | 3.558E-03 |
| Np-237 | 2.765E-07 | 9.534E-07 | 9.424E-07 | 6.878E-07 | 5.653E-07 | 7.119E-07 | 6.576E-07 | 2.846E-07 | 1.011E-06 | 1.256E-07 |
| Pu-238 | 2.491E-07 | 1.221E-06 | 1.121E-06 | 7.521E-07 | 7.478E-07 | 9.538E-07 | 5.906E-07 | 1.840E-07 | 1.358E-06 | 3.270E-07 |
| Pu-239 | 1.567E-05 | 3.012E-05 | 3.163E-05 | 2.461E-05 | 2.267E-05 | 3.027E-05 | 1.560E-05 | 1.313E-05 | 4.187E-05 | 9.276E-06 |
| Pu-240 | 2.265E-06 | 5.382E-06 | 5.436E-06 | 4.069E-06 | 4.002E-06 | 5.309E-06 | 2.731E-06 | 1.879E-06 | 7.383E-06 | 1.552E-06 |
| Pu-241 | 1.399E-05 | 6.011E-05 | 5.611E-05 | 3.844E-05 | 5.033E-05 | 6.614E-05 | 2.938E-05 | 1.105E-05 | 9.275E-05 | 1.469E-05 |
| Pu-242 | 6.017E-11 | 3.360E-10 | 3.086E-10 | 2.071E-10 | 2.825E-10 | 3.669E-10 | 1.620E-10 | 5.068E-11 | 5.195E-10 | 5.893E-11 |
| Pu-Total (g/L) | 2.622E-04 | 5.089E-04 | 5.335E-04 | 4.142E-04 | 2.509E-04 | 3.001E-04 | 2.621E-04 | 2.196E-04 | 4.331E-04 | 1.562E-04 |
| Am-241 | 2.168E-05 | 8.798E-05 | 8.515E-05 | 6.073E-05 | 3.039E-05 | 3.018E-05 | 4.951E-05 | 2.239E-05 | 4.863E-05 | 1.093E-05 |
| Am-243 | 2.033E-10 | 3.430E-09 | 3.008E-09 | 1.898E-09 | 1.159E-09 | 9.826E-10 | 1.814E-09 | 2.094E-10 | 1.753E-09 | 3.769E-10 |
| Cm-242 | 1.034E-08 | 2.514E-07 | 2.183E-07 | 1.358E-07 | 7.703E-08 | 9.701E-08 | 8.209E-08 | 1.071E-08 | 1.414E-07 | 2.676E-08 |

Table C.2. Summary of Radionuclide Tank Supernate/Salt Concentrations at Time of Leak (3 Sheets)

| Tank | S-104 | SX-107 | SX-108 | SX-109 | SX-110 | SX-111 | SX-112 | SX-113 | SX-114 | SX-115 |
|-------------------|----------------|----------------------|----------------------|----------------------|----------------|----------------|----------------|----------------|----------------|----------------|
| Assumed Leak Date | 1965 (Ci/L) | Ave. 64-67 (Ci/L) | Ave. 65-66 (Ci/L) | Ave. 64-67 (Ci/L) | 1974 (Ci/L) | 1973 (Ci/L) | 1969 (Ci/L) | 1962 (Ci/L) | 1972 (Ci/L) | 1964 (Ci/L) |
| Radionuclides | | | | | | | | | | |
| Cm-243 | 2.370E-10 | 2.490E-08 | 2.124E-08 | 1.288E-08 | 7.487E-09 | 9.285E-09 | 8.166E-09 | 2.455E-10 | 1.365E-08 | 2.598E-09 |
| Cm-244 | 7.224E-09 | 2.482E-07 | 2.141E-07 | 1.319E-07 | 8.013E-08 | 9.639E-08 | 8.123E-08 | 7.484E-09 | 1.455E-07 | 2.621E-08 |

Note: This chart selects a single waste composition (from a single selected year or average of a range of years) for each tank that leaked.

Objective is to provide the Tank Farm Vadose Zone Project with an unambiguous set of leak composition values.

Data source (HDW model-SMM Concentrations for selected tanks and for each year).

HDW = Hanford defined waste (model).

SMM = supernatant mixing model.

Once developed, waste compositions can be coupled with leak volumes to develop specific leak inventory estimates. However, published leak volume estimates (Hanlon 2001) are highly uncertain for a number of the SX tank farm leaks (Jones et al. 2000a). Thus, it was necessary to use other data sources to develop leak volume estimates. This process is discussed in the following sections.

C.3.2 GAMMA LOGGING DATA

Since the early 1960s gamma logging data have been used as a secondary tank leak monitoring system (Isaacson and Gasper 1981). In practice, strategically placed shallow boreholes (24.4 to 45.7 m [80 to 150 ft] below ground surface [bgs]), called ‘drywells,’ were routinely monitored for changes in total gamma activity. Hence, the activity is known as gross gamma logging. Drywells were located approximately 3.1 m (10 ft) from the tanks and generally 4 to 8 drywells surrounded each ‘active’ tank (that is, leak monitoring concentrated on tanks currently being used to store liquid wastes). Tanks known to have leaked (e.g., tank SX-113) where all pumpable liquids had been removed, were not given high priority to be monitored for additional leakage. For additional leak monitoring capability, 10 of the 15 tanks in the SX tank farm had laterals (i.e., horizontal pipes radiating from a central caisson) installed approximately 3.0 m (10 ft) below the base of the tank. Except for tank SX-113, each tank had three laterals radiating from a nearby caisson. As the prototype for the laterals tank leak monitoring system, tank SX-113 had five laterals installed under it.

During the routine gamma logging program, changes in gamma activity in a borehole would suggest potential leakage from a nearby waste storage tank. Although the gross gamma logging data were stored electronically from 1974 to the end of the logging program in 1994, data comparisons within any specific drywell were restricted to short time intervals. Gross gamma logging data were treated as being of value only for ‘real-time’ leak monitoring of active single-shell tanks (SSTs).

As part of the WMA S-SX vadose zone characterization, historic gross gamma logging data are assessed in Myers (1999a), and Myers (1999b). Although the gamma logging instrumentation underwent major modifications (particularly the probes) over the 20 years of data collection, the data exhibited surprising reproducibility. The data analysis also provided useful information about the potential movement of gamma emitting radionuclides over the 20-year period.

The validity of gross gamma logging methodology as a tank leak detection system was critically evaluated in *A Scientific Basis for Establishing Dry-Well Monitoring Frequencies* (Isaacson and Gasper 1981). One of the conclusions from the evaluation was that the gross gamma data provided far more insight into the migration of radionuclides in the soil than it did about potential leaks in active tanks. With the passage of time and thus decay of the short-lived mobile gamma emitting radionuclides such as ruthenium-106, the 1981 conclusions are more valid than ever.

In 1994, a baseline spectral gamma-logging program was initiated to assess the nature and extent of gamma emitting radionuclides in the tank farms vadose zone (DOE-GJPO 1995a, 1995b, 1995c; DOE-RL 1996a) by using the unique radiation emitted to identify and quantify the radionuclides. Essentially all existing drywells within each tank farm were logged with a system

designed to provide specific isotopic composition of gamma emitting radionuclides. Baseline spectral gamma logging results were published for each tank farm. The gamma-logging probe selected for the initial logging runs became saturated at approximately 1,000 pCi/g of cesium-137. Thus, in the most highly contaminated zones, quantitative values were not determined. At a later date the highly contaminated zones were re-logged using a less sensitive probe and updated results were published in supplemental tank farm reports. Ninety-eight drywells were logged in the SX tank farm and results were published in *Vadose Zone Characterization Project at the Hanford Tank Farms, SX Tank Farm Report* (DOE-GJPO 1996) and its supplement, *Addendum to the SX Tank Farm Report* (DOE-GJPO 2000). Seventy-two drywells were logged in the S tank farm and results were published in DOE-GJPO (1998) and its supplement, *Addendum to the S Tank Farm Report* (DOE-GJO 2000).

The baseline spectral gamma-logging program has made major contributions to the current tank farm vadose zone characterization efforts. The main radionuclide found was cesium-137. Only very small amounts (i.e., a few pCi/g) of cobalt-60 and/or europium-154 were found in the S and SX tank farm drywells.

C.3.3 KRIGING ANALYSIS

The SX tank farm gamma logging and soil analysis data for cesium-137 represent ‘point measurements’ along a vertical, horizontal, or slant direction. The goal of kriging analysis of the cesium-137 data was to establish mathematically defensible inventory estimates associated with the gamma contamination around each tank in the SX farm. Two separate data analyses were conducted. The first, conducted by Professor Dan Goodman, Montana State University (MSU) beginning in 1998, combined gross gamma and spectral gamma logging data with soil analysis data from borehole 41-09-39 and historical soils data (Raymond and Shdo 1966) (Goodman 2000). The MSU results are referred to as ‘MSU kriging results’ in this document. The second statistical analysis of the SX tank farm cesium-137 data, conducted by HydroGeologic, Inc. (HGL) (Sullivan et al. 2001), began with the same data set as used by MSU but also included newly acquired soils analysis data from the SX-108 slant borehole (Serne 2001d) and the updated spectral gamma logging results (DOE-GJPO 2000b).

The MSU statistical analysis focused on two objectives.

- The gross gamma logging data were evaluated to establish calibration curves so as to use the gross gamma data to develop ‘data patches’ for the regions of the spectral gamma data set lost because of detector saturation in the initial spectral gamma logging.
- The resulting enhanced gamma logging-based cesium-137 data set was coupled with soils analysis data to develop cesium-137 inventory estimates for the regions around each tank in the SX farm.

The projected cesium-137 inventory estimate for each of tank in the SX tank farm is listed in Table C.3. Inventory estimates are reported at both the 50 and 95 percentiles.

**Table C.3. SX Tank Farm Cesium-137 Inventory
Estimates from Kriging Analyses**

| Tank | MSU 50% (pCi) | MSU 95% (pCi) | HGL 50% (pCi) |
|-------------|--------------------------|--------------------------|--------------------------|
| SX-101 | 9.1E+09 | 2.1E+10 | 2.3E+10 |
| SX-102 | 0.0E+00 | 0.0E+00 | 1.5E+10 |
| SX-103 | 0.0E+00 | 0.0E+00 | 2.1E+10 |
| SX-104 | 2.7E+08 | 1.6E+09 | 7.7E+09 |
| SX-105 | 5.5E+09 | 1.3E+10 | 1.3E+10 |
| SX-106 | 0.0E+00 | 0.0E+00 | 5.9E+09 |
| SX-107 | 8.0E+15 | 1.5E+16 | 4.2E+16 |
| SX-108 | 1.4E+16 | 3.6E+16 | 3.9E+16 |
| SX-109 | 7.2E+14 | 2.3E+15 | 1.6E+15 |
| SX-110 | 2.0E+12 | 1.3E+13 | 7.5E+12 |
| SX-111 | 2.3E+11 | 1.1E+12 | 2.3E+11 |
| SX-112 | 1.8E+13 | 9.5E+13 | 2.9E+13 |
| SX-113 | 0.0E+00 | 0.0E+00 | 6.4E+07 |
| SX-114 | 0.0E+00 | 0.0E+00 | 1.9E+08 |
| SX-115 | N/R | N/R | 1.1E+14 |

HGL = HydroGeologic, Inc.

MSU = Montana State University.

N/R = not reported.

The second kriging analysis was focused on understanding the impact of the addition of the cesium-137 soils analysis data from the SX-108 slant borehole investigation on the overall cesium-137 inventory estimate. Also included in the second kriging analysis were the updated spectral gamma logging data for cesium-137 from highly contaminated zones (DOE-GJPO 2000b). Thus, the data patches from historical gross gamma data developed by MSU for that kriging analysis were not required for the HGL kriging analysis.

The first step in any kriging process is the development of a variogram model. Vertical and horizontal correlation lengths are determined during the variogram analysis. Significantly different correlation lengths were reported between the two kriging analyses.

- MSU variogram analysis led to a horizontal correlation length of 8.2 m (26.9 ft) and a vertical correlation length of 3 m (10 ft)
- HGL variogram analysis led to horizontal and vertical correlation lengths of 15 m (49 ft) and 20 m (66 ft), respectively.

The practical result of longer correlation lengths is the projection of somewhat larger plume volumes with the existing data set.

There are a number of reasons for the large correlation lengths reported in the HGL kriging analysis (Sullivan et al. 2001). The most obvious reason is the addition of the cesium-137 concentrations along the SX-108 slant borehole, giving much better definition of the vertical contamination directly below tank SX-108. However, there were also differences in approach. The MSU variogram analysis treated all of the available data within the SX tank farm while the HGL variogram analysis focused on the area around tank SX-108. The decision to estimate correlation lengths using data only from around tank SX-108 focused the analysis in the area where the maximum amount of data was available. The correlation lengths derived from the analysis of data around tank SX-108 were then used in the kriging analysis for all of the SX tank farm data. The intent was to apply the knowledge gained from detailed field investigations around tank SX-108 to the contamination found around and under other SX farm tanks.

This was justified because very similar waste types leaked from all failed SX farm tanks and the geology was assumed reasonably similar across the SX tank farm. The HGL kriging analysis also reports results of sensitivity studies associated with data processing decisions.

The cesium-137 inventory estimates developed in the HGL kriging analysis are also listed by tank in Table C.3. An example of the graphical representation of cesium-137 activity generated in the HGL kriging analysis is shown in Figures C.1 through C.7. This series of figures provide a graphical representation of the projected cesium-137 contamination as a function of activity levels.

The comparison between projected cesium-137 inventory estimates for each tank in the SX tank farm is shown in Figure C.8.

There are subjective decisions that are made in any statistical analysis involving large and diverse data sets such as those reported here where data compression is required. The HGL kriging analysis explored potential impacts of these decisions on reported results. The HGL analysis results are discussed briefly in the following paragraphs.

Both kriging analyses were forced to reduce the size of the data set prior to computations because the data set was too large to be processed with available computer systems. Both groups separated the tank farm area into a 1 m by 1 m grid size. MSU used a 1 m depth to form 1 m³ sections. The geometric mean of all cesium-137 concentration values with the 1 m³ was assigned to the center of the cube. The variogram analysis and kriging were completed with this reduced data set. The HGL data process approach was quite similar except the grid size was 1 m (3 ft) by 1 m (3 ft) by 0.5 m (1.5 ft) depth.

The geometric mean is commonly used as an approach for compressing large environmental data sets, where values span multiple orders of magnitudes (e.g., HGL data in the SX tank farm). However, other approaches could be taken. For example, a more conservative approach would be to assign the data value of the volume space as the maximum value reported within that grid volume. Or, one might chose to use the arithmetic mean. Results of the three data compression alternatives are shown in Figure C.9 for tank SX-107. A more detailed comparison between 'geometric mean' and 'maximum' values for all SX farm tanks are shown in Tables C.4 and C.5 (Sullivan et al. 2001).

Figure C.1. Three-Dimensional Perspective of Cesium-137 Contaminated Soil Above 5×10^1 pCi/g

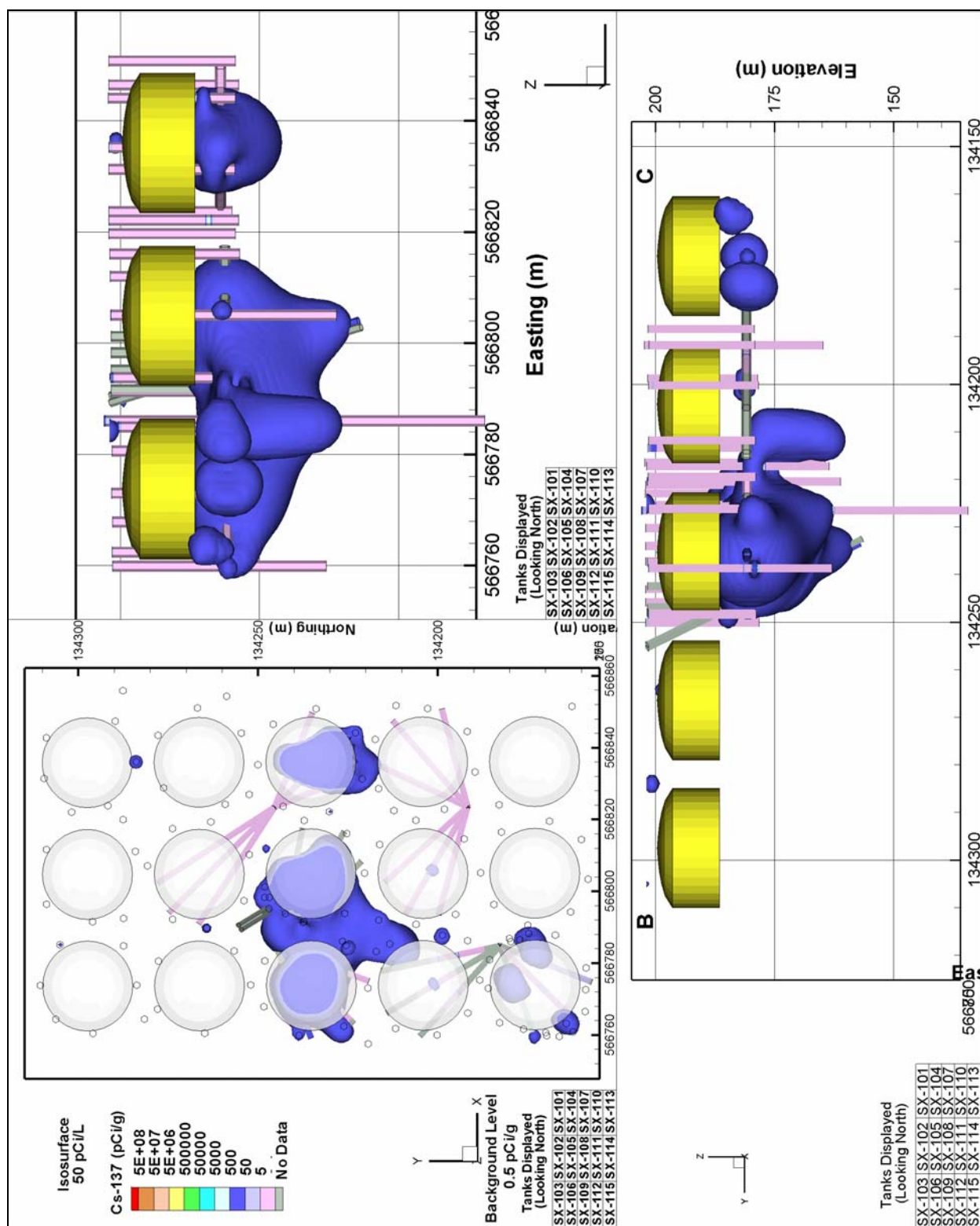


Figure C.2. Three-Dimensional Perspective of Cesium-137 Contaminated Soil Above 5×10^2 pCi/g

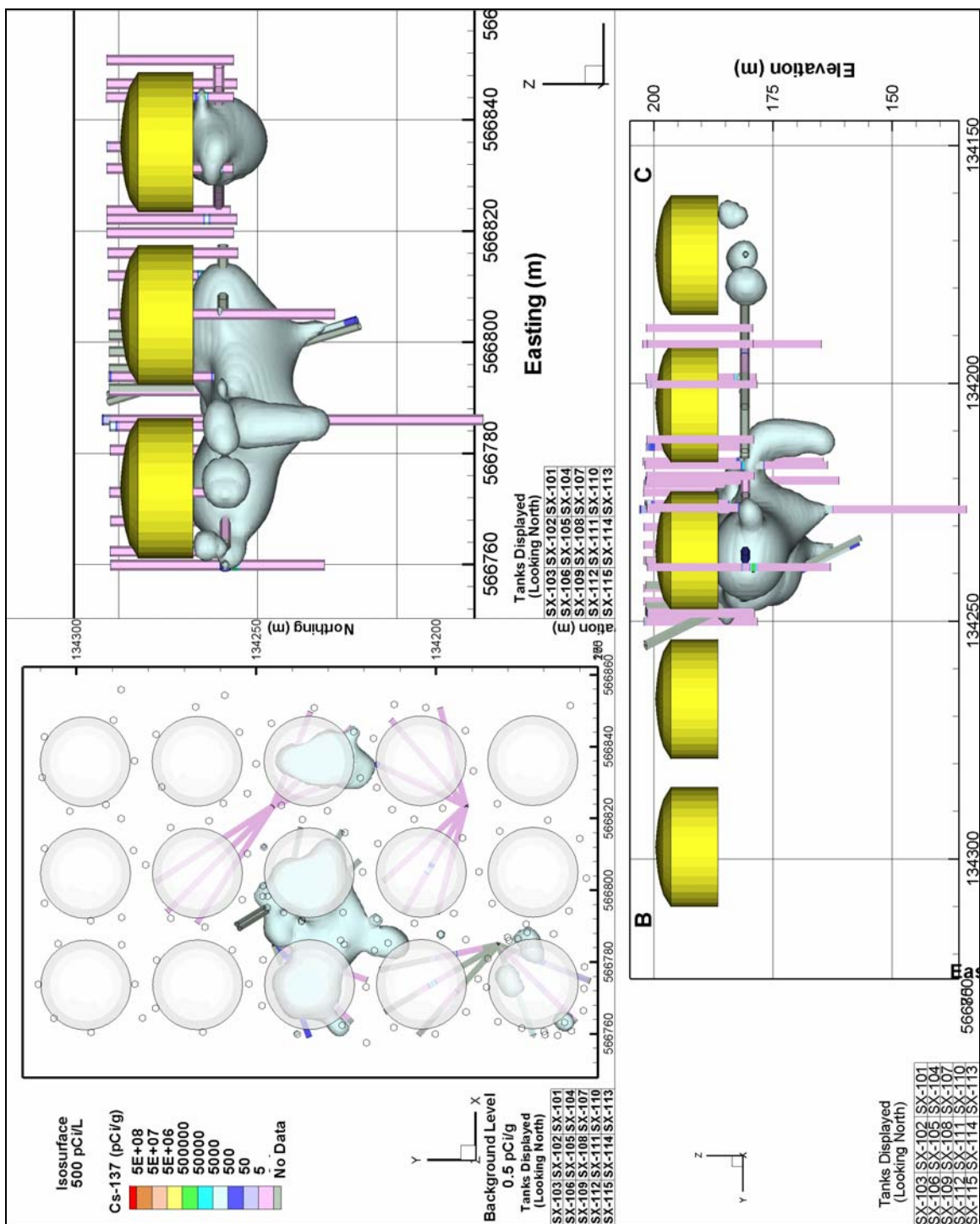


Figure C.3. Three-Dimensional Perspective of Cesium-137 Contaminated Soil Above 5×10^3 pCi/g

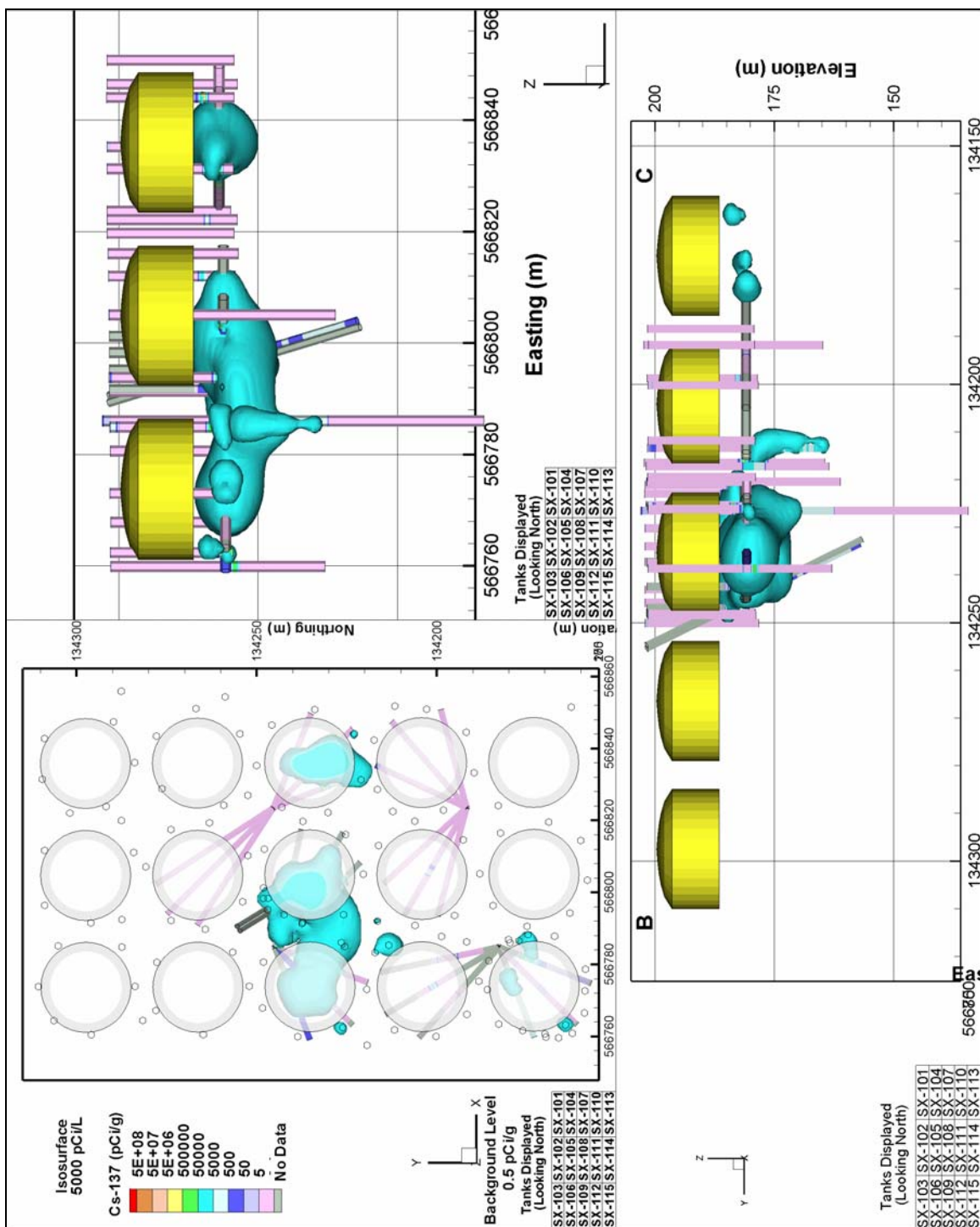


Figure C.4. Three-Dimensional Perspective of Cesium-137 Contaminated Soil Above 5×10^4 pCi/g

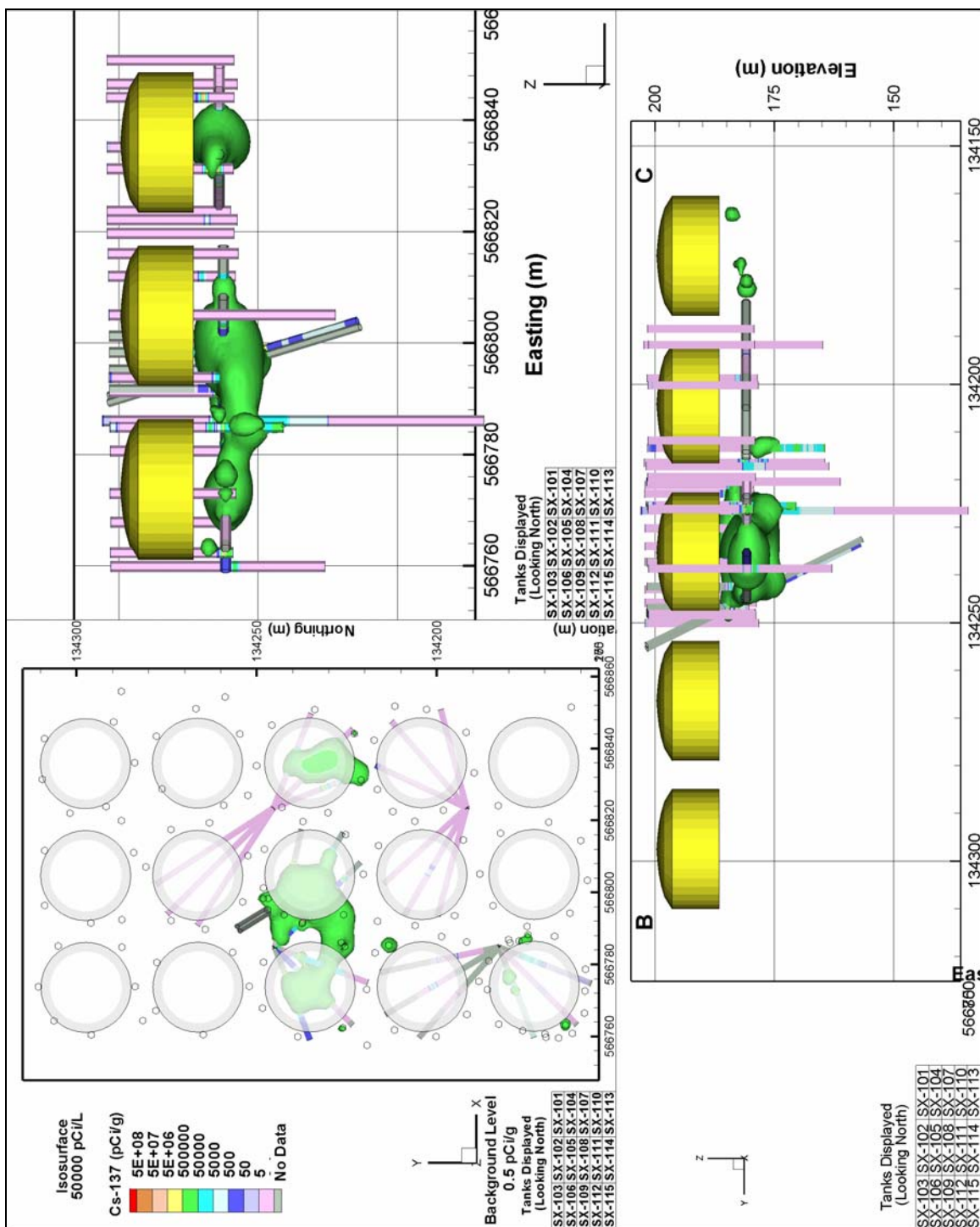


Figure C.5. Three-Dimensional Perspective of Cesium-137 Contaminated Soil Above 5×10^5 pCi/g

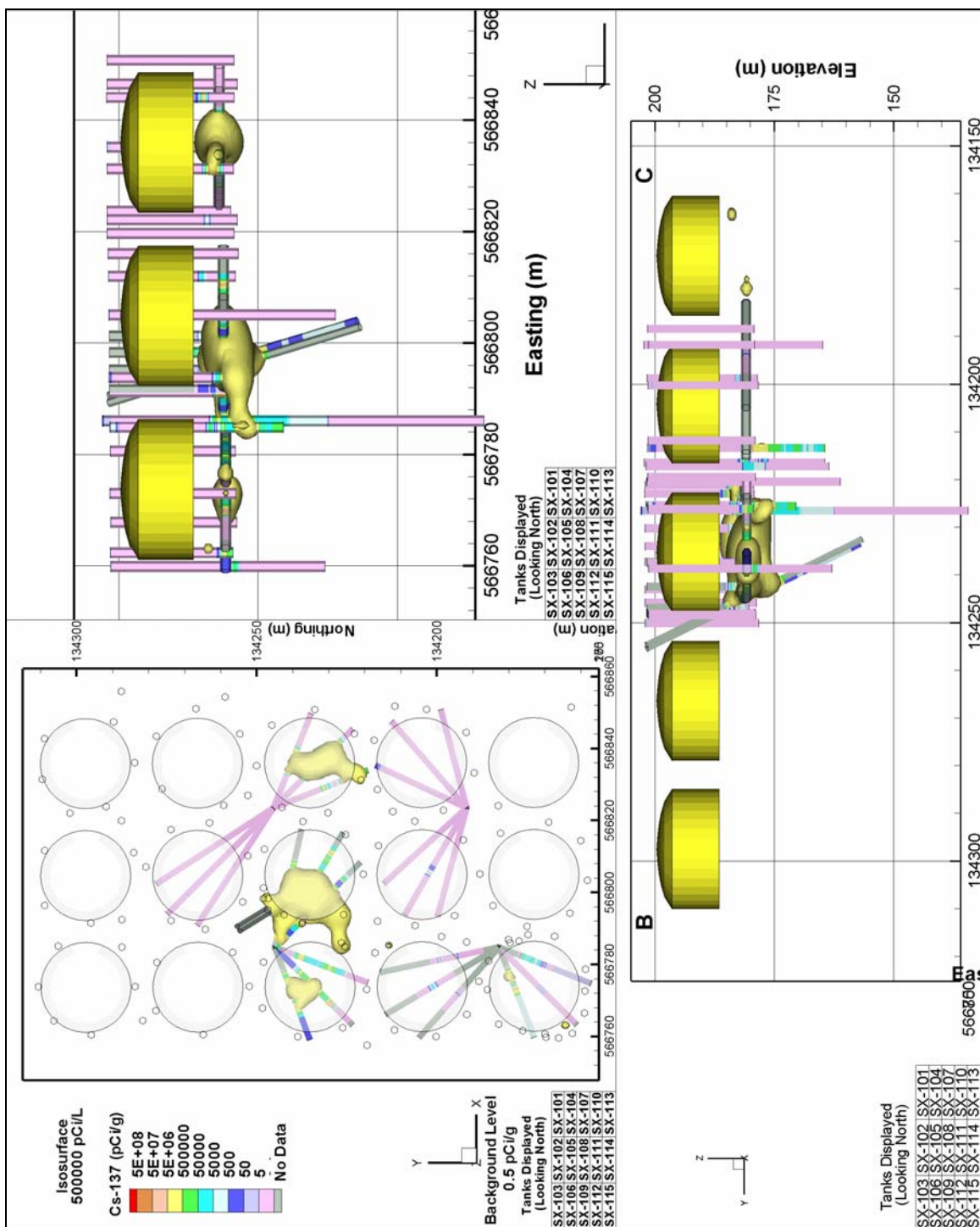


Figure C.6. Three-Dimensional Perspective of Cesium-137 Contaminated Soil Above 5×10^6 pCi/g

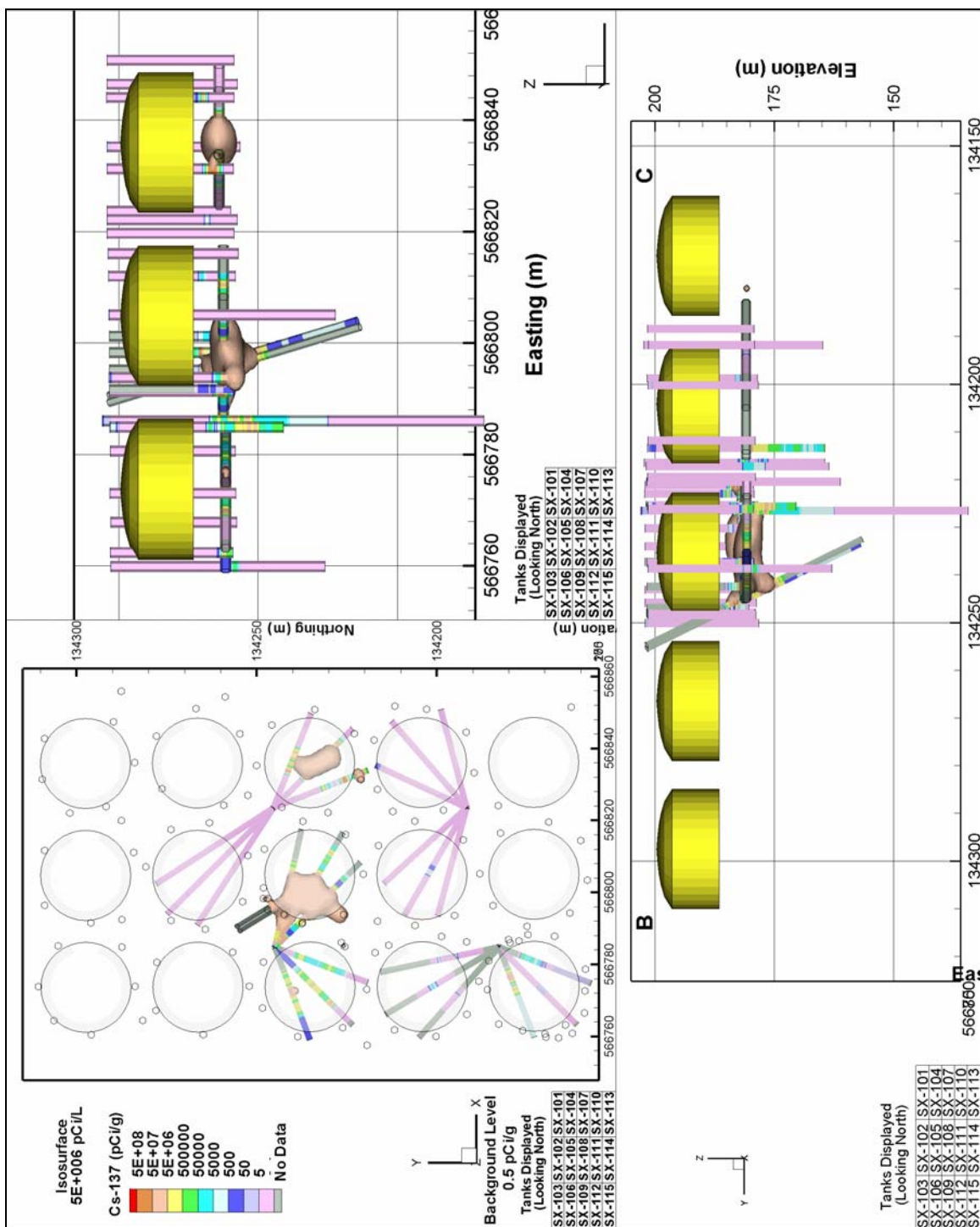


Figure C.7. Three-Dimensional Perspective of Cesium-137 Contaminated Soil Above 5×10^7 pCi/g

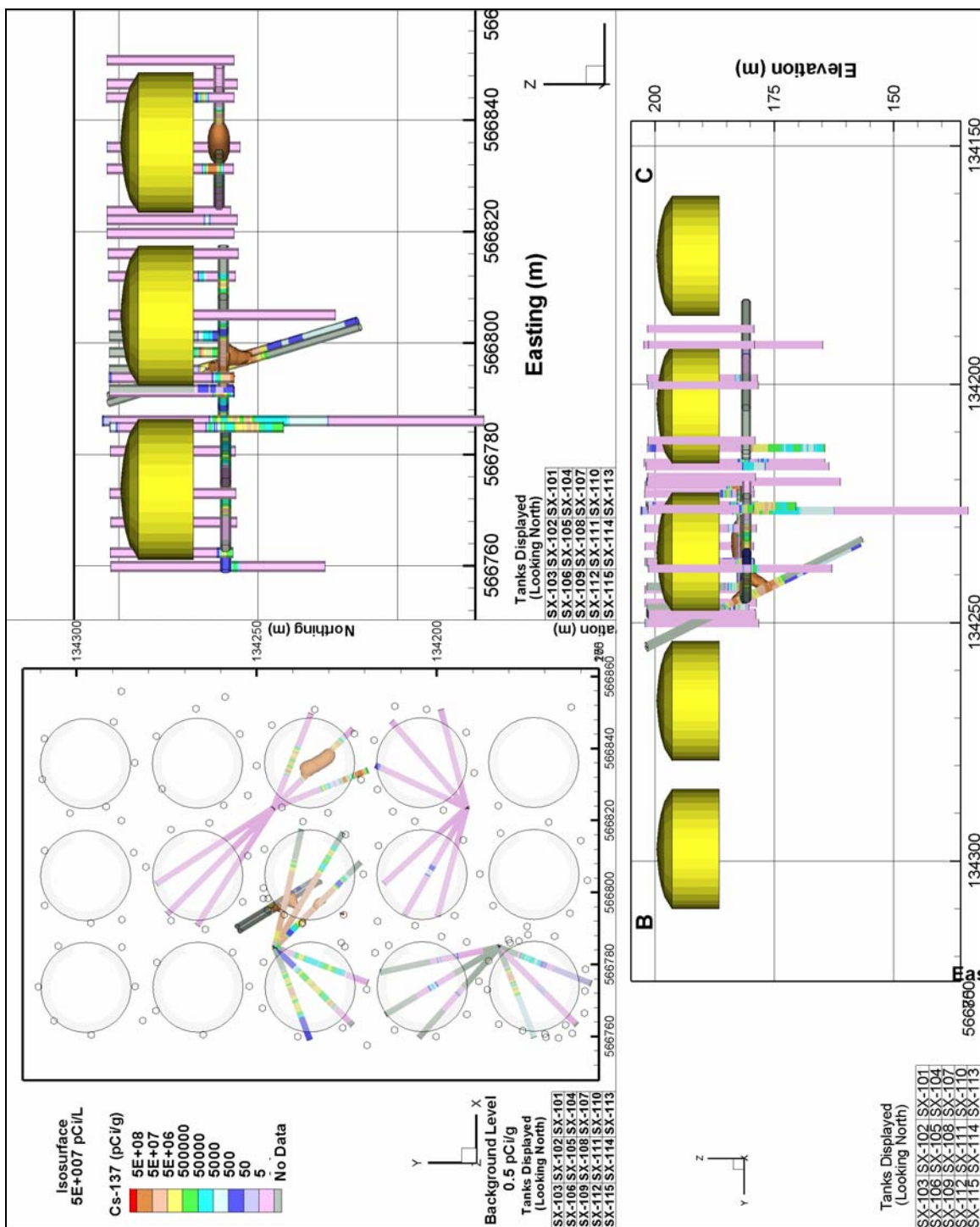
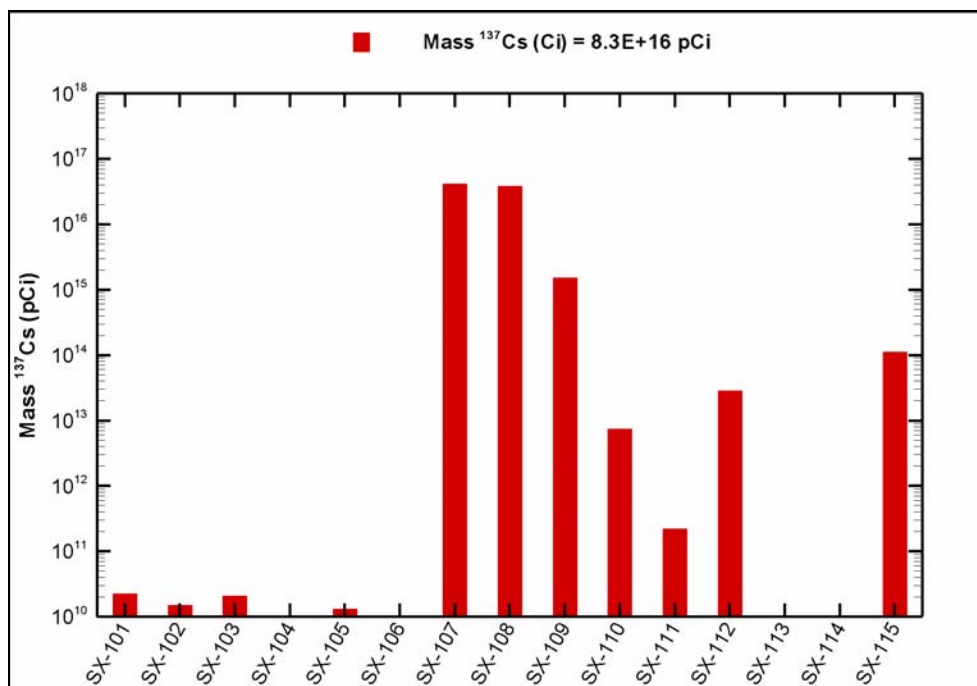
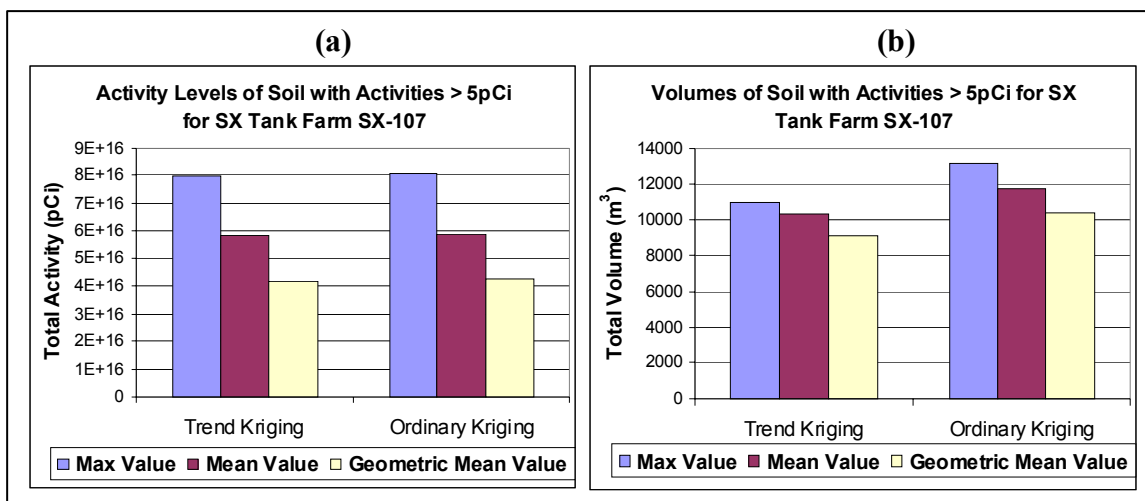


Figure C.8. Total Pico-Curies of Cesium-137 Inventory by Tank**Figure C.9. Estimated Activity Levels and Estimated Contaminated Soil Volume Using Max, Mean, and Geometric Mean Sample Data Filtering for Tank SX-107**

**Table C.4. Summary of Activity and Volume Estimates by Tank
and Activity Threshold with Geometric Mean Filtering**

| Tank | Activity/ Volume | Activity Threshold | | | | | | | |
|---------------------------|--------------------------|--------------------|---------------|----------------|------------------|-------------------|--------------------|------------------|------------------|
| | | 5 (pCi/g) | 50 (pCi/g) | 500 (pCi/g) | 5,000 (pCi/g) | 50,000 (pCi/g) | 500,000 (pCi/g) | 5E+06 (pCi/g) | 5E+07 (pCi/g) |
| SX-101 | Activity (pCi) | 2.30E+10 | 4.11E+09 | 0.00E+00 | 0.00E+00 | 0.00E+00 | 0.00E+00 | 0.00E+00 | 0.00E+00 |
| | Volume (m ³) | 1.10E+03 | 2.05E+01 | 0.00E+00 | 0.00E+00 | 0.00E+00 | 0.00E+00 | 0.00E+00 | 0.00E+00 |
| SX-102 | Activity (pCi) | 1.53E+10 | 0.00E+00 | 0.00E+00 | 0.00E+00 | 0.00E+00 | 0.00E+00 | 0.00E+00 | 0.00E+00 |
| | Volume (m ³) | 1.14E+03 | 0.00E+00 | 0.00E+00 | 0.00E+00 | 0.00E+00 | 0.00E+00 | 0.00E+00 | 0.00E+00 |
| SX-103 | Activity (pCi) | 2.12E+10 | 2.24E+08 | 0.00E+00 | 0.00E+00 | 0.00E+00 | 0.00E+00 | 0.00E+00 | 0.00E+00 |
| | Volume (m ³) | 1.31E+03 | 2.00E+00 | 0.00E+00 | 0.00E+00 | 0.00E+00 | 0.00E+00 | 0.00E+00 | 0.00E+00 |
| SX-104 | Activity (pCi) | 7.75E+09 | 0.00E+00 | 0.00E+00 | 0.00E+00 | 0.00E+00 | 0.00E+00 | 0.00E+00 | 0.00E+00 |
| | Volume (m ³) | 5.23E+02 | 0.00E+00 | 0.00E+00 | 0.00E+00 | 0.00E+00 | 0.00E+00 | 0.00E+00 | 0.00E+00 |
| SX-105 | Activity (pCi) | 1.33E+10 | 7.62E+08 | 0.00E+00 | 0.00E+00 | 0.00E+00 | 0.00E+00 | 0.00E+00 | 0.00E+00 |
| | Volume (m ³) | 1.03E+03 | 3.00E+00 | 0.00E+00 | 0.00E+00 | 0.00E+00 | 0.00E+00 | 0.00E+00 | 0.00E+00 |
| SX-106 | Activity (pCi) | 5.90E+09 | 3.35E+08 | 0.00E+00 | 0.00E+00 | 0.00E+00 | 0.00E+00 | 0.00E+00 | 0.00E+00 |
| | Volume (m ³) | 4.93E+02 | 2.00E+00 | 0.00E+00 | 0.00E+00 | 0.00E+00 | 0.00E+00 | 0.00E+00 | 0.00E+00 |
| SX-107 | Activity (pCi) | 4.22E+16 | 4.22E+16 | 4.22E+16 | 4.22E+16 | 4.22E+16 | 4.20E+16 | 4.06E+16 | 3.32E+16 |
| | Volume (m ³) | 7.82E+03 | 4.33E+03 | 2.90E+03 | 2.00E+03 | 1.36E+03 | 8.05E+02 | 3.57E+02 | 1.18E+02 |
| SX-108 | Activity (pCi) | 3.91E+16 | 3.91E+16 | 3.91E+16 | 3.91E+16 | 3.90E+16 | 3.86E+16 | 3.55E+16 | 6.20E+15 |
| | Volume (m ³) | 1.83E+04 | 1.07E+04 | 7.02E+03 | 4.69E+03 | 3.06E+03 | 1.82E+03 | 9.02E+02 | 5.35E+01 |
| SX-109 | Activity (pCi) | 1.56E+15 | 1.56E+15 | 1.56E+15 | 1.55E+15 | 1.48E+15 | 1.13E+15 | 2.20E+14 | 0.00E+00 |
| | Volume (m ³) | 1.74E+04 | 1.04E+04 | 6.58E+03 | 3.69E+03 | 1.58E+03 | 3.81E+02 | 1.55E+01 | 0.00E+00 |
| SX-110 | Activity (pCi) | 7.51E+12 | 7.50E+12 | 7.47E+12 | 7.30E+12 | 6.63E+12 | 3.88E+12 | 0.00E+00 | 0.00E+00 |
| | Volume (m ³) | 5.15E+02 | 2.05E+02 | 9.10E+01 | 3.50E+01 | 1.20E+01 | 3.00E+00 | 0.00E+00 | 0.00E+00 |
| SX-111 | Activity (pCi) | 2.26E+11 | 1.91E+11 | 1.07E+11 | 2.97E+10 | 0.00E+00 | 0.00E+00 | 0.00E+00 | 0.00E+00 |
| | Volume (m ³) | 1.72E+03 | 3.42E+02 | 4.90E+01 | 1.50E+00 | 0.00E+00 | 0.00E+00 | 0.00E+00 | 0.00E+00 |
| SX-112 | Activity (pCi) | 2.92E+13 | 2.91E+13 | 2.87E+13 | 2.67E+13 | 2.05E+13 | 7.45E+12 | 0.00E+00 | 0.00E+00 |
| | Volume (m ³) | 7.14E+03 | 2.27E+03 | 9.53E+02 | 2.82E+02 | 5.35E+01 | 6.00E+00 | 0.00E+00 | 0.00E+00 |
| SX-113 | Activity (pCi) | 6.41E+07 | 0.00E+00 | 0.00E+00 | 0.00E+00 | 0.00E+00 | 0.00E+00 | 0.00E+00 | 0.00E+00 |
| | Volume (m ³) | 6.00E+00 | 0.00E+00 | 0.00E+00 | 0.00E+00 | 0.00E+00 | 0.00E+00 | 0.00E+00 | 0.00E+00 |
| SX-114 | Activity (pCi) | 1.90E+08 | 0.00E+00 | 0.00E+00 | 0.00E+00 | 0.00E+00 | 0.00E+00 | 0.00E+00 | 0.00E+00 |
| | Volume (m ³) | 1.25E+01 | 0.00E+00 | 0.00E+00 | 0.00E+00 | 0.00E+00 | 0.00E+00 | 0.00E+00 | 0.00E+00 |
| SX-115 | Activity (pCi) | 1.14E+14 | 1.14E+14 | 1.14E+14 | 1.13E+14 | 1.07E+14 | 9.27E+13 | 5.50E+13 | 0.00E+00 |
| | Volume (m ³) | 4.24E+03 | 1.46E+03 | 6.12E+02 | 2.46E+02 | 6.70E+01 | 1.70E+01 | 3.00E+00 | 0.00E+00 |
| SX Tank Farm Totals | Activity (pCi) | 8.3011E+16 | 8.3011E+16 | 8.3011E+16 | 8.2997E+16 | 8.2814E+16 | 8.1834E+16 | 7.6375E+16 | 3.940E+16 |
| | Volume (m ³) | 62,750 | 29,375 | 18,205 | 10,945 | 6,133 | 3,032 | 1,278 | 172 |

**Table C.5. Summary of Activity and Volume Estimates by Tank
and Activity Threshold with Maximum Value Filtering**

| Tank | Activity/ Volume | Activity Threshold Level | | | | | | | |
|---------------------------|--------------------------|--------------------------|---------------|----------------|------------------|-------------------|--------------------|------------------|------------------|
| | | 5 (pCi/g) | 50 (pCi/g) | 500 (pCi/g) | 5,000 (pCi/g) | 50,000 (pCi/g) | 500,000 (pCi/g) | 5E+06 (pCi/g) | 5E+07 (pCi/g) |
| SX-101 | Activity (pCi) | 6.29E+10 | 1.54E+10 | 1.96E+09 | 0.00E+00 | 0.00E+00 | 0.00E+00 | 0.00E+00 | 0.00E+00 |
| | Volume (m ³) | 2.56E+03 | 7.55E+01 | 1.50E+00 | 0.00E+00 | 0.00E+00 | 0.00E+00 | 0.00E+00 | 0.00E+00 |
| SX-102 | Activity (pCi) | 5.62E+10 | 0.00E+00 | 0.00E+00 | 0.00E+00 | 0.00E+00 | 0.00E+00 | 0.00E+00 | 0.00E+00 |
| | Volume (m ³) | 3.19E+03 | 0.00E+00 | 0.00E+00 | 0.00E+00 | 0.00E+00 | 0.00E+00 | 0.00E+00 | 0.00E+00 |
| SX-103 | Activity (pCi) | 7.60E+10 | 9.26E+09 | 0.00E+00 | 0.00E+00 | 0.00E+00 | 0.00E+00 | 0.00E+00 | 0.00E+00 |
| | Volume (m ³) | 3.50E+03 | 6.80E+01 | 0.00E+00 | 0.00E+00 | 0.00E+00 | 0.00E+00 | 0.00E+00 | 0.00E+00 |
| SX-104 | Activity (pCi) | 3.61E+10 | 1.53E+09 | 0.00E+00 | 0.00E+00 | 0.00E+00 | 0.00E+00 | 0.00E+00 | 0.00E+00 |
| | Volume (m ³) | 1.74E+03 | 1.30E+01 | 0.00E+00 | 0.00E+00 | 0.00E+00 | 0.00E+00 | 0.00E+00 | 0.00E+00 |
| SX-105 | Activity (pCi) | 7.03E+10 | 1.19E+10 | 9.85E+09 | 4.77E+09 | 0.00E+00 | 0.00E+00 | 0.00E+00 | 0.00E+00 |
| | Volume (m ³) | 3.66E+03 | 1.25E+01 | 2.50E+00 | 5.00E-01 | 0.00E+00 | 0.00E+00 | 0.00E+00 | 0.00E+00 |
| SX-106 | Activity (pCi) | 5.71E+10 | 5.78E+09 | 4.03E+09 | 0.00E+00 | 0.00E+00 | 0.00E+00 | 0.00E+00 | 0.00E+00 |
| | Volume (m ³) | 3.09E+03 | 1.05E+01 | 2.00E+00 | 0.00E+00 | 0.00E+00 | 0.00E+00 | 0.00E+00 | 0.00E+00 |
| SX-107 | Activity (pCi) | 8.08E+16 | 8.08E+16 | 8.08E+16 | 8.08E+16 | 8.08E+16 | 8.05E+16 | 7.86E+16 | 6.44E+16 |
| | Volume (m ³) | 9.94E+03 | 5.22E+03 | 3.54E+03 | 2.52E+03 | 1.79E+03 | 1.19E+03 | 6.38E+02 | 2.12E+02 |
| SX-108 | Activity (pCi) | 5.02E+16 | 5.02E+16 | 5.02E+16 | 5.02E+16 | 5.01E+16 | 4.96E+16 | 4.60E+16 | 9.84E+15 |
| | Volume (m ³) | 2.27E+04 | 1.16E+04 | 7.60E+03 | 5.24E+03 | 3.51E+03 | 2.14E+03 | 1.08E+03 | 8.15E+01 |
| SX-109 | Activity (pCi) | 3.77E+15 | 3.77E+15 | 3.77E+15 | 3.76E+15 | 3.67E+15 | 3.06E+15 | 9.61E+14 | 0.00E+00 |
| | Volume (m ³) | 2.19E+04 | 1.26E+04 | 8.33E+03 | 5.20E+03 | 2.68E+03 | 8.49E+02 | 6.60E+01 | 0.00E+00 |
| SX-110 | Activity (pCi) | 1.11E+14 | 1.11E+14 | 1.11E+14 | 1.10E+14 | 1.09E+14 | 1.04E+14 | 8.35E+13 | 0.00E+00 |
| | Volume (m ³) | 1.50E+03 | 2.83E+02 | 1.37E+02 | 6.50E+01 | 3.00E+01 | 1.15E+01 | 4.00E+00 | 0.00E+00 |
| SX-111 | Activity (pCi) | 1.16E+12 | 1.08E+12 | 9.70E+11 | 4.52E+11 | 1.11E+11 | 0.00E+00 | 0.00E+00 | 0.00E+00 |
| | Volume (m ³) | 4.16E+03 | 5.92E+02 | 1.79E+02 | 1.65E+01 | 5.00E-01 | 0.00E+00 | 0.00E+00 | 0.00E+00 |
| SX-112 | Activity (pCi) | 6.16E+13 | 6.14E+13 | 6.07E+13 | 5.82E+13 | 4.82E+13 | 2.76E+13 | 0.00E+00 | 0.00E+00 |
| | Volume (m ³) | 1.21E+04 | 3.50E+03 | 1.26E+03 | 4.57E+02 | 8.90E+01 | 1.30E+01 | 0.00E+00 | 0.00E+00 |
| SX-113 | Activity (pCi) | 8.42E+08 | 0.00E+00 | 0.00E+00 | 0.00E+00 | 0.00E+00 | 0.00E+00 | 0.00E+00 | 0.00E+00 |
| | Volume (m ³) | 7.00E+01 | 0.00E+00 | 0.00E+00 | 0.00E+00 | 0.00E+00 | 0.00E+00 | 0.00E+00 | 0.00E+00 |
| SX-114 | Activity (pCi) | 6.16E+09 | 0.00E+00 | 0.00E+00 | 0.00E+00 | 0.00E+00 | 0.00E+00 | 0.00E+00 | 0.00E+00 |
| | Volume (m ³) | 4.64E+02 | 0.00E+00 | 0.00E+00 | 0.00E+00 | 0.00E+00 | 0.00E+00 | 0.00E+00 | 0.00E+00 |
| SX-115 | Activity (pCi) | 2.69E+14 | 2.69E+14 | 2.69E+14 | 2.68E+14 | 2.60E+14 | 2.27E+14 | 1.46E+14 | 0.00E+00 |
| | Volume (m ³) | 5.30E+03 | 1.82E+03 | 8.27E+02 | 3.97E+02 | 1.54E+02 | 3.80E+01 | 6.00E+00 | 0.00E+00 |
| SX Tank Farm Totals | Activity (pCi) | 1.35E+17 | 1.35E+17 | 1.35E+17 | 1.35E+17 | 1.35E+17 | 1.34E+17 | 1.26E+17 | 7.43E+16 |
| | Volume (m ³) | 95,867 | 35,735 | 21,873 | 13,894 | 8,260 | 4,232 | 1,795 | 294 |

C.3.4 INVENTORY ESTIMATES FOR WASTE MANAGEMENT AREA S-SX TANK LEAKS

Leak volume estimates and projected inventory estimates for WMA S-SX tank leaks are listed in Tables C.6 and C.7 (Jones et al. 2000a). Leak inventory estimates for tanks SX-107, SX-108, and SX-109 were based on cesium-137 inventories developed by the MSU kriging analysis (Goodman 2000). Leak volumes for these three tanks were estimated from cesium-137 inventory estimates (Goodman 2000) coupled with waste composition estimates (see Section C.3.1). Inventory estimates for tanks S-104, SX-113, and SX-115 were based on documented leak volumes (Hanlon 2001; Jones et al. 2000a). For these three cases, leak volumes were combined with tank waste inventory estimates (see Section C.3.1) to develop inventory estimates for each tank leak.

The following discussion focuses on potential modifications to the published WMA S-SX inventory estimates based on the updated HGL kriging results.

Inventory and leak volume estimates developed in Jones et al. (2000a) are listed in Tables C.6 and C.7. The estimates were made using the waste tank compositions (discussed in Section C.3.1) and the leak volumes as estimated from the cesium-137 inventory in the soil (discussed in Section C.3.3). The inventory estimates shown in Tables C.6 and C.7 for tanks SX-107, SX-108, and SX-109 were developed using 95 percentile cesium-137 data from MSU (Goodman 2000). That is, these inventory estimates were biased high by using the 95 percentile data rather than the mean or 50 percentile values. The decision to use the higher values was driven by an assumption that the cesium-137 plume estimates failed to reflect realistic estimates of the cesium-137 inventories directly below the tanks. (This was one of the conclusions discussed in the MSU report [Goodman 2000] and was used as one of the technical justifications for drilling the SX-108 slant borehole.)

Those estimates remain as reasonable estimates for use in leak impact assessment studies. The HGL kriging analysis was more robust than the MSU efforts because only experimentally determined measurements were used by HGL, and HGL correlation lengths were based on a single tank (i.e., tank SX-108) where the most data were available then applied to all SX farm tanks.

The inventory estimates for tanks SX-107, SX-108, and SX-109 were developed using the 95 percentile MSU kriging data. If the HGL kriging results had been used in developing the inventory estimates, the values for tanks SX-108 and SX-109 listed in Tables C.6 and C.7 would have changed very little. However, the tank SX-107 inventory estimates would have been slightly higher than those reported for tank SX-108 in Tables C.6 and C.7. Leak inventory estimates for tanks S-104, SX-113, and SX-115 were based on historical leak volumes. Leak volumes from tanks SX-113 and SX-115 are well documented (Hanson et al. 1962; Raymond and Shdo 1966) whereas the leak volume from tank S-104 is significantly more uncertain. The 24,000 gal (91,000 L) leak volume currently reported in *Waste Tank Summary Report for Month Ending March 31, 2001* (Hanlon 2001) for tank S-104 is based on long-term liquid level decreases (Agnew et al. 1997). However, the waste footprint projected from field investigations using cone penetrometer techniques and spectral gamma logging data fail to document the inventory estimates shown in Tables C.6 and C.7 for tank S-104. Thus, the tank S-104 inventory estimates listed in Tables C.6 and C.7 are conservative.

**Table C.6. Estimated Inventory Lost to Vadose Zone
in the S and SX Tank Farms (2 Sheets)**

| Chemical | Estimated S-104 Inventory Loss (kg) | Estimated SX-107 Inventory Loss (kg) | Estimated SX-108 Inventory Loss (kg) | Estimated SX-109 Inventory Loss (kg) | Estimated SX-113 Inventory Loss (kg) | Estimated SX-115 Inventory Loss (kg) |
|------------------|--|---|---|---|---|---|
| Leak Vol. | 24,000 gal^a | 63,500 gal^b | 15,200 gal^b | 989 gal^b | 15,000 gal^a | 50,000 gal^a |
| Na | 1.82E+04 | 9.90E+03 | 2.37E+04 | 1.54E+03 | 1.05E+04 | 1.57E+04 |
| Al3 | 3.83E+03 | 2.00E+03 | 4.78E+03 | 3.11E+02 | 1.95E+03 | 4.24E+03 |
| Fe (Total) | 1.81E+01 | 8.87E+00 | 2.12E+01 | 1.38E+00 | 9.47E+00 | 2.25E+01 |
| Cr | 7.81E+02 | 4.71E+02 | 1.13E+03 | 7.33E+01 | 5.08E+02 | 5.03E+02 |
| Bi | 1.71E-04 | 0.00E+00 | 0.00E+00 | 0.00E+00 | 0.00E+00 | 2.63E-03 |
| La | 2.79E-10 | 0.00E+00 | 0.00E+00 | 0.00E+00 | 0.00E+00 | 4.31E-09 |
| Hg | 6.49E-02 | 1.90E-04 | 4.54E-04 | 2.95E-05 | 0.00E+00 | 2.40E-01 |
| ZrO(OH)2 | 1.15E-05 | 0.00E+00 | 0.00E+00 | 0.00E+00 | 0.00E+00 | 1.77E-04 |
| Pb | 1.07E+01 | 3.13E-02 | 7.48E-02 | 4.87E-03 | 0.00E+00 | 3.96E+01 |
| Ni | 1.66E+01 | 8.36E+00 | 2.00E+01 | 1.30E+00 | 8.94E+00 | 1.93E+01 |
| Sr | 0.00E+00 | 0.00E+00 | 0.00E+00 | 0.00E+00 | 0.00E+00 | 0.00E+00 |
| Mn | 3.27E-04 | 0.00E+00 | 0.00E+00 | 0.00E+00 | 0.00E+00 | 5.04E-03 |
| Ca | 5.82E+01 | 2.85E+01 | 6.82E+01 | 4.44E+00 | 3.05E+01 | 7.22E+01 |
| K | 1.09E+02 | 6.33E+01 | 1.52E+02 | 9.86E+00 | 6.92E+01 | 8.21E+01 |
| U-Total | 1.19E+02 | 4.58E+01 | 1.10E+02 | 7.14E+00 | 5.74E+01 | 1.61E+02 |
| Pu-Total | 2.39E-02 | 1.17E-02 | 2.80E-02 | 1.82E-03 | 1.25E-02 | 2.97E-02 |
| TOC wt% C | 1.28E+02 | 0.00E+00 | 0.00E+00 | 0.00E+00 | 0.00E+00 | 0.00E+00 |
| free OH | 0.00E+00 | 0.00E+00 | 0.00E+00 | 0.00E+00 | 0.00E+00 | 0.00E+00 |
| OH | 1.40E+04 | 7.66E+03 | 1.83E+04 | 1.19E+03 | 7.72E+03 | 1.35E+04 |
| NO3 | 1.70E+04 | 7.40E+03 | 1.77E+04 | 1.15E+03 | 9.96E+03 | 3.87E+03 |
| NO2 | 6.87E+03 | 4.49E+03 | 1.07E+04 | 6.99E+02 | 3.50E+03 | 9.23E+03 |
| CO3 | 8.73E+01 | 4.28E+01 | 1.02E+02 | 6.66E+00 | 4.57E+01 | 8.35E+01 |
| PO4 | 5.02E-03 | 0.00E+00 | 0.00E+00 | 0.00E+00 | 0.00E+00 | 4.89E-02 |
| SO4 | 2.81E+02 | 1.95E+02 | 4.68E+02 | 3.04E+01 | 1.58E+02 | 3.46E+02 |
| Si (as SiO32-) | 1.94E+02 | 1.57E+02 | 3.76E+02 | 2.45E+01 | 9.66E+01 | 2.33E+02 |
| F | 8.00E-04 | 0.00E+00 | 0.00E+00 | 0.00E+00 | 0.00E+00 | 4.94E-02 |
| Cl | 4.57E+02 | 2.65E+02 | 6.33E+02 | 4.12E+01 | 2.89E+02 | 1.83E+02 |
| C6H5O7 | 8.22E-03 | 0.00E+00 | 0.00E+00 | 0.00E+00 | 0.00E+00 | 1.27E-01 |
| EDTA | 1.69E-06 | 0.00E+00 | 0.00E+00 | 0.00E+00 | 0.00E+00 | 7.32E-03 |
| HEDTA | 1.41E-06 | 0.00E+00 | 0.00E+00 | 0.00E+00 | 0.00E+00 | 5.75E-03 |
| glycolate | 6.14E-05 | 0.00E+00 | 0.00E+00 | 0.00E+00 | 0.00E+00 | 7.10E-02 |
| acetateE- | 6.37E-06 | 0.00E+00 | 0.00E+00 | 0.00E+00 | 0.00E+00 | 5.80E-03 |
| oxalate | 2.63E-12 | 0.00E+00 | 0.00E+00 | 0.00E+00 | 0.00E+00 | 3.58E-09 |

**Table C.6. Estimated Inventory Lost to Vadose Zone
in the S and SX Tank Farms (2 Sheets)**

| Chemical | Estimated S-104 Inventory Loss (kg) | Estimated SX-107 Inventory Loss (kg) | Estimated SX-108 Inventory Loss (kg) | Estimated SX-109 Inventory Loss (kg) | Estimated SX-113 Inventory Loss (kg) | Estimated SX-115 Inventory Loss (kg) |
|------------------|--|---|---|---|---|---|
| Leak Vol. | 24,000 gal^a | 63,500 gal^b | 15,200 gal^b | 989 gal^b | 15,000 gal^a | 50,000 gal^a |
| DBP | 3.86E-05 | 0.00E+00 | 0.00E+00 | 0.00E+00 | 0.00E+00 | 9.58E-02 |
| butanol | 3.86E-05 | 0.00E+00 | 0.00E+00 | 0.00E+00 | 0.00E+00 | 4.40E-02 |
| NH3 | 1.87E+00 | 3.96E+01 | 9.48E+01 | 6.17E+00 | 2.06E+01 | 4.21E+01 |
| Fe(CN)6 | 0.00E+00 | 0.00E+00 | 0.00E+00 | 0.00E+00 | 0.00E+00 | 0.00E+00 |

^aLeak volumes from Hanlon (2001).

^bLeak volumes estimated from Montana State University kriging analysis of gamma logging data (Goodman 2000).

**Table C.7. Estimated Inventory Lost to Vadose Zone
in the S and SX Tank Farms (Radionuclides) (2 Sheets)**

| Radionuclide | Estimated S-104 Inventory Loss Ci | Estimated SX-107 Inventory Loss Ci | Estimated SX-108 Inventory Loss Ci | Estimated SX-109 Inventory Loss Ci | Estimated SX-113 Inventory Loss Ci | Estimated SX-115 Inventory Loss Ci |
|---------------------|--|---|---|---|---|---|
| H-3 | 7.12E+00 | 1.34E+01 | 3.20E+01 | 2.08E+00 | 4.61E+00 | 1.43E+01 |
| C-14 | 5.53E-01 | 6.37E-01 | 1.52E+00 | 9.92E-02 | 3.57E-01 | 6.95E-01 |
| Ni-59 | 6.99E-02 | 7.46E-02 | 1.79E-01 | 1.16E-02 | 4.46E-02 | 8.38E-02 |
| Ni-63 | 6.53E+00 | 7.28E+00 | 1.74E+01 | 1.13E+00 | 4.17E+00 | 8.20E+00 |
| Co-60 | 2.21E-01 | 6.11E-01 | 1.46E+00 | 9.52E-02 | 1.41E-01 | 6.74E-01 |
| Se-79 | 1.17E-01 | 1.22E-01 | 2.92E-01 | 1.90E-02 | 7.58E-02 | 1.33E-01 |
| Sr-90 | 4.52E+03 | 2.69E+03 | 6.44E+03 | 4.19E+02 | 2.88E+03 | 3.38E+03 |
| Y-90 | 4.53E+03 | 2.69E+03 | 6.44E+03 | 4.19E+02 | 2.88E+03 | 3.38E+03 |
| Zr-93 | 5.54E-01 | 6.01E-01 | 1.44E+00 | 9.36E-02 | 3.58E-01 | 6.56E-01 |
| Nb-93m | 4.53E-01 | 4.37E-01 | 1.05E+00 | 6.80E-02 | 2.93E-01 | 4.77E-01 |
| Tc-99 | 3.87E+00 | 5.03E+00 | 1.21E+01 | 7.84E-01 | 2.50E+00 | 5.52E+00 |
| Ru-106 | 1.66E-06 | 1.51E-04 | 3.62E-04 | 2.36E-05 | 3.94E-07 | 1.68E-04 |
| Cd-113m | 1.71E+00 | 2.71E+00 | 6.50E+00 | 4.23E-01 | 1.10E+00 | 2.98E+00 |
| Sb-125 | 3.35E-01 | 2.23E+00 | 5.34E+00 | 3.48E-01 | 2.07E-01 | 2.48E+00 |
| Sn-126 | 1.80E-01 | 1.84E-01 | 4.40E-01 | 2.86E-02 | 1.16E-01 | 2.00E-01 |
| I-129 | 7.44E-03 | 9.53E-03 | 2.28E-02 | 1.48E-03 | 4.80E-03 | 1.04E-02 |
| Cs-134 | 6.32E-03 | 1.33E-01 | 3.19E-01 | 2.08E-02 | 3.56E-03 | 1.48E-01 |
| Cs-137 | 1.14E+04 | 1.71E+04 | 4.10E+04 | 2.67E+03 | 7.34E+03 | 1.88E+04 |
| Ba-137m | 1.08E+04 | 1.62E+04 | 3.87E+04 | 2.52E+03 | 6.94E+03 | 1.78E+04 |
| Sm-151 | 4.19E+02 | 4.28E+02 | 1.03E+03 | 6.67E+01 | 2.71E+02 | 4.68E+02 |
| Eu-152 | 4.14E-02 | 1.08E-01 | 2.59E-01 | 1.69E-02 | 2.65E-02 | 1.18E-01 |
| Eu-154 | 5.33E+00 | 1.49E+01 | 3.56E+01 | 2.32E+00 | 3.41E+00 | 1.64E+01 |
| Eu-155 | 1.96E+00 | 5.49E+00 | 1.31E+01 | 8.55E-01 | 1.25E+00 | 6.00E+00 |
| Ra-226 | 8.15E-06 | 4.90E-06 | 1.17E-05 | 7.64E-07 | 5.24E-06 | 5.50E-06 |
| Ra-228 | 1.88E-07 | 1.85E-10 | 4.44E-10 | 2.89E-11 | 3.51E-11 | 2.90E-06 |
| Ac-227 | 4.72E-05 | 2.85E-05 | 6.81E-05 | 4.43E-06 | 3.04E-05 | 3.15E-05 |
| Pa-231 | 1.75E-04 | 1.36E-04 | 3.26E-04 | 2.12E-05 | 1.13E-04 | 1.47E-04 |
| Th-229 | 1.49E-08 | 1.32E-08 | 3.16E-08 | 2.05E-09 | 6.70E-09 | 8.36E-08 |
| Th-232 | 2.52E-08 | 5.24E-10 | 1.25E-09 | 8.16E-11 | 9.32E-11 | 3.87E-07 |
| U-232 | 3.83E-06 | 1.42E-06 | 3.41E-06 | 2.22E-07 | 8.26E-07 | 3.44E-05 |
| U-233 | 7.37E-06 | 3.78E-08 | 9.05E-08 | 5.89E-09 | 3.15E-08 | 1.13E-04 |
| U-234 | 4.09E-02 | 1.85E-02 | 4.43E-02 | 2.88E-03 | 1.88E-02 | 7.25E-02 |
| U-235 | 1.73E-03 | 7.37E-04 | 1.77E-03 | 1.15E-04 | 8.09E-04 | 2.80E-03 |
| U-236 | 9.69E-04 | 8.69E-04 | 2.08E-03 | 1.35E-04 | 2.97E-04 | 4.29E-03 |

**Table C.7. Estimated Inventory Lost to Vadose Zone
in the S and SX Tank Farms (Radionuclides) (2 Sheets)**

| Radionuclide | Estimated S-104 Inventory Loss Ci | Estimated SX-107 Inventory Loss Ci | Estimated SX-108 Inventory Loss Ci | Estimated SX-109 Inventory Loss Ci | Estimated SX-113 Inventory Loss Ci | Estimated SX-115 Inventory Loss Ci |
|---------------------|--|---|---|---|---|---|
| U-238 | 3.96E-02 | 1.53E-02 | 3.66E-02 | 2.38E-03 | 1.92E-02 | 5.36E-02 |
| Np-237 | 2.52E-02 | 2.08E-02 | 4.97E-02 | 3.24E-03 | 1.62E-02 | 2.39E-02 |
| Pu-238 | 2.27E-02 | 2.49E-02 | 5.96E-02 | 3.87E-03 | 1.05E-02 | 6.21E-02 |
| Pu-239 | 1.43E+00 | 6.95E-01 | 1.66E+00 | 1.08E-01 | 7.48E-01 | 1.76E+00 |
| Pu-240 | 2.07E-01 | 1.20E-01 | 2.87E-01 | 1.86E-02 | 1.07E-01 | 2.95E-01 |
| Pu-241 | 1.28E+00 | 1.24E+00 | 2.98E+00 | 1.94E-01 | 6.30E-01 | 2.79E+00 |
| Pu-242 | 5.49E-06 | 6.85E-06 | 1.64E-05 | 1.07E-06 | 2.89E-06 | 1.12E-05 |
| Am-241 | 1.98E+00 | 1.88E+00 | 4.50E+00 | 2.93E-01 | 1.28E+00 | 2.08E+00 |
| Am-243 | 1.85E-05 | 6.70E-05 | 1.60E-04 | 1.04E-05 | 1.19E-05 | 7.16E-05 |
| Cm-242 | 9.43E-04 | 4.87E-03 | 1.17E-02 | 7.59E-04 | 6.11E-04 | 5.09E-03 |
| Cm-243 | 2.16E-05 | 4.75E-04 | 1.14E-03 | 7.39E-05 | 1.40E-05 | 4.94E-04 |
| Cm-244 | 6.59E-04 | 4.78E-03 | 1.14E-02 | 7.44E-04 | 4.27E-04 | 4.98E-03 |

C.3.5 SPECIATION ANALYSIS

Significant quantities of high-level waste (HLW) were lost to the soil column from large underground tanks in WMA S-SX during long-term storage of the wastes produced in the Reduction-Oxidation (REDOX) Plant. An understanding of the mechanisms of soil/waste reactions controlling the movement of tank waste through the vadose zone requires knowledge of waste components on a molecular level. However, this level of tank waste chemistry is generally not available since this level of understanding was not required for the original plant operations or for long-term storage and waste management. *REDOX Technical Manual* (GE 1951) and the updated flowsheets from *Standard Inventories of Chemicals and Radionuclides in Hanford Site Tank Wastes* (Kupfer et al. 1998) provide clear guidance as to the conditions required for successful operations of separations process but only limited understanding of the underlying fundamental chemistry. Thus, the most practical approach for developing an understanding of the chemical species present in leaked tank waste comes from a chemical equilibria-based computer model that develops speciation of bulk waste components.

Chemical thermodynamic-based models of aqueous systems can be applied to predict reaction products if the controlling thermodynamic parameters are sufficiently well understood. However, the tank waste mixtures are extremely complex and many of the required thermodynamic parameters are only poorly understood. Any thermodynamic-based modeling exercise involving a tank waste matrix requires many approximations and assumptions. Thus, speciation modeling results must be treated with considerable caution.

The initiative was to conduct preliminary scoping studies using the Environmental Simulation Program (ESP), a thermodynamic-based chemical process simulator that has been widely applied at the Hanford Site (MacLean and Eager 1998). ESP is currently used to simulate transfers, mixing, and treatment of tank wastes for both the waste feed delivery project and vitrification pretreatment. It has been used to simulate processing of plutonium solutions, the clean salt waste treatment process, sluicing of tank wastes, and other nuclear-waste related processing.

The ESP is designed to model the processing of complex, concentrated aqueous solutions, organic liquids, solids, and vapors. It uses sophisticated thermodynamic models to predict the activity coefficients and equilibrium constants of most species and equilibrium relationships that can exist in tank wastes, or during processing of plant wastes. It can be used to calculate the equilibrium or time dependent composition of mixtures of solids, liquids, and gases.

The ESP calculates the thermodynamic equilibrium of all phases by minimizing the chemical potential of a system in an iterative process (Stern et al. 1997). The equilibrium constants for aqueous and solid species are calculated using the Helgeson-Kirkham-Flowers Equation of State (Stern et al. 1997), thermodynamic properties, or temperature and pressure dependent correlations of experimental data. Activity coefficients, partial molar densities, and other properties of aqueous species are calculated using the Bromley-Zemaitis or Pitzer excess property models (Stern et al. 1997).

ESP comes with several databanks covering most of the elements and compounds found or expected in Hanford Site tank wastes (Stern et al. 1996). These are supplemented with custom databanks that have been prepared specifically for simulating the processing of tank wastes.

Special databanks combined with associated chemistry models are used for almost all waste-related simulations.

As discussed in Section C.3.1, the compositions of the wastes in SSTs at the time of suspected leaks were developed using the HDW model (Agnew 1997). The HDW model provides supernatant compositions that were combined with leak volumes to project leak inventory estimates (Jones et al. 2000a). The tank waste supernatant compositions were then used as input to the ESP model with the goal of developing a better understanding of chemical speciation of the wastes at the time of suspected leaks. One of the weak points of the HDW model is its inability to reliably predict acid/base parameters such as pH or free hydroxide ion concentrations. However, the historical records (GE 1951; Harmon 1949; Barney 1976) clearly show that it was well known that the solution chemistry of REDOX HLW was dominated by the aluminum ion solubility and the aluminum solubility was controlled by the free hydroxide ion concentration. The selection of the free hydroxide concentration will dictate the thermodynamic modeling results for the REDOX HLW systems. Thus, much of the speciation modeling work discussed here focused on developing a better understanding of aluminum ion chemistry in the REDOX waste matrix. Such an understanding is potentially important in geochemical processes impacting tank waste movement in the subsurface.

The speciation calculation results reported in Jones et al. (2000a) use the tank waste compositions predicted by the HDW model at the times of the leaks for tanks S-104, SX-108, and SX-115. The previously reported results are supplemented here with additional modeling runs addressing the free hydroxide issue. These results are compared with results from Litchner et al. (2001). Corrections to errors in technetium-99 speciation estimates in Jones et al. (2000a) are also discussed briefly.

C.3.5.1 Aluminum Solubility in Reduction-Oxidation Wastes

One of the major characteristics of the REDOX HLW was the very high aluminum ion concentrations found in this waste stream (GE 1951). Aluminum ion solubility is closely coupled with the ‘free’ hydroxide ion concentration. An understanding of the aluminum ion chemistry in the REDOX HLW matrix is required in order to develop reasonable leak inventory estimates and address questions about waste-soil chemical reactions.

Aluminum nitrate was used as a ‘salting out’ agent in the REDOX liquid-liquid exchange columns to facilitate transfer of uranium and plutonium from the aqueous to organic phase. The high aluminum ion levels in the waste streams led to the development of carefully controlled processes for concentrating and neutralizing the HLW stream prior to being discharged to the SSTs (GE 1951). Considerable care was taken to avoid the precipitation of aluminum oxides during the concentration and neutralization processes because the formation of aluminum oxide solids in the waste stream led to problems in pumping the wastes. Since the long-term HLW management goals (Tomlinson 1963) required many waste transfers between tanks and processing facilities prior to final solidification, it is reasonable to assume that the free hydroxide concentration in the REDOX HLW streams would have been maintained at high enough levels to maintain essentially all of the aluminum ions in the solution phase (Barney 1975). However, there are inconsistencies in the historical records.

GE (1951) states that it was necessary to neutralize the HLW stream to a pH 13 to obtain a 'nearly clear liquid.' However, the manual also states that 25% to 30% excess caustic was required to reach that pH. Because the aluminum neutralization involved the reaction of 1 mole of aluminum with 4 moles of hydroxide to form sodium aluminate ($\text{NaAl}(\text{OH})_4$), a 25% to 30% excess caustic leads to 1 to 1.2 moles excess hydroxide being added per mole aluminum, during the neutralization process. Because the total aluminum concentration in the neutralized waste stream was approximately 1.2 moles, one would expect the free hydroxide concentration to be as high as 1.2 to 1.4 moles. However, some of the excess hydroxide would be neutralized by the excess nitric acid (1.2%), dichromate, iron, and uranium. Nevertheless, the excess hydroxide concentration in the waste stream going to the SSTs, would likely have been around 1 mole. The free hydroxide concentration would, of course, increase as the wastes were concentrated by self-evaporation in the tanks. REDOX boiling wastes were concentrated by a factor of approximately two until the beginning of 1963. After that point it appears the REDOX wastes were concentrated by a factor of closer to three in tanks SX-107, SX-108, and SX-109.

The arbitrary selection of 0.1 mole hydroxide for the preliminary speciation calculations reported in Jones et al. (2000a) was based on statements in GE (1951). However, the statement in GE (1951) that the waste was neutralized to pH 13 probably has little relationship to the hydrogen ion (or hydroxide ion) concentration in the waste. It is likely the pH 13 simply reflected an operations parameter that, in reality, only reflects the potential developed between a glass electrode and the reference electrode (likely to have been a calomel electrode). In a well-controlled laboratory environment, pH measurements can be converted to hydrogen ion activity (and concentration) in relatively simple systems. However, such a conversion is likely impossible in the REDOX waste matrix. Glass pH electrodes are, by design, highly selective for hydrogen ions but many also respond to sodium ion activity. Above pH 10, this 'sodium ion error' can become quite significant. There are also issues associated with the liquid junction potentials in the reference electrode. Finally, pH measurements are meaningful only if matrix-matched standards are available to calibrate the pH measurement system. Little is known about the pH monitoring systems or their operations in the REDOX Plant. Analysis of the REDOX process flowsheets leads to the conclusion that the hydroxide was at least an order of magnitude higher than the value used in Jones et al. (2000a).

The initial ESP speciation modeling of REDOX HLW, reported in Jones et al. (2000a), assumed a 0.1 mole free hydroxide concentration resulting in essentially all of the aluminum residing in the solid phase as aluminum hydroxide. Because of the uncertainty about the correct hydroxide concentration in the REDOX HLW, a sensitivity study was completed using the ESP model to assess the aluminum ion solubility in the waste matrix over a range of free hydroxide concentrations. The projected aluminum solubility data at 50 and 100 °C (122 and 212 °F) are shown in Figures C.10 and C.11. The aluminum solubility increases with increasing hydroxide reaching a maximum at 1 mole at 100 °C (212 °F) and 2 moles at 50 °C (122 °F), with essentially all of the aluminum in solution, as aluminum hydroxide. GE (1951) states that acidic REDOX HLW was cooled to slightly less than 50 °C (122 °F) prior to neutralization with 50% caustic. It is also stated that the wastes were neutralized to a 'near-clear' solution. Statements from GE (1951) coupled with aluminum solubility modeling results would suggest that the wastes contained in excess of 1 mol/L free hydroxide. Thus, it is almost certain that the HLW leaving the REDOX Plant would have contained in excess of 1 mol/L free hydroxide. The modeling results show the solubility to increase at higher temperatures therefore it is likely that essentially all

aluminum ions remained in the solution phase during the boiling phase of the REDOX waste processing in the SX tank farm. This suggests that leaked tank wastes would have contained high levels of both aluminum ions and free hydroxide. This conclusion is supported by speciation calculations reported in Litchner (2001). The Litchner (2001) results are briefly described in Section C.3.5.2.

Figure C.10. Solubility of Aluminum in Tank SX-108 Waste at 100 °C (212 °F)

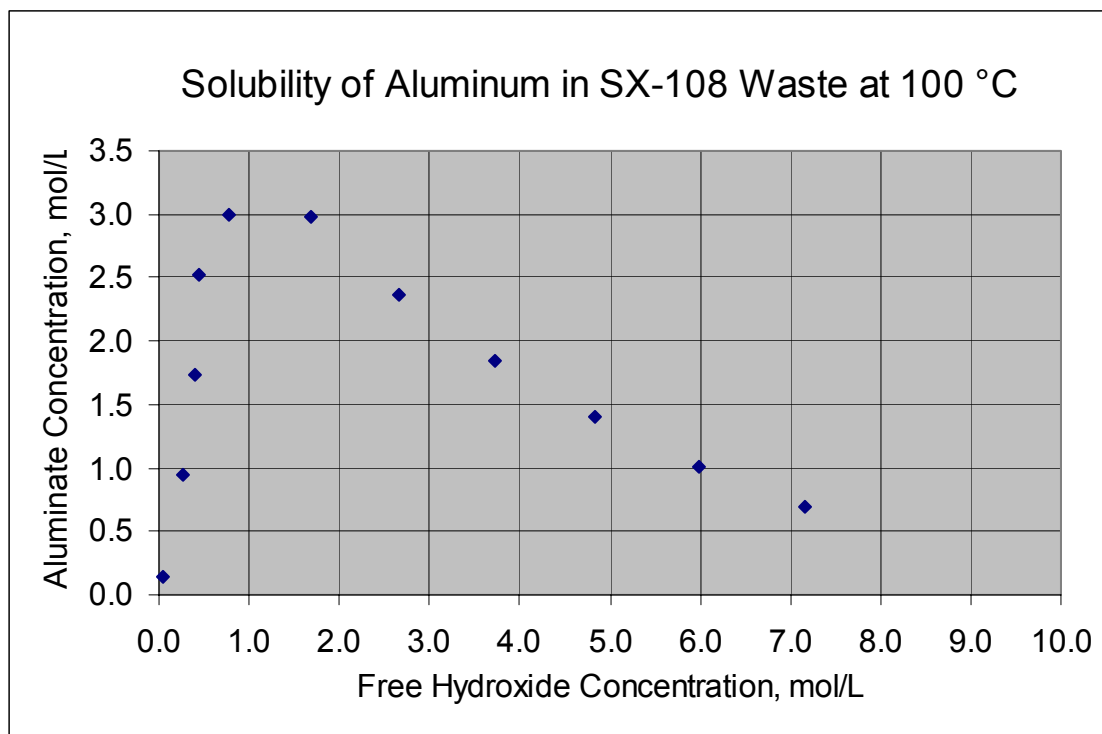
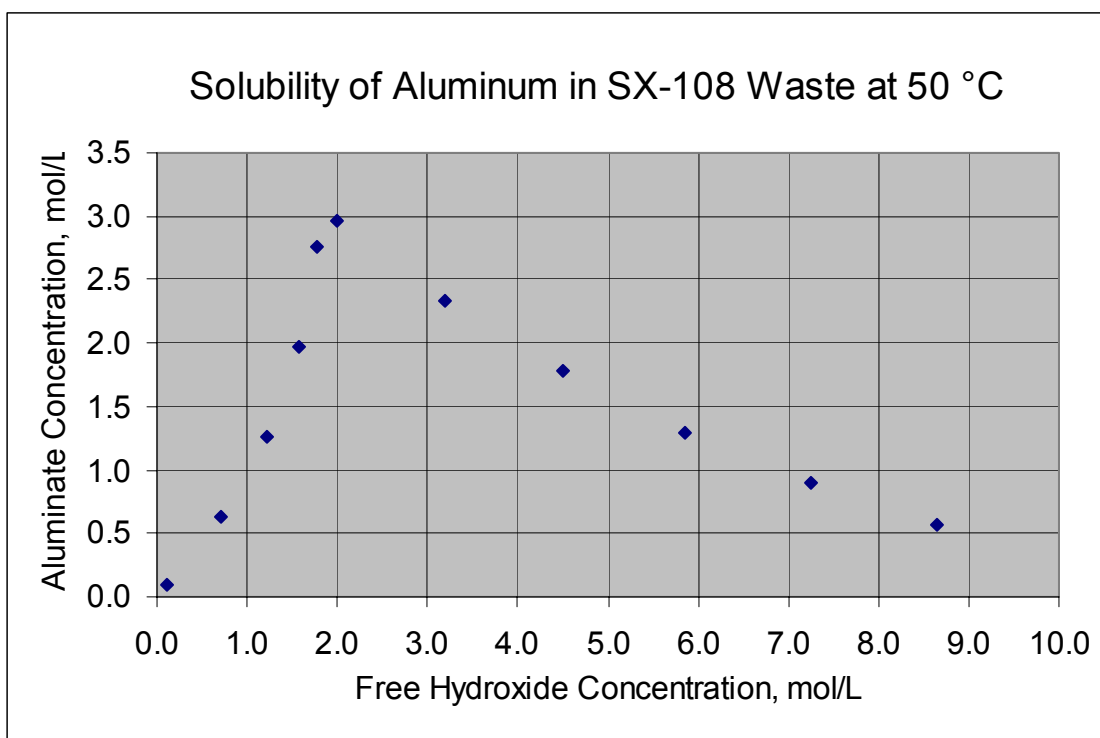


Figure C.11. Solubility of Aluminum in Tank SX-108 Waste at 50 °C (122 °F)

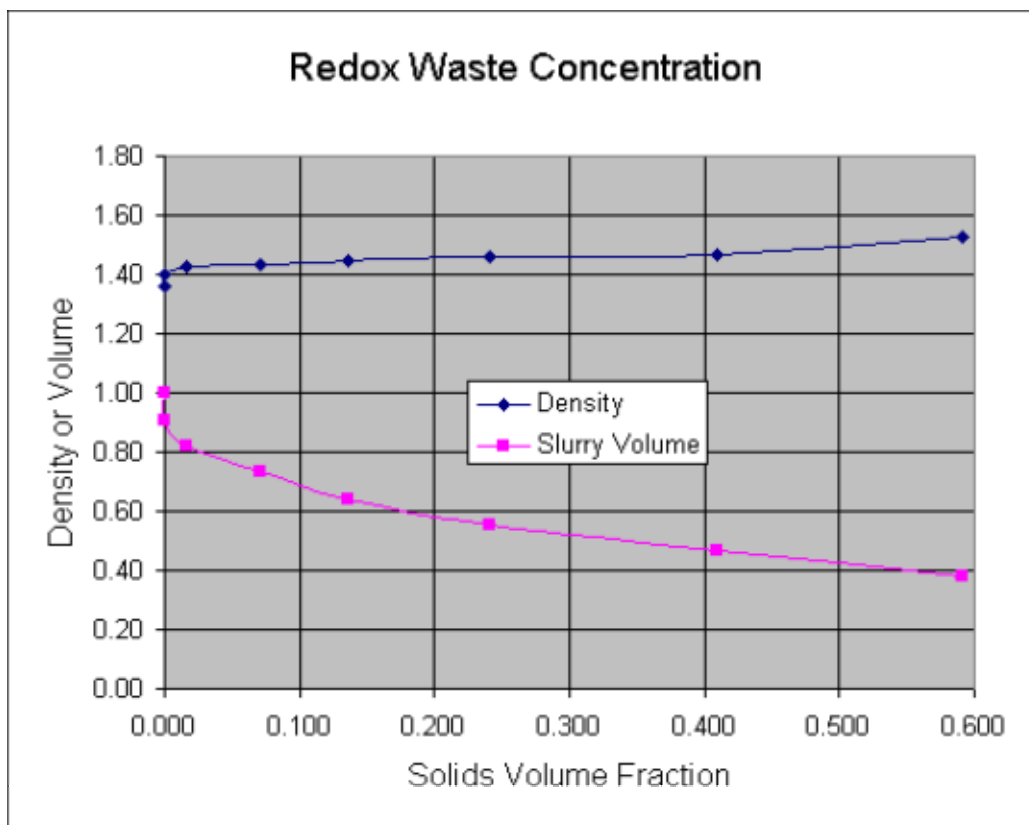
The second speciation modeling run evaluated the changes in solution composition as water was removed from the system. A REDOX HLW waste composition containing only major components was taken from GE (1951). Maximum aluminum ion solubility required 2.60 mol/L free hydroxide. The results shown in Tables C.8 and C.9 indicate the sodium nitrate is the first solid that precipitates from solution as water is removed. The aluminum ion solubility is not exceeded until approximately 45 % of the water is removed. These results are consistent with evaporator operations while removing water from high aluminum wastes (Barney 1975). Results are shown graphically in Figure C.12.

**Table C.8. REDOX High-Level Waste Components
During Volume Reduction (with Constant OH⁻)**

| REDOX High-Level Waste (50 °C) – moles | | | | | | | | Liq. Vol. |
|--|----------------------------------|--------------------|------------------------------|----------------------|--------------------------|-------------------|------------|-----------|
| OH ⁻ | Al(OH) ₄ ⁻ | NaAlO ₂ | NO ₃ ⁻ | NaNO ₃ aq | Total NO ₃ aq | NaNO ₃ | Liq. Dens. | |
| 2.60 | 1.40 | 0.00 | 2.02 | 2.21 | 4.23 | 0.00 | 1.36 | 1.00 |
| 2.60 | 1.40 | 0.00 | 1.79 | 2.44 | 4.23 | 0.00 | 1.40 | 0.91 |
| 2.60 | 1.40 | 0.00 | 1.42 | 2.48 | 3.90 | 0.33 | 1.43 | 0.82 |
| 2.60 | 1.40 | 0.00 | 0.87 | 1.99 | 2.86 | 1.37 | 1.43 | 0.73 |
| 2.60 | 1.40 | 0.00 | 0.41 | 1.50 | 1.91 | 2.32 | 1.45 | 0.64 |
| 2.60 | 1.05 | 0.36 | 0.14 | 1.05 | 1.19 | 3.04 | 1.46 | 0.56 |
| 2.60 | 0.37 | 1.03 | 0.03 | 0.63 | 0.66 | 3.57 | 1.47 | 0.47 |
| 2.60 | 0.05 | 1.36 | 0.00 | 0.23 | 0.23 | 4.00 | 1.53 | 0.38 |

Table C.9. REDOX High-Level Waste Components Assuming Water Removal Only

| moles/liter | | | | | Liq. Vol. | Solid Vol. | Solid Vol. Frac. |
|-------------|-----------------------|--------------------|-------------------|----------------------|-----------|------------|------------------|
| OH- | Al(OH) ₄ - | NaAlO ₂ | NO ₃ - | NaNO ₃ aq | | | |
| 2.60 | 1.40 | 2.02 | 2.22 | 4.23 | 1.00 | 0.000 | 0.000 |
| 2.86 | 1.54 | 1.96 | 2.68 | 4.65 | 0.91 | 0.000 | 0.000 |
| 3.22 | 1.73 | 1.75 | 3.07 | 4.82 | 0.81 | 0.013 | 0.016 |
| 3.82 | 2.06 | 1.29 | 2.92 | 4.21 | 0.68 | 0.052 | 0.071 |
| 4.68 | 2.52 | 0.73 | 2.70 | 3.43 | 0.56 | 0.088 | 0.137 |
| 6.18 | 2.48 | 0.34 | 2.48 | 2.82 | 0.42 | 0.134 | 0.241 |
| 9.43 | 1.34 | 0.12 | 2.28 | 2.40 | 0.28 | 0.191 | 0.409 |
| 16.60 | 0.29 | 0.00 | 1.48 | 1.48 | 0.16 | 0.226 | 0.591 |

Figure C.12. REDOX Waste Chemistry During Water Removal

C.3.5.2 Los Alamos National Laboratory Speciation Results for Tank SX-108

The results reported in Litchner (2001) represent a far more detailed solution thermodynamic investigation than the results reported in Jones et al. (2000a). Litchner (2001) uses the Pitzer-based formulation for calculation activity coefficients. This approach is more consistent with contemporary geochemical modeling studies.

Any assessment of the soil-waste reactivity requires reasonable estimates of the chemical species present in the tank waste at the time of the leak. Litchner (2001) begins with estimated tank waste compositions reported in Jones et al. (2000a). The initial step in any speciation modeling exercise is the development a charge balance for the system. Jones et al. (2000a) fixes the hydroxide at 0.1 mole and allows the sodium ion to vary until the overall charge balance is reached, leading to sodium ion concentration near 12 moles. Litchner (2001) chooses to maintain the sodium ion concentration developed by the HDW model and allows hydroxide to be varied until a charge balance is reached. At equilibrium in tank SX-108 at 100 °C (212 °F), Litchner (2001) predicts the hydroxide to be 5.1 moles and a pH of 14.1 with essentially all of the aluminum to be in solution as aluminum hydroxide. The Litchner (2001) speciation results are consistent with the conditions one would predict from process flowsheet data. Thus, these results are the preferred data set for geochemical modeling studies.

C.3.5.3 Technetium-99 Speciation

Technetium-99 has been identified as the major radioisotope of concern in recent risk evaluations at the Hanford Site. Based on theoretical calculations and Hanford Site reactor production records, it is believed that approximately 33,000 Ci of technetium-99 were produced at Hanford and processed through the various plutonium recovery processes (Kupfer et al. 1998). Currently, the fate of this technetium-99 is unclear. Although it is assumed in Kupfer et al. (1998) that for tank inventory estimates all of the technetium-99 produced in the plutonium-production reactors is currently stored in the 177 HLW tanks at the Hanford Site, it is widely understood that some fraction of the technetium-99 was shipped offsite as an impurity in the recovered uranium (Roberts et al. 1962), lost during intentional discharges of tank wastes to the soil column in the 1950s (Waite 1991; Corbin et al. 2001), and lost during various tank waste leak events. In addition to the uncertainty about the quantities and location of technetium-99 within the Hanford HLW tanks, there is considerable uncertainty about the chemical species of technetium-99 in individual tanks (Kovach et al. 1999). Thus, the preliminary speciation modeling results suggesting that major fractions of the technetium-99 could reside in the solid phase as potassium pertechnetate (KTcO_4) in highly concentrated REDOX HLW (Jones et al. 2000a) were of considerable interest.

Initial modeling runs indicated that the majority of technetium-99 in wastes in tank SX-108 was incorporated into the solid phase as potassium pertechnetate but in the more dilute tank SX-115 wastes the technetium-99 remained in the solution phase (Jones et al. 2000a). The implication was that technetium-99 was being 'salted out' of solution because of extremely high salt concentrations of these supernates. If the technetium-99 were predominately in the solid phase then the quantity of technetium-99 lost during a leak event would be reduced, as would the long-term risk. The possibility of technetium-99 being salted out of solution because of high ionic strengths could have had significant impacts on other tank waste related activities such as

waste retrieval and vitrification operations. Thus, the technetium-99 modeling results were critically reviewed.

A detailed review of the supporting information reported along with the speciation modeling results indicated that the potassium pertechnetate solubility was being driven by an unrealistically large activity coefficient term. Resolution of this issue was referred back to OLI Systems¹, the software vendor, for resolution. The vendor reported that a programming error was found in the code. Basically, the silicate ion activity was being summed with pertechnetate activity leading to errors in solubility estimates. After correcting this programming error, the model predicted that all technetium-99 remained in the solution phase in each SX farm tank waste composition. Although, to date, no technetium-99 analysis data have been found for REDOX HLW, the suggestion that technetium-99 tends to remain in the solution phase is consistent with experimental data for plutonium-uranium extraction HLW (Godfrey 1971).

¹ OLI Systems, Inc., Morris Plains, New Jersey.

C.4.0 GEOLOGY

This section presents a general discussion on the vadose zone geology in the vicinity of the SX tank farm.

C.4.1 REGIONAL GEOLOGIC SETTING

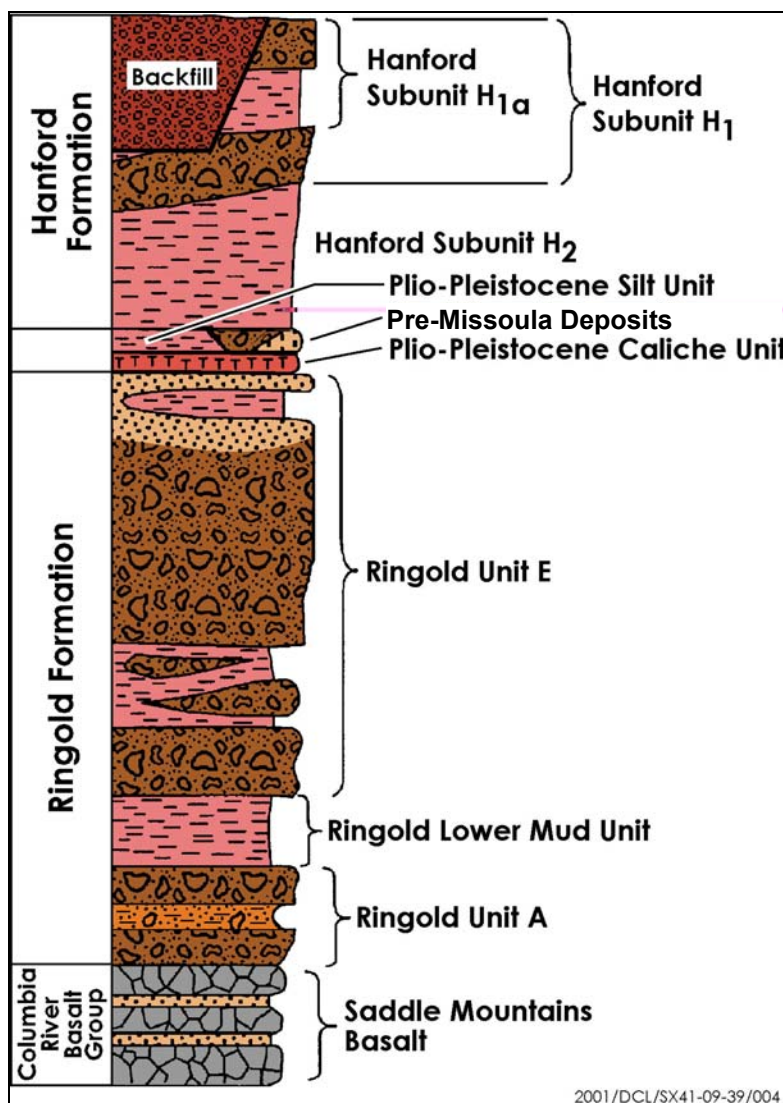
The Hanford Site is located within the Columbia Plateau of southeastern Washington State. This broad plain, situated between the Cascade Mountains to the west and the Rocky Mountains to the east, is underlain by a thick sequence of Miocene age tholeiitic basalt flows (the Columbia River Basalt Group). These basalt flows have been folded and faulted, creating broad structural and topographic basins, separated by asymmetric anticlinal ridges. Sediments of late Miocene, Pliocene, and Pleistocene age have accumulated up to 518 m (1,700 ft) thick in some of these basins. The Hanford Site lies within one of the larger of these basins, the Pasco Basin. This basin is partially bisected by the Umtanum-Gable Mountain anticline creating two subordinate synclinal basins. The largest of these is the Cold Creek syncline, which is further subdivided into two basins, the Wye Barricade depression and the Cold Creek depression. The Cold Creek depression underlies the principal WMAs of the Hanford Site, the 200 East and 200 West Areas.

The generalized stratigraphy beneath the Hanford Site consists of, in ascending order, the Columbia River Basalt Group, the Ringold Formation, the Plio-Pleistocene unit, and the Hanford formation (Figure C.13). Thin veneers of Holocene alluvium, colluvium, and/or eolian sediments discontinuously overlie these principal geologic units. More thorough descriptions of the regional geology, including the saturated zone of this area, are found in *Geology of the Separations Areas, Hanford Site, South-Central Washington* (Tallman et al. 1979), *Consultation Draft Site Characterization Plan* (DOE 1988); *200 West Groundwater Aggregate Area Management Study Report* (DOE-RL 1993); and “Geohydrologic Setting of the Hanford Site, South-Central Washington” (Lindsey et al. 1994).

C.4.2 GEOLOGY OF THE S AND SX TANK FARMS

The S and SX tank farms were constructed into the upper Hanford formation sediments underlying 200 West Area, along the north limb of the Cold Creek syncline. Stratigraphic units underlying or adjacent to the tank farms (in descending order) include backfill materials, lower Hanford formation sediments, the Plio-Pleistocene unit, and the Miocene- to Pliocene-age Ringold Formation.

Figure C.13. Generalized, Composite Stratigraphy for the Late Cenozoic Sediments Overlying the Columbia River Basalt Group on the Hanford Site

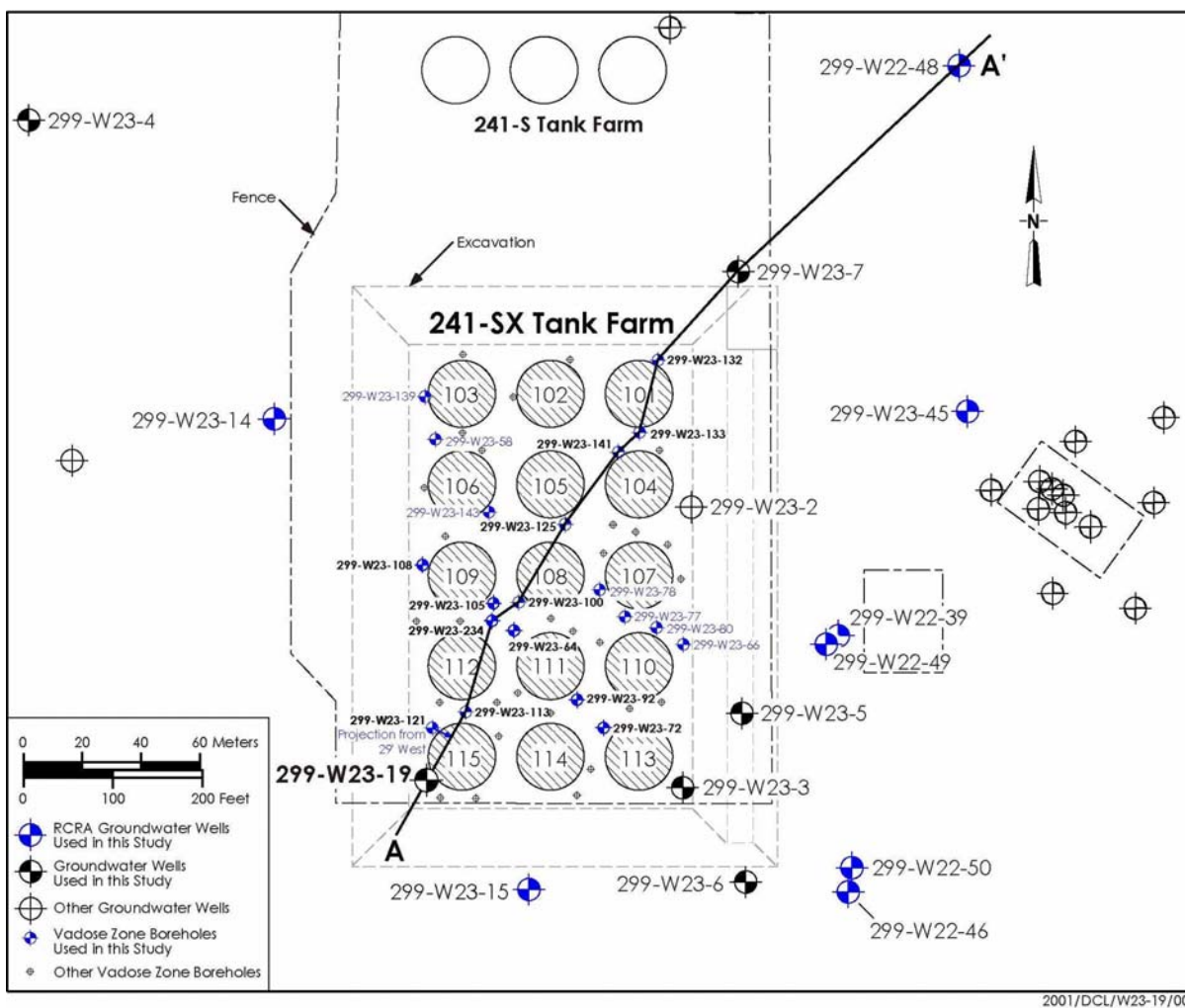


Sources: Johnson and Chou (1998); Johnson and Chou (1999).

The geology beneath the S and SX tank farms has been the subject of numerous reports. *Geology of the 241-SX Tank Farm* (Price and Fecht 1976a) presents an initial detailed interpretation of the geology. *Vadose Zone Characterization Project at the Hanford Tank Farms* (DOE 1996) presents an interpretation of the geology that is based primarily on groundwater monitoring wells constructed around the perimeter of the tank farm in the early 1990s. *Results of Phase I Groundwater Quality Assessment for Single-Shell Tank Waste Management Areas S-SX at the Hanford Site* (Johnson and Chou 1998) updates and refines the geologic interpretation. *Findings of the Extension of Borehole 41-09-39, 241-SX Tank Farm* (Myers et al. 1998) and *Geologic and Geochemical Data Collected from Vadose Zone Sediments from Borehole SX 41-09-39 in the S/SX Waste Management Area and Preliminary Interpretations* (Serne et al. 2001b) present detailed discussions on the geologic materials penetrated by the extension of borehole 41-09-39 (299-W23-234). *Subsurface Conditions Description for the S-SX Waste Management Area* (Johnson et al. 1999) further describes the geology and other subsurface contaminants. *Vadose Zone Geology of Boreholes 299-W22-50 and 299-W23-19 S-SX Waste Management Area Hanford Site, South-Central Washington* (Lindsey et al. 2000) provides additional interpretations on the geology, facilitated by the collection of near continuous split-spoon samples from boreholes 299-W22-50 and 299-W23-19. Geochemical analyses on vadose zone samples collected from borehole 299-W23-19, drilled through a contaminated zone immediately adjacent to SST SX-115, is the focus of this report (Figure C.14).

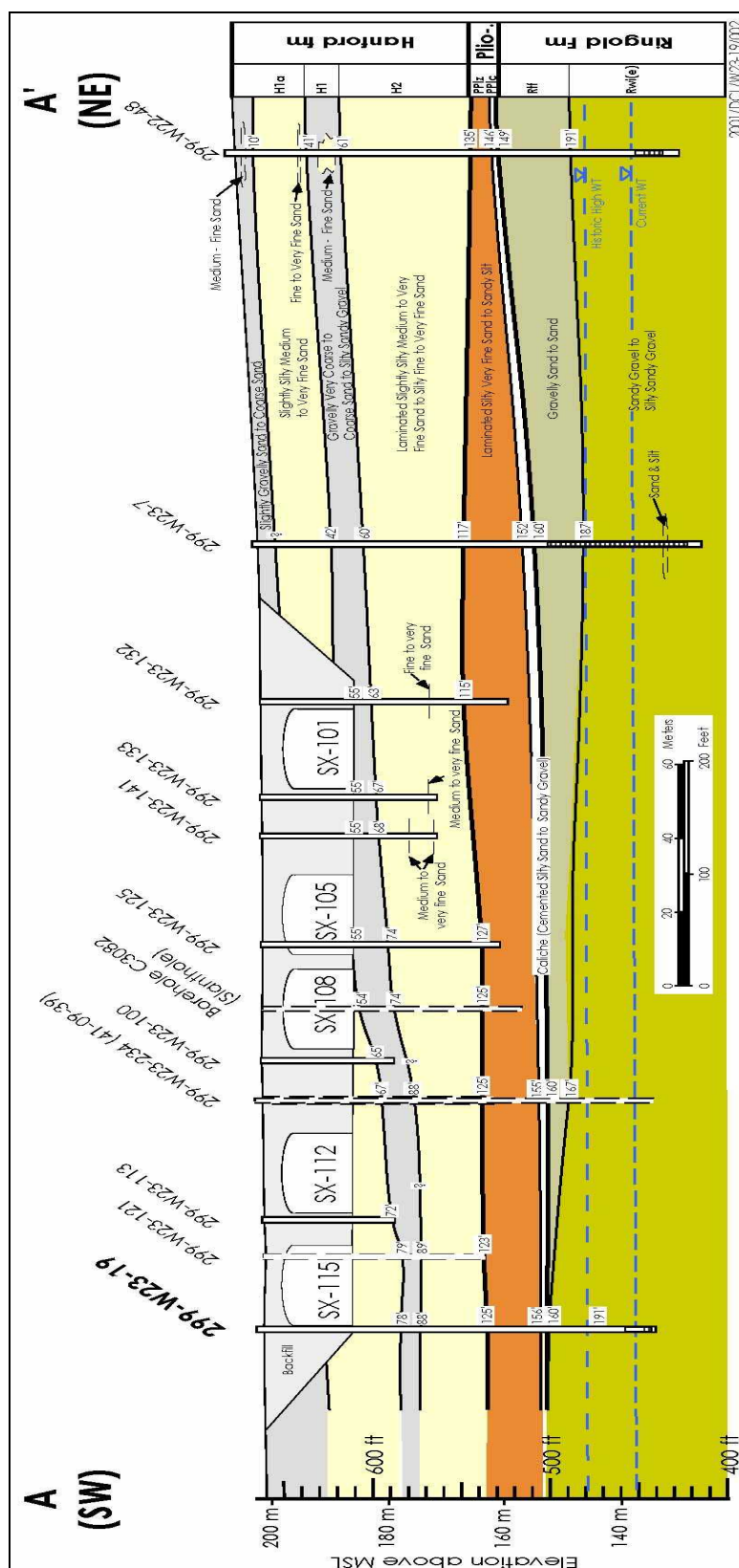
Borehole Data Package for Wells 299-W22-48, 299-W22-49, and 299-W22-50 at Single Shell Tank Waste Management Areas S-SX at the Hanford Site (Horton and Johnson 2000) contains a compilation of data packages on three groundwater monitoring wells (299-W22-48, 299-W22-49, and 299-W22-50) completed near the SX tank farm in 1999 and 2000. Most recently, *Subsurface Interpretation of the SX Tank Farm, Hanford Site, Washington Based on Gamma-Ray Logging* (Sobczyk 2000) presents a reinterpretation on the geology based on gross gamma-ray logs of 98 boreholes within the SX tank farm and the most recently published geology reports of the area (Johnson et al. 1999; Lindsey et al. 2000). Lastly, *Modeling Data Package for S-SX Field Investigation Report* (Khaleel et al. 2000) contains a detailed data package to support numerical simulation of the S and SX tank farms.

A hydrogeologic cross-section, constructed from a series of densely spaced boreholes beneath the SX tank farm is presented in Figure C.15. Some slight discrepancies may occur between the depths of the geologic contacts presented in this appendix and those presented in other documents, due to the various source of uncertainty in the geologic data sets and an individual geologist's interpretation. Johnson et al. (1999) describes the various sources of uncertainty for locating the stratigraphic contacts within a borehole as well as those uncertainties for drawing correlations between boreholes. That document identifies the principal sources of uncertainty as related to the drilling and sampling techniques, logging of the boreholes, and uncertainties in the geometric shape of the sedimentary units. Two different geostatistical techniques are used in Johnson et al. (1999) to evaluate the stratigraphy/depth uncertainty and finds that both techniques indicate that the stratigraphy beneath the S and SX tank farms is relatively consistent across the area. The optimal depths for stratigraphic correlations between different data sets were also found to be typically accurate to within 0.6 to 3 m (2 ft to 10 ft).

Figure C.14. SX Tank Farm and Vicinity Showing Location of Borehole 299-W23-19

Note: Location of cross-section A-A', represented in Figure C.15.

Figure C.15. Hydrogeologic Cross-Section of the Vadose Zone Beneath the SX Tank Farm



The stratigraphic terminology used in this report is summarized in Table C.10. The general stratigraphic interpretation presented here differs somewhat from that presented in Lindsey et al. (2000). The coarse (gravelly) materials found near the middle of the Hanford formation (correlative with Hanford H1 unit in Lindsey et al. [2000]) are interpreted to correlate across the tank farm and to represent a laterally continuous coarse unit distinct from the overlying and underlying finer sand units. Lindsey et al. (2000) suggests that these coarser materials are not continuous but rather represent thin, lenticular, discontinuous gravelly beds within stratified sand sheets of the Hanford formation. These differences are in interpretation only.

C.4.2.1 Columbia River Basalt Group

The Columbia River Basalt Group (composed of approximately 50 basalt flows) is more than 3,000 m (10,000 ft) thick and forms the bedrock beneath the Hanford Site. Sedimentary interbeds are sandwiched between the basalt flows, particularly in the uppermost Saddle Mountains Basalt. These interbeds, along with the porous basalt flow tops and flow bottoms, form confined aquifers that extend across the Pasco Basin (Reidel 1997).

The surface of the Columbia River Basalt Group lies at an elevation of approximately 26 m (85 ft) above mean sea level beneath the S and SX tank farms (a depth of approximately 175 m [575 ft] and dips gently to the southwest towards the axis of the Cold Creek syncline (Price and Fecht 1976a; DOE-RL 1993).

C.4.2.2 Ringold Formation

The Ringold Formation lies directly on top of the Columbia River Basalt Group and is approximately 125 m (410 ft) thick beneath the S and SX tank farms. The group locally consists of three principal stratigraphic units: (1) the fluvial gravels of unit A, (2) a fine-grained, paleosol-lacustrine sequence referred to as the lower mud unit, and (3) fluvial gravels of unit E (Figure C.13). The Ringold unit E gravels, depicted as Rwi(e) on Table C.10, are interpreted as equivalent to the Ringold Member of Wooded Island exposed along the White Bluffs, located along the eastern margin of the Hanford Site (Lindsey 1996). Ringold unit E grades upwards into fluvial sands of the upper Ringold unit (DOE-RL 1993), interpreted as an equivalent to the Ringold member of Taylor Flat (Rtf on Table C.10). Ringold unit E forms the main unconfined aquifer beneath the 200 West Area.

DOE-RL (1993) shows that the thickness of fluvial Ringold unit A is approximately 30 m (100 ft). Tallman et al. (1979) describes this unit as a silty-sandy gravel that is composed predominantly of gravel supported by a coarse-to-fine sand matrix with intercalated, lenticular beds of sand and silt.

The thickness of the lower mud unit is approximately 12 to 30 m (40 to 100 ft) (Tallman et al. 1979; DOE-RL 1993). This unit consists of predominantly mud (i.e., silt and clay); the lower portion contains well-developed argillic to calcic paleosol sequence (DOE 1988). The high clay content (up to 43% by weight) and the low hydraulic conductivity (perhaps as low as 10^{-12} ft/day) of this sequence acts to locally confine groundwater within unit A and form a base for the uppermost unconfined aquifer (Last et al. 1989).

**Table C.10. Stratigraphic Terminology Used in this Report
for the Vadose Zone Beneath the SX Tank Farm**

| Stratigraphic Symbol* | Formation | Facies/Subunit | Description | Genesis |
|-----------------------|-----------------------|------------------------------------|--|---|
| Holocene/Fill | NA | Backfill | Poorly sorted gravel to medium sands and silt derived from the Hanford formation (Price and Fecht 1976a). | Anthropogenic |
| H1a | Hanford formation | Unit H1b - gravelly sand | Top coarse sand and gravel sequence equivalent to the Johnson et al. (1999) 'Gravel Unit B.' | Cataclysmic flood deposits |
| | | Unit H1a - slightly silty sand | Upper fine sand and silt sequence | |
| H1 | | Unit H1 | Middle Coarse Sand and Gravel Sequence equivalent to 'Gravel Unit A' described by Johnson et al. (1999) and 'Hanford Unit A' described by Sobczyk (2000). | |
| H2 | | Unit H2 | Lower Fine Sand and Silt Sequence | |
| PPlz and/or H/PP1 | Plio-Pleistocene unit | Upper | Very Fine Sand to Clayey Silt Sequence is interstratified silt to silty very fine sand and clay deposits at least partially correlative with the 'early Palouse soils' described by Tallman et al. (1979) and DOE (1988) and the 'unnamed Hanford formation [?]' or Plio-Pleistocene Deposits [?]' described by Lindsey et al. (2000), and the H/PP deposits in Wood et al. (2001). | Fluvial and/or eolian deposits (with some weakly developed paleosols) |
| PPlc | | Lower | Carbonate-Rich Sequence. Weathered and naturally altered sandy silt to sandy gravel, moderately to strongly cemented with secondary pedogenic calcium carbonate. | Well-developed calcic paleosol or sequence of calcic soils. |
| Rtf | Ringold Formation | Member of Taylor Flat | Interstratified sand and silt deposits , equivalent to the Upper Ringold unit described by Tallman et al. (1979) and DOE (1988). | Fluvial and overbank-paleosol deposits |
| Rwi(e) | | Member of Wooded Island, subunit E | Moderate to strongly cemented, well-rounded gravel and sand deposits , and interstratified finer-grained deposits. | Fluvial |

*After Lindsey et al. (2000).

The thickness of unit E is estimated to be approximately 75 to 85 m (250 to 280 ft) (Tallman et al. 1979; DOE-RL 1993). This unit consists of well-rounded, clast-supported pebbles and small cobbles in a matrix of sand and mud. The amount of cementation is variable, with the lower portion of this unit described as moderately to well-indurated conglomerate (Tallman et al. 1979). However, zones of poorly indurated gravel and sand also occur within this zone. The upper part of the unit is generally poorly indurated. Borehole data in the immediate vicinity of the SX tank farm indicate that this upper portion is dominated by sandy gravel and muddy sandy gravel, with sand to muddy sand beds becoming more prevalent toward the top of the unit.

A relict erosional and weathered surface occurs at the top of the Ringold Formation beneath the SX tank farm (DOE 1988; Slate 1996; Slate 2000). The uppermost portion of this paleosurface is highly weathered and often cemented with secondary pedogenic calcium carbonate, referred to in this appendix as the carbonate-rich facies (subunit PPlc) of the Plio-Pleistocene unit (Table C.10). The northwest-southeast trending trough-shaped surface appears to conform to an ancestral Cold Creek channel and drainage system that developed following late Pliocene incision of the Ringold Formation, and prior to early Pleistocene cataclysmic flooding, during the period between approximately 2 to 3 million years ago (DOE 1988). The SX tank farm lies north of the ancestral Cold Creek paleochannel and the eroded Ringold paleosurface dips to the southwest beneath the SX tank farm. The attitude on this surface may have increased since late Pliocene-early Pleistocene time as a result of tectonic deformation associated with the Cold Creek syncline (Slate 1996; Slate 2000).

C.4.2.3 Plio-Pleistocene Unit

The Plio-Pleistocene unit lies unconformably on the tilted and truncated Ringold Formation that formed following incision and downcutting of the Ringold Formation by the ancestral Columbia River system, which began about 3.4 million years ago (DOE 1988). These deposits are inferred to have a late Pliocene to early Pleistocene age on the basis of stratigraphic position.

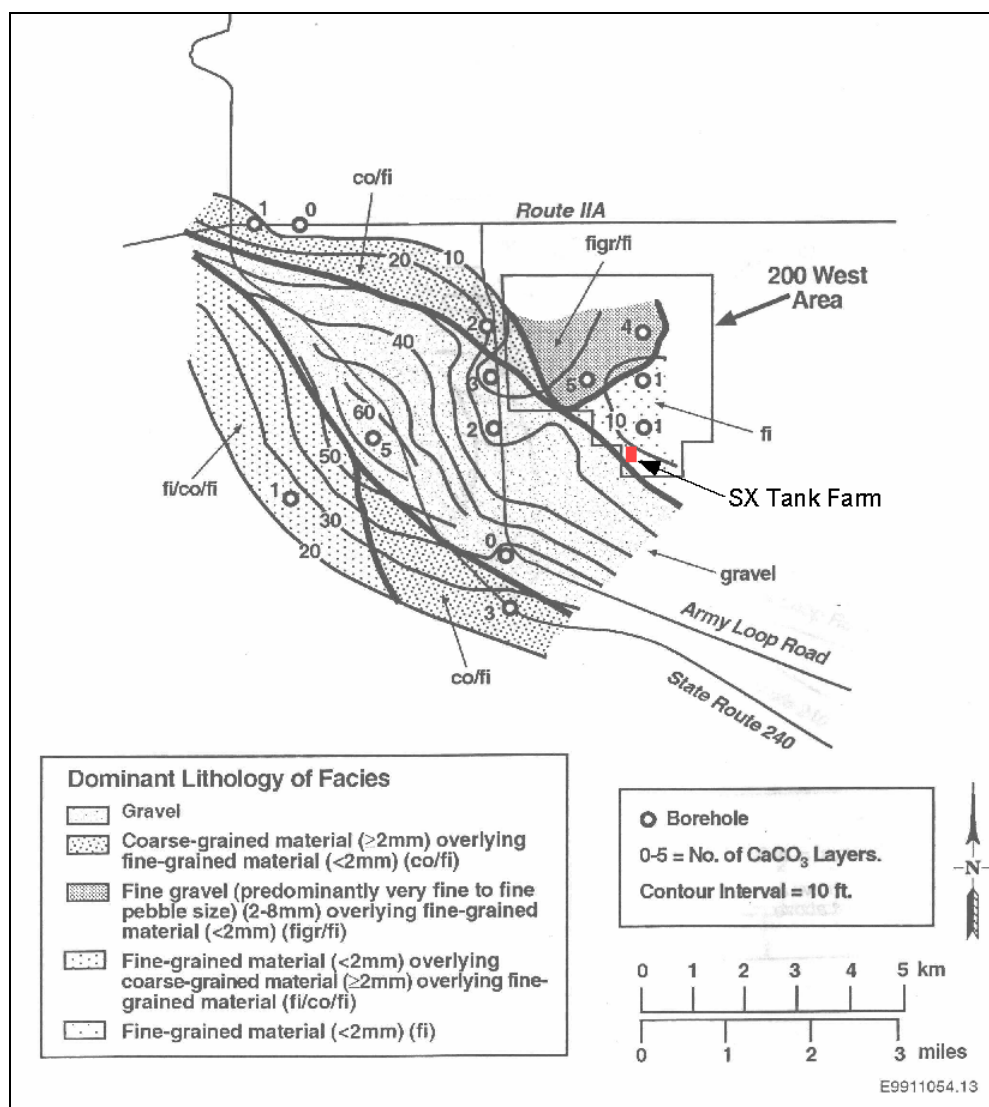
The Plio-Pleistocene unit includes all material overlying the Ringold Formation, including the weathered horizon at the top of the Ringold Formation, and beneath cataclysmic flood deposits of the Hanford formation (Lindsey et al. 1994). The Plio-Pleistocene unit includes the ‘early Palouse soils’ described in *An Eolian Deposit Beneath 200-West Area* (Brown 1960), Tallman et al. (1979), and DOE (1988); the ‘Pre-Missoula Gravels’ (or equivalent); the ‘unnamed Hanford Formation [?] or Plio-Pleistocene Deposits [?]’ described in Lindsey et al. (2000); and H/PP(?) deposits described in *Subsurface Conditions Description of the T-TX-TY Waste Management Area* (Wood et al. 2001).

Two distinct facies of the Plio-Pleistocene unit are recognized beneath the SX tank farm; these consist of an upper (PPlz) and lower (PPlc) subunit (Table C.10). The upper subunit PPlz is characterized by an abundance of silt, signified by the letter ‘z,’ and the lower subunit PPlc is characterized by an abundance of pedogenic calcium carbonate cement, signified by the letter ‘c.’ The combined total thickness of the Plio-Pleistocene unit is up to 13.1 m (43 ft) in the vicinity of the SX tank farm (Figure C.15). Subunit PPlz is relatively thick (up to 10.7 m [35 ft]), compared to the subunit PPlc, which measures only 1 to 4 m (4 to 13 ft) in thickness.

Subunit PPlc. The lower subunit PPlc represents a highly weathered paleosurface that developed atop the Ringold Formation (Brown 1959; Brown 1960), which represents a long period of surficial weathering in a semi-arid climate, similar to climatic conditions that exist today. Root traces and animal borrows, as well as other relict soil structures, point to a pedogenic origin for the calcium carbonate, although “Buried Carbonate Paleosols Developed in Pliocene-Pleistocene Deposits of the Pasco Basin, South-Central Washington” (Slate 1996) and *Nature and Variability of the Plio-Pleistocene Unit in the 200 West Area of the Hanford Site* (Slate 2000) also suggest the calcium carbonate could be associated with precipitation from paleo-groundwater levels. Calcium carbonate contents as high as 70 wt% have been reported within subunit PPlc elsewhere within the 200 West Area; however, the calcium carbonate content generally does not exceed 25 wt% in the vicinity of the SX tank farm. The calcium carbonate content from 3 randomly chosen boreholes within the SX tank farm did not exceed 10 wt%. Other names used for subunit PPlc, including ‘caliche’ and ‘calcrete’ are somewhat misleading because they imply a single, homogeneously cemented layer, which is not the case. Considerable internal variation exists, within subunit PPlc, often with multiple carbonate-cemented zones present (Bjornstad 1990; Slate 1996; Slate 2000; Wood et al. 2001).

The calcium carbonate overprint may occur on a variety of lithologies including silt, sand, felsic sand, and gravel as well as basaltic sand and gravel (Lindsey et al. 2000). In places, pedogenic alteration occurs directly on top of Ringold gravels (Rwi[e]) or sands (Rtf). In other places, the carbonate horizons occur within younger, pedogenically altered, fine-grained, eolian or sidestream-alluvial deposits overlying the Ringold Formation. The top of subunit PPlc is well defined by a coincident significant increase in calcium carbonate and decrease in mud content and sorting accompanied by a sudden and sustained decrease in total gamma activity (i.e., potassium-40) on borehole geophysical logs (DOE 1988; Last et al. 1989; Bjornstad 1990; Wood et al. 2001). In general, the top of subunit PPlc is easily identified by a sudden drop in total gamma activity that is usually, but not always, accompanied by a significant increase in calcium carbonate.

While the top subunit PPlc is relatively easy to recognize, considerable variation may exist internally within the subunit due to natural heterogeneity inherent of soils and soil processes that vary under different physical, chemical, and biological conditions (e.g., moisture, grain size, aspect, mineralogy, bioturbation, microbial activity). Added to this is the complicating factor that the land surface during Plio-Pleistocene time was undergoing many changes under the influence of local fluvial and eolian activity resulting in variable rates of aggradation, degradation, and soil development. Normally, only a single paleosol horizon is present within the lower Plio-Pleistocene unit within the SX tank farm, suggesting slow or negligible aggradation and/or subsequent erosion during paleosol development. This is in contrast to other areas to the west and south, which show up to five separate calcic horizons (Figure C.16) separated by relatively noncalcareous, uncemented sand; silt; and even indigenous, basaltic sand and/or gravel (Slate 1996; Slate 2000; Wood et al. 2001). Multiple carbonate horizons within the subunit PPlc are indicative of several periods of calcic-soil development interrupted temporarily by periodic aggradational events (e.g., localized overbank flood, eolian accumulation, channel fill). The evolution of calcic paleosols and their morphogenetic development are discussed further in Slate (1996; 2000) and Wood et al. (2001).

Figure C.16. Lithofacies Distribution for the Lower Plio-Pleistocene Subunit PPlc

Modified from Slate (2000).

In WMA T-TX-TY, which is 1,800 m (5,900 ft) north of the SX tank farm, the top of subunit PPlc dips to the southwest at about 1° (Wood et al. 2001). At least some of the dip reflects the paleo-topography that existed during subaerial weathering of the eroded Ringold Formation surface. This is inferred based on the relief on top of subunit PPlc, which is almost double that of the underlying Ringold Formation lower mud unit. Therefore, it appears that during development of subunit PPlc there was a gentle dip to the land surface to the southwest toward the Cold Creek valley axis. Since Plio-Pleistocene time this surface has been steepened further by continued long-term downwarping along the north limb of the Cold Creek syncline (DOE 1988).

Another recognized facies of the Plio-Pleistocene unit is a coarse-grained side-stream-alluvial facies (Bjornstad 1984; DOE 1988; Slate 1996; Slate 2000), which is laterally equivalent to subunit PPlc to the south and west of SX tank farm. The side-stream alluvial facies (gravel facies in Figure C.16) fills and is restricted to the northwest-southeast trending, ancestral Cold Creek channel, located south and west of the 200 West Area. The eastern edge of this gravel facies occurs along the southwest boundary of 200 West Area near the SX tank farm (Figure C.16). North and east of the 200 West Area, the Plio-Pleistocene unit is generally not present, having been scoured away during either post-Ringold erosion and/or Pleistocene cataclysmic flooding.

C.4.2.3.1 Subunit PPlz. Unconformably overlying subunit PPlc is the upper subunit PPlz which consists of interstratified, uncemented fine sand, silt, and/or clay that only displays occasional, very weak soil development in the vicinity of the SX tank farm. Based on its fine-grained texture and relatively high natural-gamma activity on geophysical logs, this unit can be correlated across most of the 200 West Area (Wood et al. 2001). Subunit PPlz sediments appear to be predominantly fluvial-overbank type deposits intercalated with some eolian deposits (Lindsey et al. 2000; Slate 2000; Wood et al. 2001). Subunit PPlz is at least partially correlative with the ‘early Palouse soils’ described by previous reports (Brown 1960; Tallman et al. 1979; Bjornstad 1984; Last et al. 1989; Bjornstad 1990; and DOE 1988); the ‘unnamed Hanford Formation [?] or Plio-Pleistocene Deposits [?]’ described in Lindsey et al. (2000); and the H/PP(?) unit described in Wood et al (2001).

The upper Plio-Pleistocene unit contains moderate amounts (up to a few weight percent) of calcium carbonate (Table C.11), generally more than the overlying Hanford formation. As discussed previously, however, subunit PPlz may also locally have more calcium carbonate than the underlying subunit PPlc if samples from subunit PPlc come from noncalcic zones between paleosols within subunit PPlc.

Table C.11. Example of Granulometric and Calcium Carbonate Data from Drive-Barrel Samples of Subunit PPlz Encountered Beneath the SX Tank Farm

| Borehole /Depth | CaCO ₃ % | Gravel >2 mm | Sand | | | | | Mud <0.063 mm | Class |
|---------------------|---------------------|--------------|--------------------|-------------------|--------------------|--------------------|--------------------------|---------------|-------|
| | | | Very Coarse 1-2 mm | Coarse 0.5-1.0 mm | Medium 0.25-0.5 mm | Fine 0.125-0.25 mm | Very Fine 0.063-0.125 mm | | |
| 299-W23-5 120 ft | 2.6 | 0.0 | 1.8 | 1.9 | 4.8 | 12.3 | 31.1 | 48 | mS |
| 299-W23-5 125 ft | 2.3 | 0.0 | 1.6 | 7.0 | 9.2 | 7.3 | 8.1 | 66.8 | sM |

The source of the calcium carbonate within the two subunits appears distinctly different. Within subunit PPlc, most of the calcium carbonate appears as stringers or in massive horizons, which formed in situ as a result of pedogenesis (Wood et al. 2001). Within subunit PPlz, on the other hand, the calcium carbonate is evenly disseminated and does not occur in discrete zones; therefore, it is interpreted to be detrital in origin (Wood et al. 2001). In fact, the bulk of the detrital, calcium carbonate mineral grains in subunit PPlz are probably derived from the disintegration and mechanical re-working and re-deposition of the underlying subunit PPlc.

The contact between subunits PPlz and PPlc is distinctive and easily identified. Subunit PPlz consists of relatively loose, stratified, non-pedogenically altered, well-sorted silt to very fine sand in contrast to poorly-sorted, weathered, and carbonate-cemented deposits of subunit PPlc. Also distinctive is a sudden increase in total gamma activity upward across the contact (DOE 1988; Last et al. 1989; Bjornstad 1990; Johnson et al. 1999). The upper contact of subunit PPlz with the overlying Hanford formation, on the other hand, often appears gradational, both texturally and structurally, and thus is often difficult to identify based on lithologic observations alone, especially in the vicinity of the SX tank farm. Because of this uncertainty, in the past subunit PPlz has been combined and queried with the lower Hanford formation in some recent reports (Lindsey et al. 2000; Wood et al. 2001). For the purposes of this study it was determined that the total gamma activity on borehole geophysical logs can effectively be used to identify the upper contact for the Plio-Pleistocene unit. Accordingly, a subtle decrease in total gamma activity appears to be associated with the top of subunit PPlz, probably as a result of a lower silt/clay content within the Hanford formation. Therefore, we recommend that this change in total-gamma activity and grain size be used to define the upper contact for subunit PPlz.

C.4.2.4 Hanford Formation

Pleistocene-age deposits of the Hanford formation overlie the Plio-Pleistocene unit and represent the dominant vadose zone materials directly beneath the SX tank farm. The Hanford formation is the informal name given to all deposits from Ice Age cataclysmic floods including any intercalated non-flood deposits.

The Hanford formation can generally be divided into three facies: (1) gravel-dominated, (2) sand-dominated, and (3) silt-dominated, also referred to as coarse-grained deposits, plane-laminated sand facies, and rhythmite facies, respectively (Baker et al. 1991). The coarse-grained facies have also been referred to as the 'Pasco gravels,' and the rhythmite

facies as 'Touchet Beds.' The Hanford formation is thickest (up to 65 m [215 ft]) in the vicinity of the 200 Areas beneath Cold Creek bar (Figure C.17).

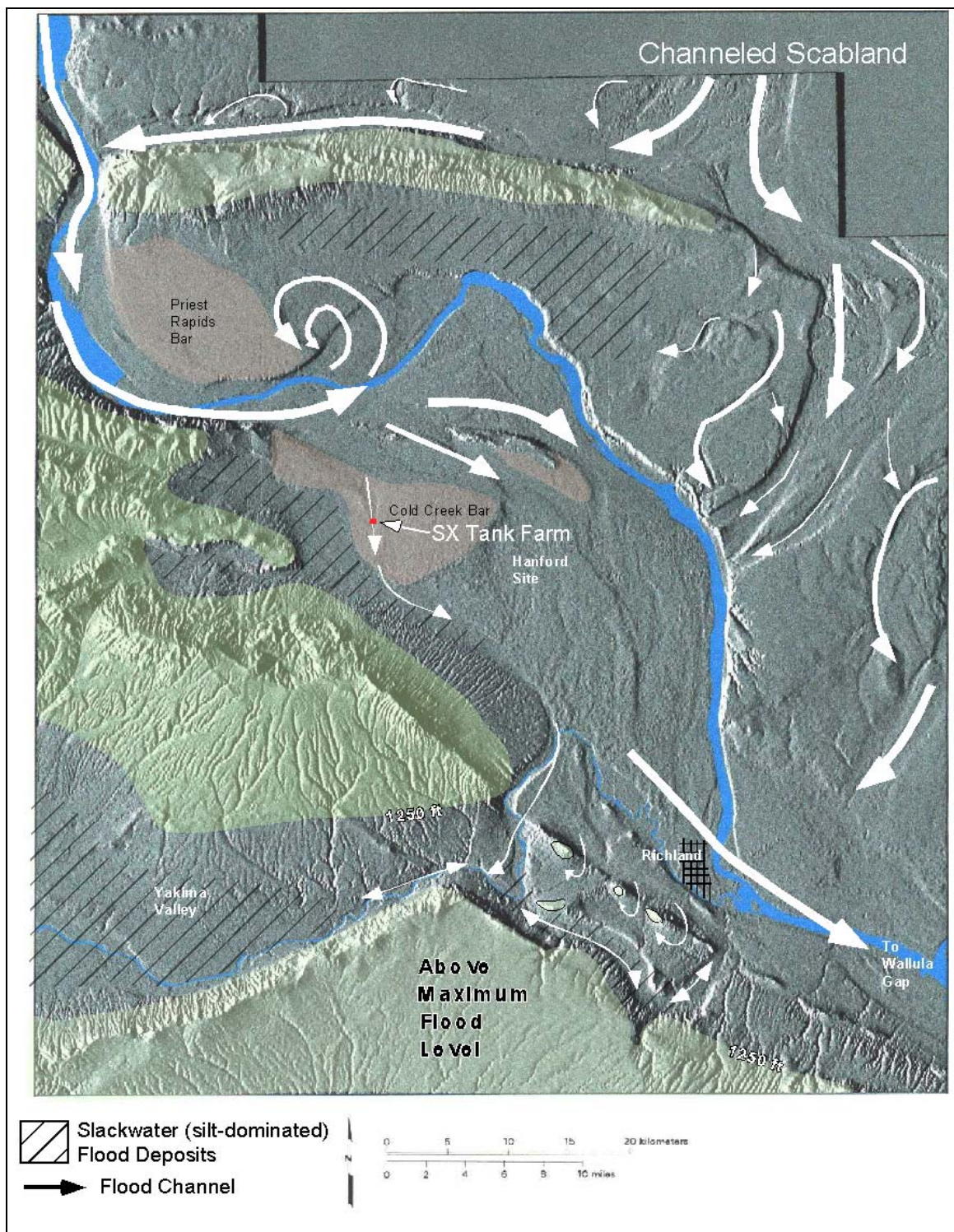
The gravel-dominated facies generally consists of poorly-sorted coarse-grained basaltic sand and granule to boulder gravel. These deposits occasionally display an open framework texture, massive bedding, plane to low-angle bedding, and large-scale fore-set bedding in outcrop. The gravel clasts (dominated by basalt) are usually subangular to subrounded. The gravel-dominated facies was deposited by high-energy floodwaters in or immediately adjacent to the main cataclysmic flood channel ways (Figure C.17).

The sand-dominated facies consists of fine- to coarse-grained sand and granule gravel displaying plane lamination and bedding and, less commonly, plane bedding and channel-fill sequences in outcrop. These sands may contain small pebbles and rip-up clasts in addition to pebble-gravel interbeds and silty interbeds less than 1 m (3 ft) thick. The silt content of these sands is variable, but where it is low a well-sorted and open framework texture is common. These sands typically are basaltic, commonly being referred to as black, gray, or 'salt-and-pepper' sands. The laminated sand facies was deposited at higher elevations where the floodwaters were starved of gravel, and/or adjacent to main flood channel ways during the waning stages of flooding (Figure C.17). This is a transitional facies between the gravel-dominated facies and the silt-dominated facies. The sand-dominated facies is the predominant facies of the Hanford formation beneath the SX tank farm.

The silt-dominated facies consists of rhythmically bedded, ripple-cross-laminated sand and silt, and fine- to coarse-grained sand grading upward to plane laminated silt. Individual rhythmites range from a few centimeters to several tens of centimeters thick (Myers and Price 1979; DOE 1988; Baker et al. 1991). These sediments were deposited under slack-water conditions and in back-flooded areas (DOE 1988), mostly around the margins of the basins (Figure C.17). The silt-dominated facies is the predominant facies of the Hanford formation south and west of the SX tank farm.

The Hanford formation beneath the SX tank farm is mostly represented by sand-dominated facies consisting of fine-grained sands intercalated with coarse sand and gravel and thinner lenses of silt. The basal portion of the Hanford formation is predominantly silty fine sand, described by DOE (1996) and Lindsey et al. (2000) as Hanford subunit H2 (Table C.10). A sandy gravel to coarse sand facies dominates the middle portion of the Hanford formation, which is then overlain by a slightly silty medium sand and finally by a slightly gravelly coarse sand. The middle coarse sand to gravel facies makes up the Hanford subunit H1 described in DOE (1996), Johnson et al. (1999), and Lindsey et al. (2000). The slightly silty medium sand and overlying slightly gravelly coarse sand is equivalent to the Hanford subunit H1a (Johnson et al. 1999; Lindsey et al. 2000).

Figure C.17. Digital Elevation Model Map of a Portion of the Pasco Basin Showing Routes and Facies Distributions for the Last Pleistocene Cataclysmic Floods



C.4.2.4.1 Subunit H2. The lower fine sand and silt sequence of the Hanford formation, H2 subunit, consists primarily of interstratified silty sands. This sequence generally thins from about 24.3 m (80 ft) east of the SX tank farm to approximately 10.7 m (35 ft) west of the tank farm (Figure C.15). Johnson and Chou (1998) suggests that this thinning may signify some scouring on top of the subunit, perhaps associated with a secondary flood channel similar to the north-south trending flood channel that bisects Cold Creek bar in Figure C.17. The grain-size within the Hanford H2 subunit appears to coarsen upward slightly (see Table C.12). Sobczyk (2000) and Johnson et al. (1999) report that the top of this unit generally dips about 6° to the southwest with some local relative highs and lows present throughout. Below subunit H2 are slightly finer-grained deposits of interstratified very fine sand, silt, and clay associated with the upper Plio-Pleistocene subunit PPlz. As mentioned previously, the base of the Hanford formation is indicated by a diagnostic increase in total-gamma activity on borehole geophysical logs.

C.4.2.4.2 Subunit H1. Subunit H2 is bounded above by subunit H1, and is a coarse unit dominated by gravel to gravelly sand and intercalated coarse sand (Table C.12) that appears to correlate beneath the SX tank farm (Figure C.15). This middle sequence—referred to as ‘Gravel Unit A’ in Johnson et al. (1999) and as ‘Hanford Unit A’ in Sobczyk (2000)—is equivalent to the H1 unit described in DOE (1996) and Lindsey et al. (2000). Subunit H1 ranges in thickness from 1 m (3 ft) to nearly 10 m (30 ft) beneath the SX tank farm. Sobczyk (2000) reports subunit H1 to be thickest beneath tank SX-102 (Figure C.14) where coarse-grained flood deposits backfilled an apparent channel eroded into the top of the underlying subunit H2.

Recent particle size results using dry sieving for 100 selected samples from 7 wells drilled in and around the tank farm reveal that this unit averages approximately 30% gravel, 66% sand, and only 4 % mud (see Appendix A). This is compared to the materials directly above and below it, that both average less than 1% gravel, nearly 90% sand, and 9% mud. Based on the modified Folk/Wentworth classification scheme, the classification of the average particle size for subunit H1 falls near the boundary between the sandy gravel and gravelly sand classes.

C.4.2.4.3 Subunit H1a. Above the middle coarse facies of the subunit H1 lies an upper fine sand to silty-sand sequence equivalent to subunit H1a described in Lindsey et al. (1994; 2000), and the ‘silty sand’ described in Sobczyk (2000). This sequence consists predominantly of interstratified slightly-silty medium to very fine sands (Table C.12) and ranges in thickness from 0 m (0 ft) where it was removed during excavation of the tank farm to about 9 to 12 m (30 to 40 ft) to the southwest (Figure C.15). Sobczyk (2000) reports that the top of this unit dips slightly (approximately 2°) to the southwest. Sobczyk (2000) also suggests that this unit may become coarser textured to the west.

C.4.2.4.4 Top Coarse Sand and Gravel Sequence (Hanford Subunit H1 - Coarse Unit B). A coarse-grained sand to gravelly sand unit (Table C.12) overlies the fine sand sequence of subunit H1a, and may be intercalated with some sandy gravel to the west. This unit is equivalent to Gravel Unit B (Johnson et al. 1999) and Hanford Unit B (Sobczyk 2000). It is the uppermost stratigraphic unit in the tank farm area, but is completely missing beneath the tank farm, where it was removed during construction. In surrounding boreholes, however, this unit ranges from a few meters in thickness to east to up 12 m (40 ft) to the west.

Table C.12. Data from Drive Barrel and Split-Spoon Samples of the Hanford Formation Beneath SX Tank Farm located in Figure C.14

| Hanford Subunit | Borehole /Depth | CaCO ₃ % | Gravel >2 mm | Sand (mm) | | | | | Mud <0.06 3 mm | Class | Average Bulk Density from 299-W22-50* |
|-----------------|--------------------|---------------------|--------------|--------------------|-------------------|--------------------|-----------------|--------------------------|----------------|-------|---------------------------------------|
| | | | | Very Coarse 1-2 mm | Coarse 0.5-1.0 mm | Medium 0.25-0.5 mm | Fine 0.125-0.25 | Very Fine 0.063-0.125 mm | | | |
| H1a | 299-W23-72 55 ft | 1.4 | 0.4 | 0.5 | 1 | 19.1 | 43.1 | 22.1 | 13.9 | (m)S | 1.95 |
| | 299-W23-92 80 ft | NA | 2.1 | 3 | 12.1 | 20.4 | 31.2 | 19.8 | 11.4 | (m)S | |
| H1 | 299-W23-72 70 ft | 1.7 | 10.7 | 23.7 | 28.7 | 16.7 | 8.3 | 6.0 | 6.0 | gS | 2.27 |
| | 299-W23-92 90 ft | NA | 16.3 | 16.9 | 27.9 | 18.5 | 8.1 | 5.7 | 6.6 | gS | |
| | 299-W23-108 85 ft | NA | 41.8 | 24.5 | 14.5 | 7.1 | 3.9 | 3.3 | 5.0 | sG | |
| H2 | 299-W23-72 100 ft | 1.7 | 0.0 | 0.2 | 2.1 | 37.6 | 29.7 | 15.2 | 15.3 | (m)S | 2.05 |
| | 299-W23-92 110 ft | NA | 0.8 | 1.0 | 9.4 | 40.0 | 22.2 | 14.6 | 12.0 | (m)S | |
| | 299-W23-92 120 ft | NA | 2.8 | 2.2 | 1.7 | 9.6 | 33.5 | 34.9 | 15.4 | (m)S | |
| | 299-W23-108 110 ft | NA | 1.8 | 0.1 | 1.8 | 13.2 | 26.6 | 30.9 | 15.7 | mS | |

Source: Horton and Johnson (2000).

NA = not analyzed.

C.4.2.5 Backfill

Geology of the 241-SX Tank Farm (Price and Fecht 1976a) describes the backfill surrounding the HLW tanks of the SX tank farm as consisting predominantly of poorly sorted cobbles, pebbles, and coarse to medium sands to silt derived from the Hanford formation. Lindsey et al. (2000) describes the backfill as relatively non-cohesive, friable, massive sand with variable amounts of silt and pebbles. A hardened zone at the base of the backfill, extending to a depth of approximately 18.6 m (61 ft) that was significantly harder and drier than the overlying materials was also observed.

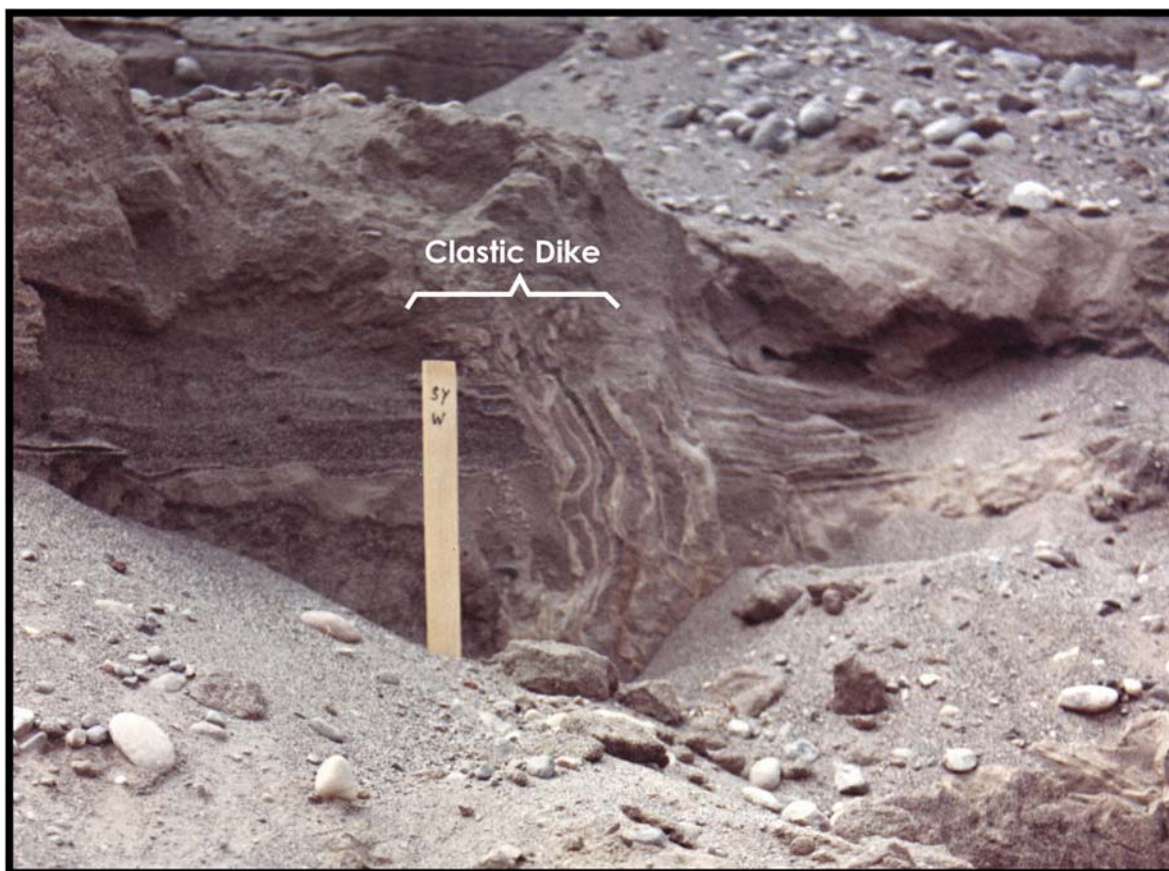
Engineering drawings (H-237985, Sheets 1 and 2) show that the tank farm was excavated to create three terraces for construction of cascading tanks. This excavation extended to an elevation of 185.3 m (608 ft) on the west side and 185.9 m (610 ft) on the east side.

C.4.2.6 Clastic Dikes

Clastic dikes are vertical to near-vertically oriented sedimentary structures that cut across horizontal bedding planes. These dikes have been observed in all types and ages of geologic materials found beneath the Hanford Site including basalt; interbed sediments; the Ringold Formation; and the sands, mud, and gravels of the Hanford formation (Fecht et al. 1999). They are especially notable within the sand- and silt-dominated facies of the Hanford formation where they have been observed to be a few centimeters to more than a meter thick and extend to depths of 36 m (120 ft) or more. Clastic dikes may significantly impact contaminant transport through the vadose zone based on their differing orientation versus the traditional horizontal strata common in the Hanford formation.

Price and Fecht (1976a) states that clastic dikes were detected in the SX tank farm but that they could not be mapped. Clastic dikes (and/or polygonally patterned ground often associated with them) have also been observed at a number of locations surrounding the SX tank farm, including the SY tank farm to the north, the Environmental Restoration and Disposal Facility to the east, and throughout Cold Creek Valley to the south and west (including the former 216-S-16 pond). Tallman et al. (1979) indicates that identification of clastic dikes in this area was also based on examination of cable-tool drilling samples. Horton and Johnson (2000) reports that possible clastic dikes had been encountered by two or three recently installed RCRA groundwater monitoring wells (299-W22-48 and 299-W22-50). Lindsey et al. (2000) also notes a few structures suggestive of clay skins on clastic dikes in split-spoon samples from well 299-W22-50.

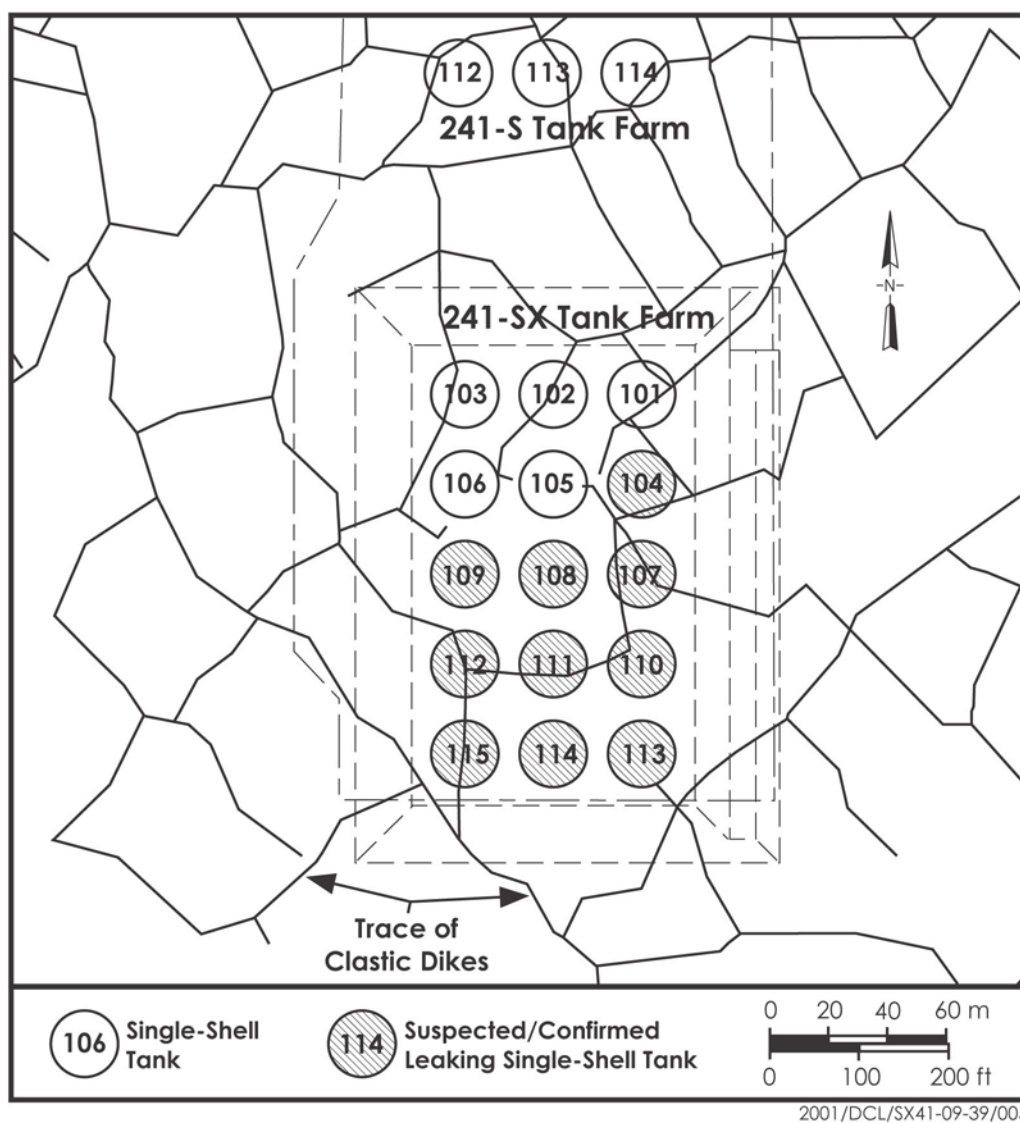
Figure C.18 illustrates one of the clastic dikes observed in walls of the excavation for the SY tank farm located approximately 300 m (1,000 ft) to the north of the SX tank farm (Price and Fecht 1976b).

Figure C.18. Clastic Diak in the SY Tank Farm Excavation

2001/DCL/SX41-09-39/002

Johnson et al. (1999) projects a plausible network of clastic dikes for the SX tank farm (Figure C.19) based on polygonally patterned ground mapped between Army Loop Road and State Highway 240 and scaled based on the best cell size estimate from *An Atlas of Clastic Injection Dikes of the Pasco Basin and Vicinity* (Fecht et al. 1999).

**Figure C.19. Projection of a Hypothetical Network of
Clastic Dikes onto Waste Management Area S-SX**



Source: Johnson et al. (1999).

C.5.0 MOISTURE CONTENT AND MATRIC POTENTIAL MEASUREMENTS

Moisture content and matric potential measurements are available for a number of boreholes in WMA S-SX (Myers 2000; Serne et al. 2001a, 2001b, 2001c). Many of the conclusions based on the measured matric potentials (Serne et al. 2001a, 2001b, 2001c) are presented in Section 3.2.1, in the context of recharge estimates for the tank farms. The primary purpose of this section is to present the measured data on moisture content and matric potential.

Moisture content measurements were made for sediments in the drywells surrounding the SX tank farm (Myers 2000). Matric potentials were measured for samples from two clean RCRA boreholes, 299-W22-48 and 299-W22-50 (Serne et al. 2001a), and also for the two contaminated boreholes: borehole 41-09-39 near tank SX-108 (Serne et al. 2001b) and borehole 299-W23-19 south of the SX tank farm (Serne et al. 2001c).

C.5.1 MOISTURE CONTENT FOR DRYWELL SEDIMENTS

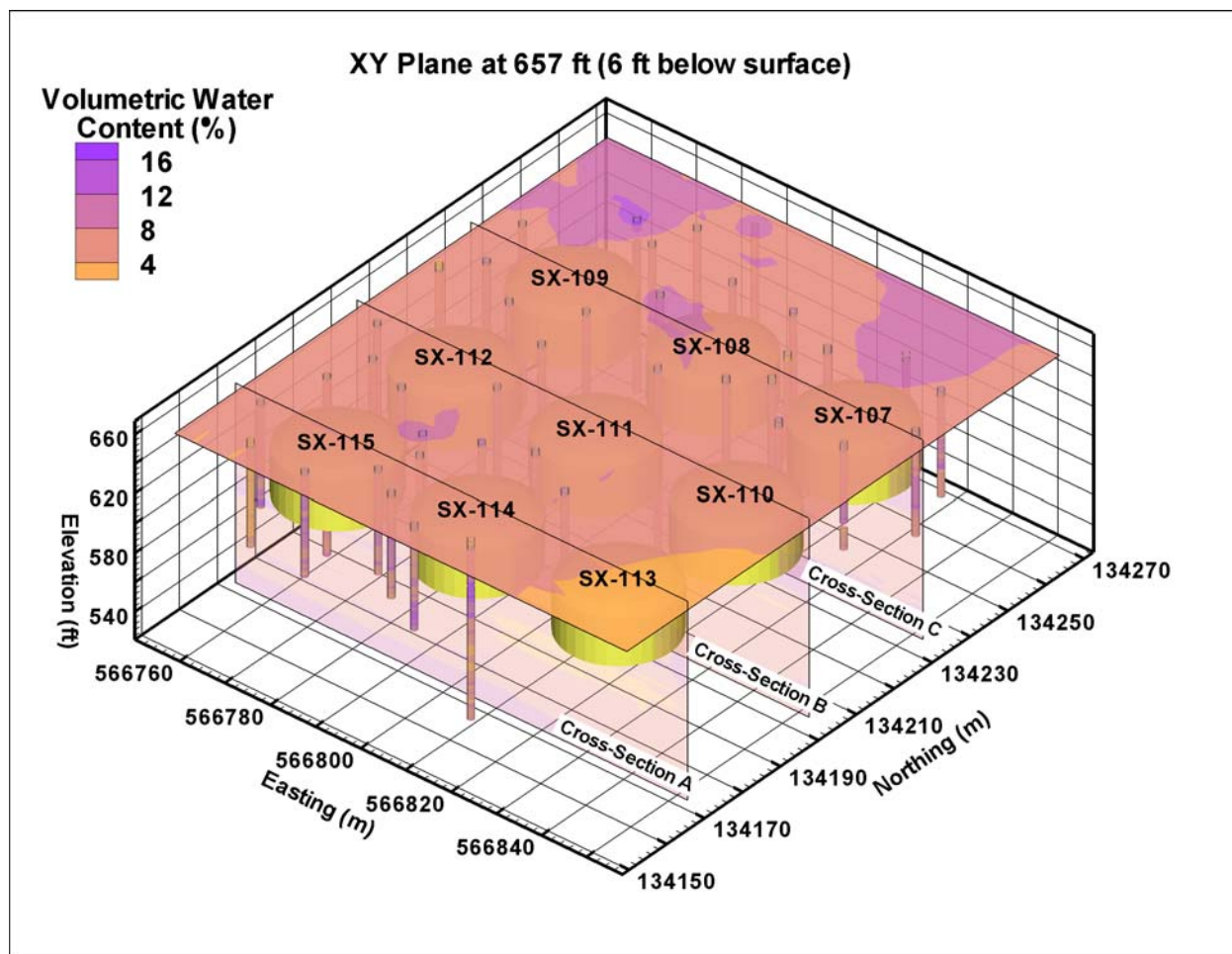
The drywells at SX tank farm are generally within 1.5 to 3 m (5 to 10 ft) from the outside walls of the tanks. The drywells extend to various depths, typically between 22.8 and 30 m (75 and 100 ft). There are presently 98 drywells within the SX tank farm.

Within the backfill surrounding the SX tank farm, the measurements suggest that there is relatively consistent moisture content of 8 to 10 % (volumetric), with a moderate increase in moisture at the base of the excavation (Figure C.20). The increased moisture content is possibly due to the increased compaction that took place during farm construction. In the undisturbed soils beneath the excavation, the presence of gravelly zones results in much lower moisture content, typically in the range of 4 to 6 vol%, with some drier zones. Thin zones of higher moisture content are evident below the tank farm excavation (Figure C.21). These thin zones are consistent with the presence of lenses or beds of silty fine sands noted in the Hanford formation. Deeper drywells exhibit a consistent increase in moisture content at a depth of about 38 m (125 ft) (Figure C.21). This depth corresponds to the approximate depth of the more massive fine, silty sands and sandy silts of the lower Hanford formation or Plio-Pleistocene unit.

Regions of greater than 12 % moisture content (volumetric) were detected (Figure C.20). One of these zones was located east of tank SX-115. This location is defined by the high moisture content in a narrow zone in a single drywell at a depth about 21.3 m (70 ft). A second zone of high moisture content was identified north of tank SX-109 and appears as a halo starting at about 1.5 m (5 ft) bgs (Figure C.21). Research into the location of utilities serving the tank farm reveals that these readings are from a depth close to the terminus of an active water line. The presence of areas of noticeably wetter zones in vicinity of water distribution pipes points to the probability that these pipes may be significant sources of recharge.

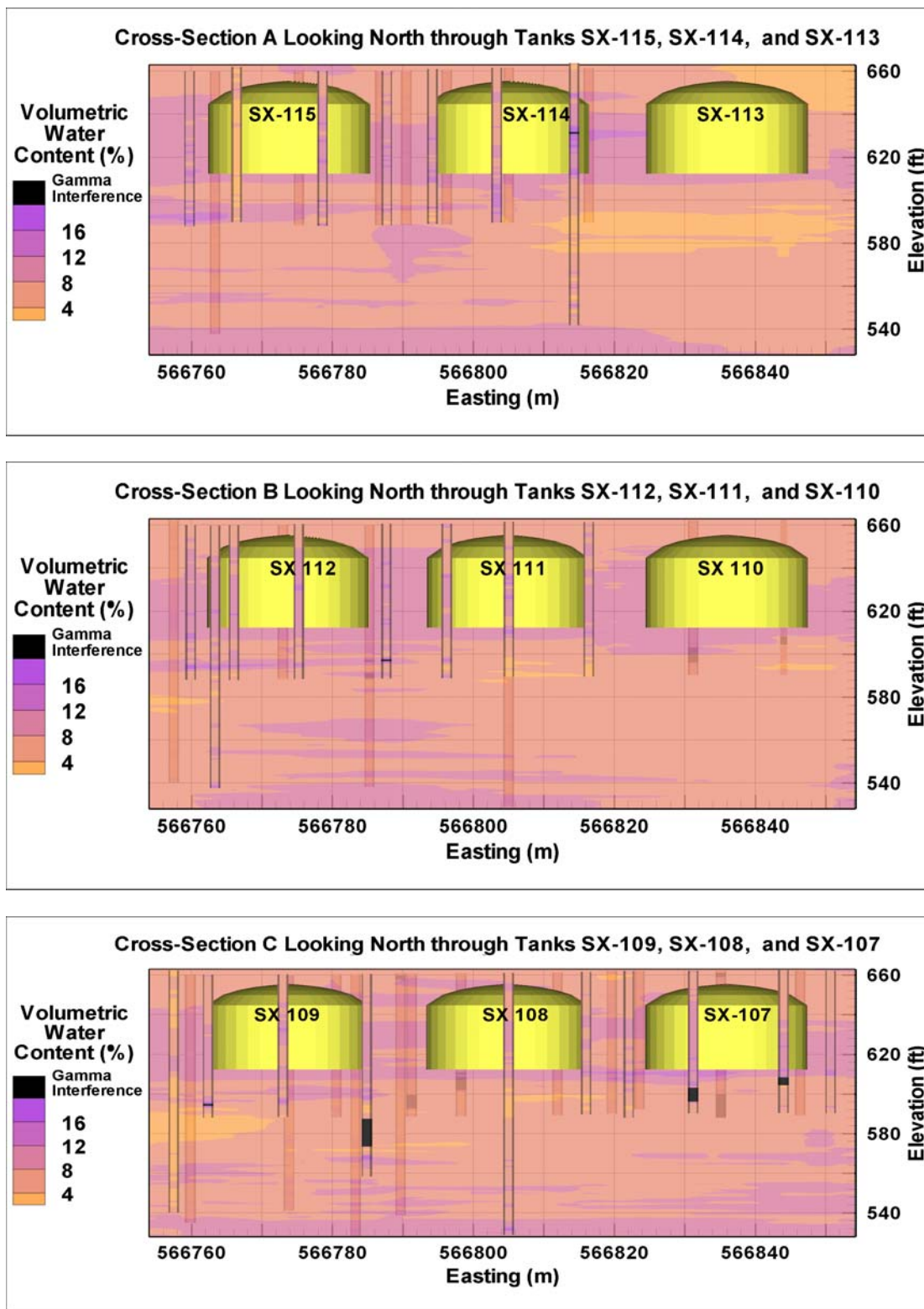
In summary, the geologic environment of the SX tank farm plays a significant role in controlling the distribution of moisture with increasing depth. The distribution of moisture content, on the basis of drywell measurements, helps to identify areas where potential sources of recharge from water-line leaks may exist.

**Figure C.20. Measured Moisture Contents for the
Drywell Sediments Beneath SX Tank Farm**



Source: Myers (2000).

Figure C.21. Moisture Content Distribution for the Drywell Sediments for Three Cross-Sections

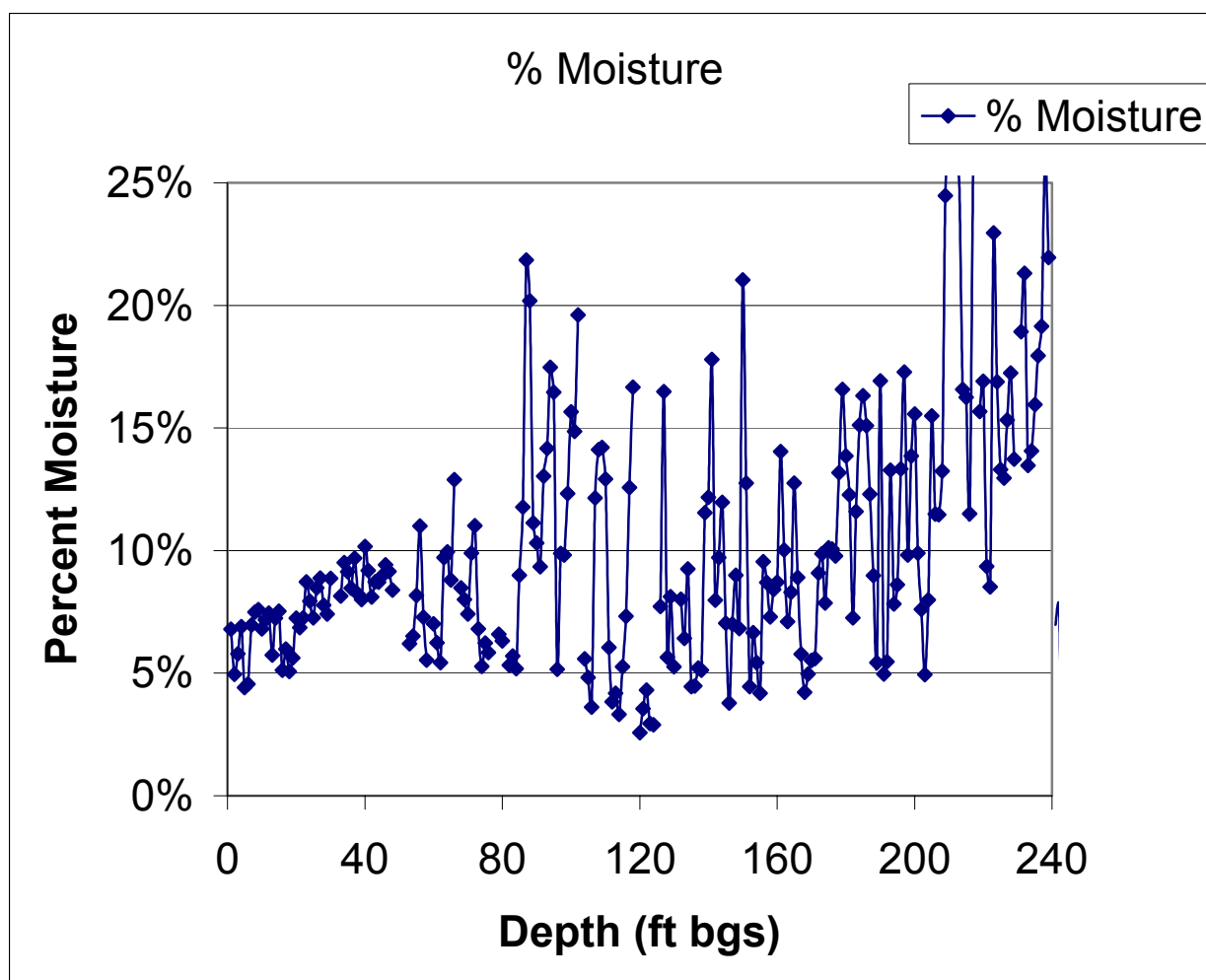


Source: Myers (2000).

C.5.2 MEASUREMENTS FOR BOREHOLES 299-W23-19, 299-W22-48, AND 299-W22-50

The gravimetric moisture content for sediments from borehole 299-W23-19 are shown in Figure C.22. The moisture content profile shows several high peaks within the Hanford formation coarse facies and the Hanford formation fine laminated sands. At 26.5 and 28.7 m (87 and 94 ft) bgs within the coarse unit, the higher moisture contents correspond to thin lenses of finer grained material. Within the fine unit there are wetter zones at 31 and 36 m (102 and 118 ft) bgs that do not seem to correlate with subtle changes in particle size. Within the Plio-Pleistocene unit fine grained facies there are 3 wet zones at 38.7, 43, and 45.7 m (127, 141, and 150 ft) bgs that correspond to thin zones of finer grained material. Wetter zones within the Ringold Formation may correspond to zones where water was added during hard tooling. Hard tooling was initiated at 49 m (161 ft) bgs and continued periodically down to 63.4 m (208 ft) bgs.

Figure C.22. Gravimetric Moisture Content Distribution for the Sediment Profile at Borehole 299-W23-19



Source: Serne et al. (2001c).

The moisture content profile in Figure C.22 is consistent with the measured data in Figure C.20 for near-surface sediments. The profile data in Figure C.22 are also consistent with those in Figure C.21 at about 21 m (70 ft) bgs and at about 37 m (120 ft) bgs. However, the observed high moisture contents at about 27 m (90 ft) bgs in Figure C.22 are not present in Figure C.21 near tank SX-115.

Matric potential measurements for samples from borehole 299-W23-19 and clean RCRA boreholes (299-W22-48 and 299-W22-50) are shown in Figure C.23. The soil suction (negative of matric potential) data are reported as head values in feet, consistent with reported depths bgs.

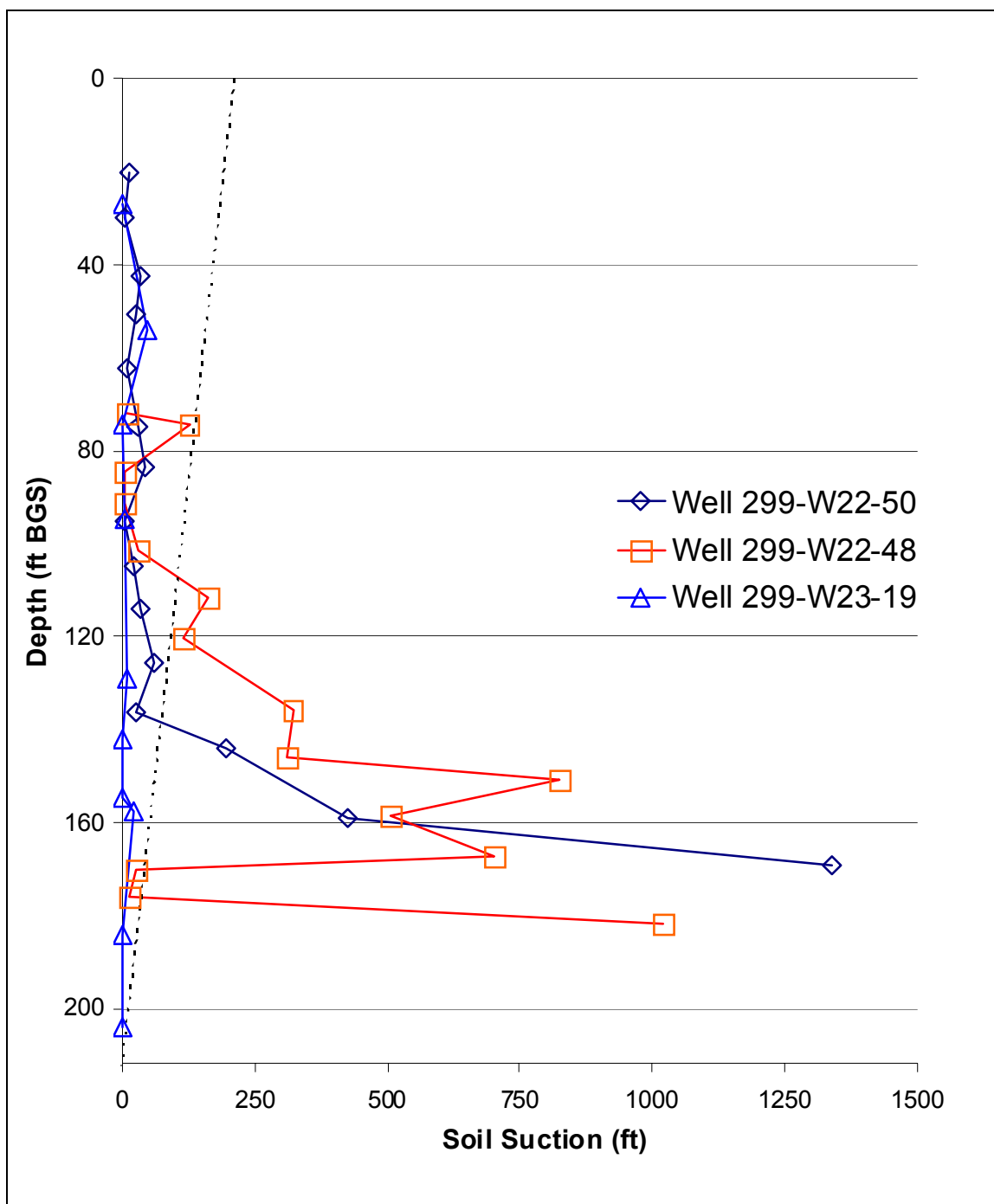
The higher the suction values, the less recharge is expected. On Figure C.23, an equilibrium line is also shown. Measured soil suction values to the left of the equilibrium line indicate that drainage (recharge) is occurring while values to the right of the line indicate that evaporation (drying or upward flow) conditions persist. As discussed in *Geologic and Geochemical Data Collected from Vadose Zone Sediments from Borehole 299-W23-19 [SX-115] in the S/SX Waste Management Area and Preliminary Interpretations* (Serne et al. 2001c), for RCRA boreholes 299-W22-48 and 299-W22-50 it appears that water from winter rains and snowmelt (or perhaps other sources) have penetrated the soil profile to depths of about 30 m (100 ft) bgs. However, below that depth the sediments from these two uncontaminated boreholes are significantly drier (i.e., to the right of the equilibrium line) compared to the sediments found in contaminated borehole 299-W23-19.

For borehole 299-W23-19 3 m ([10 ft] to the south-south-west of the side of tank SX-115), the suctions are low (sediments are relatively wet) throughout the profile and drainage is predicted to be the highest of any of the three boreholes. Note that borehole 299-W23-19 was drilled using air rotary and therefore no water was added during drilling. This is unlike the RCRA groundwater wells 299-W23-48 and 299-W22-50 boreholes, where water was added during hard tooling process of cable tool drilling. As discussed in Serne et al. (2001c), unit gradient conditions persist throughout the profile for borehole 299-W23-19 sediments but not for two clean boreholes outside the tank farm operations area. The accelerated drainage from water-line leaks south of tank SX-115 is believed to be the primary reason for the relatively low suction values (and higher recharge) for sediments from borehole 299-W23-19. Nonetheless, as discussed in Serne et al. (2001c), for this location an estimated recharge rate of between 50 to 100 mm/yr (2 to 4 in./yr) would be in line with the observed drainage rates from bare gravel surface soils at the Hanford Site (Gee et al. 1992).

C.5.3 MEASUREMENTS FOR BOREHOLE 41-09-39

Thirty sleeve sediment samples from the extension borehole for 41-09-39 near tank SX-108 were analyzed for and moisture content and matric suction. The data, tabulated in Table C.13 and shown in Figure C.24, indicate that of the 30 samples 18 are at matric suctions lower (wetter) than the elevation of the sample above the water table (Serne et al. 2001b). As shown in Figure C.24, when the suction for a sample is less than the sample's elevation-above the water table, the sample is draining. As discussed in Serne et al. (2001b), in contrast to the other contaminated borehole 299-W23-19 matric suction values for samples from borehole 41-09-39 suggest a much drier moisture regime. Note that, because of extreme variability and uncertainty in some of the measurements, not all the data (Table C.13) are plotted in Figure C.24.

Figure C.23. Soil Suction Profiles for 299-W22-48, 299-W22-50 and 299-W23-19 Borehole Samples



Note: Dashed line is the equilibrium soil suction line. Drainage occurs only for values to left of the equilibrium line.

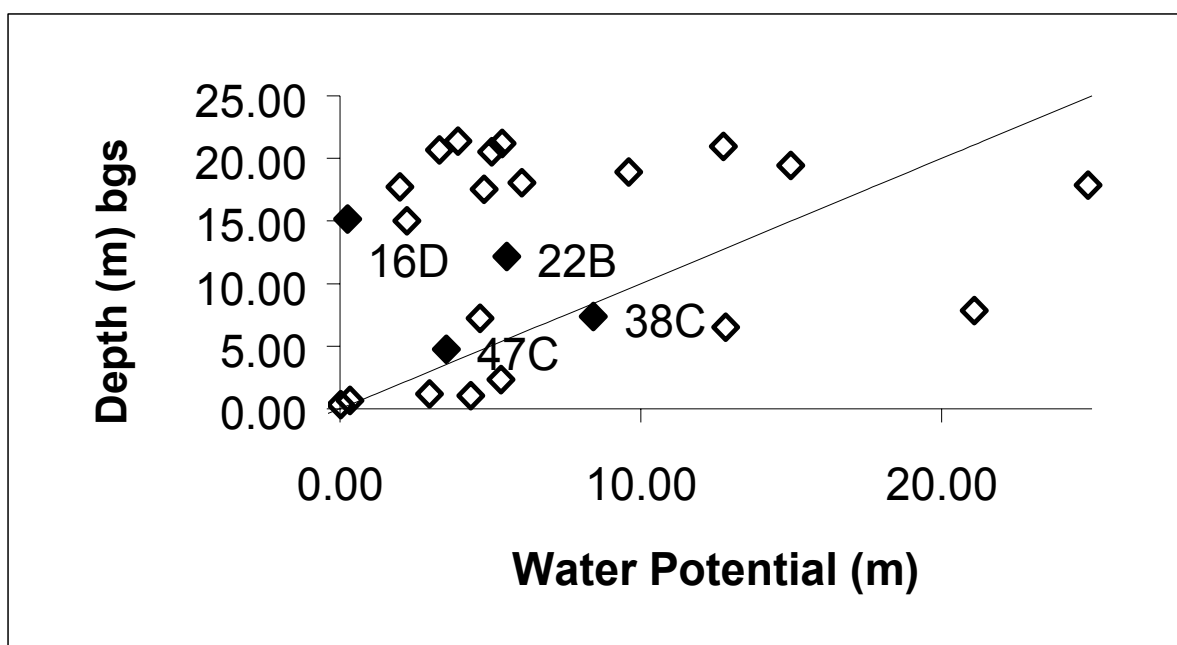
Source: Serne et al. (2001c).

**Table C.13. Water Content and Matric Suction Values
for Samples from Borehole 41-09-39**

| Sample | Depth (ft bgs) | Water content (g/g) | Suction (m) | Sample | Depth (ft bgs) | Water Content (g/g) | Suction (m) |
|--------|-------------------|---------------------------|----------------|--------|-------------------|---------------------------|----------------|
| 6F | 141.9 | 0.11 | 3.93 | 37C | 186.2 | 0.026 | 21.08 |
| 6E | 142.4 | 0.096 | 5.38 | 38C | 187.8 | 0.029 | 8.42 |
| 6D | 143.3 | 0.218 | 12.74 | 38B | 188.3 | 0.019 | 4.65 |
| 6C | 144.1 | 0.26 | 3.3 | 39A | 189.5 | 0.018 | 50.16 |
| 6B | 144.7 | 0.229 | 5.03 | 40A | 190.7 | 0.051 | 12.83 |
| 7C | 146.4 | 0.112 | 26.81 | 47C | 196.4 | 0.066 | 3.53 |
| 8C | 148.3 | 0.074 | 14.99 | 50A | 199.4 | 0.039 | 96.42 |
| 8B | 149.9 | 0.097 | 9.6 | 56C | 204.3 | 0.077 | 5.34 |
| 9A | 152.8 | 0.139 | 6.04 | 56B | 205.0 | 0.066 | 27.75 |
| 10C | 153.4 | 0.136 | 24.86 | 56A | 205.6 | 0.054 | 30.77 |
| 10B | 153.9 | 0.147 | 2 | 58C | 208.1 | 0.102 | 2.97 |
| 10A | 154.5 | 0.196 | 4.8 | 58B | 208.6 | 0.106 | 4.34 |
| 16D | 162.3 | 0.133 | 0.25 | 59C | 209.8 | 0.125 | 0.33 |
| 16C | 162.8 | 0.135 | 2.21 | 59A | 210.9 | 0.25 | 0.02 |
| 22B | 172.0 | 0.052 | 5.54 | 64A | 213.3 | 0.132 | 0.03 |

Source: Serne et al. (2001b).

Figure C.24. Matric Suction Profile for Samples from Borehole 41-09-39



Source: Serne et al. (2001b).

Serne et al. (2001b) presents three possibilities for the borehole 41-09-39 core samples having higher matric suction. The first is that much less drainage (recharge) is occurring at this borehole location than was observed at the other location at borehole 299-W23-19. The second is that the samples were disturbed enough during coring that the water content and possibly the density were altered enough to increase the matric suction values. The third is the possible drying effect due to heat load from the high-heat tank SX-108.

C.6.0 GEOCHEMISTRY

Numerous studies have been completed during the characterization of the WMA S-SX vadose zone that provide geochemistry information related to vadose zone contamination. Data provided by these studies are discussed in other sections and appendices of this WMA S-SX Field Investigation Report. Those investigations are briefly described here with appropriate references to other sections of this document for more detailed discussion.

The first and most extensive effort is the characterization of soil samples from the boreholes that have been drilled in support of this RCRA facility investigation. These include three characterization boreholes within WMA S-SX and two RCRA groundwater monitoring boreholes east of WMA S-SX. Soil samples were extensively analyzed for mineralogy and particle size distribution. Water and acid extracts were taken to measure water chemistry and radionuclide content. In a few samples, porewater was extracted without dilution from the soils and analyzed. These data are discussed in greater detail in Appendix B.

Several laboratory studies were completed to determine the chemical reactions controlling the mobility of cesium-137 and chromium. The results show that cesium-137 sorption is strongly influenced by the concentration of competing cations (primarily sodium and to a lesser extent potassium) for sorption sites and cesium-137 mobility has ranged from very high to very low. Chromium studies indicate that some retardation of chromium migration can occur by oxidation-reduction reactions. Cesium-137 and chromium studies are discussed in greater detail in Appendix D, Sections D.3.0 and D.4.0, respectively. Isotopic fission products were measured in borehole soils to gain insight on multiplicity of tank sources and their distribution in the soil column (Appendix D, Sections D.6.1, D.6.2, and D.6.3).

Finally, several modeling studies were completed to evaluate or incorporate geochemical parameters and their influence on contaminant migration. These included thermodynamic simulations to predict tank fluid chemistry (Appendix D, Section D.7.3) and flow and transport estimates of aqueous species migration (Appendix D, Section D.7.1 and D.7.4)

C.7.0 GROUNDWATER CONTAMINATION

Several groundwater monitoring wells around WMA S-SX have been contaminated during the last decade by constituents (primarily technetium-99, nitrate, and chromium) whose sources are postulated to be derived from one or more tank leaks (Johnson and Chou 1998; Johnson and Chou 1999b). Relatively high technetium-99 concentrations downgradient of WMA S-SX and occurrences of relatively high technetium-99/nitrate ratios similar to presumed tank liquid ratios have been the primary observations suggesting a link between observed groundwater contamination and tank leak contamination in the vadose zone. These data are also summarized in Johnson et al (1999). Since that report was issued, additional groundwater contamination data have been collected. This section summarizes some of the additional data provided in Johnson and Chou (2001). Where relevant to the discussion, data collected more recently than Johnson and Chou (2001) are also discussed in the main text.

The most recent groundwater contamination data from groundwater samples in several groundwater monitoring wells continue to support the hypothesis that the tank farm is the source of the contaminants. Sampling with depth was conducted at 4 new wells including well 299-W23-19 near tank SX-115, well 299-W22-48 east of S tank farm, well 299-W22-49 east of SX tank farm, and well 299-W22-50 at the southeast corner of the SX tank farm. Chemical species and radionuclide concentrations measured in these wells are listed in Tables C.14, C.15, and C.16. Technetium-99/nitrate and tritium/technetium-99 ratios are shown in Figures C.25 and C.26, respectively. Some outstanding features include the following.

- **Well 299-W23-19** – Shallow samples (0 to 6 cm and 1 m [0 to 5.5 in. and 3 ft]) were first taken in October 1999. Later samples in 2000 were taken at greater depth. There is relatively little variability with depth. Of note are the very high technetium-99 concentrations which continue to be high. Also, maximum technetium-99/nitrate ratios of 0.11 are observed, indicating a tank waste source.
- **Well 299-W22-48** – Moderate contaminant concentrations are observed. However, intermediate technetium-99/nitrate ratios of 0.039 occur, which may indicate a tank waste source.
- **Well 299-W22-49** – Moderate amounts of contaminants occur. The relatively high tritium/technetium-99 ratio indicates a non-tank farm source.
- **Well 299-W22-50** – Moderate contaminant concentrations occur. Maximum technetium-99/nitrate ratios of 0.11 are observed, indicating a tank waste source. The presence of increased nitrate and carbon tetrachloride at about 68 m (223 ft) indicates that an additional source, presumably the regional contamination plumes created by crib discharges, has contributed to contamination at this location.

In particular, technetium-99 groundwater concentrations measured in March 2001 have reached 81,500 pCi/L in well 299-W23-19.

Table C.14. Observed Contaminant Concentrations in Shallow and Extended Well 299-W23-19 Completions Near Tank SX-115

| Constituent (unit) | Shallow Temporary Screen (1.5 m) | | Permanent Screen (9.1 m) | |
|------------------------------------|----------------------------------|------------------------------|------------------------------|------------------------------|
| | October 1999 ^a | | March 2000 | June 2000 |
| | Passive (Kabis, 0–6 cm) | Pumped ^b (1 m) | Pumped ^c (2 m) | Pumped ^c (2 m) |
| Technetium-99 (pCi/L) ^d | 48,050 | 39,000 | 52,300 | 63,700 |
| Chromium (µg/L) ^e | 84 | 63 | 90 | 87 |
| Nitrate, as NO ₃ (mg/L) | 560 | 434 | 491 | 562 |
| Tritium (pCi/L) | 92,000 | 91,000 | 95,800 | 92,000 |
| Specific Conductance (µS/cm) | 1,199 | 1,003 | 968 | 1,237 |
| Sulfate (mg/L) | 18 | 16 | 18 | 17 |
| Calcium (mg/L) | 118 | 96 | 127 | 120 |
| Magnesium (mg/L) | 39 | 32 | 41 | 40 |
| Sodium (mg/L) | 34 | 34 | 42 | 43 |
| Chloride (mg/L) | 15 | 12 | 16 | 16 |

^aValues reported represent duplicate averages.^b1.5 m (5 ft) screened interval with pump intake set at 1 m (3 ft) below the static water level.^c9.1 m (30 ft) screened interval with pump intake set at 2 m (6 ft) below the static water level.^dConcentration values of 81,500 pCi/L were measured in the March 2001 sample.^eConcentration values of 138 µg/L were measured in the March 2001 sample.**Table C.15. Depth Distribution of Key Contaminants at SX Tank Farm Wells**

| Well | Sample Date | Depth (m) | Mode | Contaminants | | | | | |
|------------|-------------|-----------|------|-----------------------------|---------------------------|--------------|---------------------------|-------------|----------------------------|
| | | | | ⁹⁹ Tc (pCi/L) | NO ₃ (µg/L) | Cr (µg/L) | ³ H (pCi/L) | U (µg/L) | CCl ₄ (µg/L) |
| 299-W22-48 | 10/26/99 | 0.6 | DT/B | 39.5 | 17,132 | 3.2U | 122U | 0.2 | 0.4 |
| | 03/30/00 | 2.3 | S | 720 | 18,593 | 7.1 | 249U | 3.23 | 4 |
| 299-W22-49 | 11/04/99 | 0.5 | DT | 32.5 | 13,546 | 3.2U | 22,000 | 0.82 | 0.6 |
| | 03/30/00 | 2.3 | S | 58.3 | 9,296 | 4.6U | 22,000 | 3.27 | 6 |
| | 11/08/99 | 6.7 | DT | 2.96U | 7,880 | 3.2U | 18,900 | 0.92 | 1 |
| 299-W22-50 | 11/23/99 | 0.2 | DT/B | 4,240 | 57,991 | 3.0U | 31,400 | 0.78 | 13 |
| | 04/03/00 | 2.3 | S | 3,230 | 30,102 | 10.4 | 24,200 | 4.29 | 11 |
| | 11/29/99 | 6.7 | DT | 812 | 12,838 | 3.0U | 19,900 | 3.34 | 5.6 |
| | 12/14/99 | 11.9 | DT | 7.03U | 2,125 | 3.0U | 969 | 1.09 | 0.94 |
| | 12/15/99 | 28.7 | DT | 0U | 1,151 | 3.0U | 304 | 0.58 | 1.5 |
| | 12/17/99 | 53.0 | DT | 0U | 3,187 | 3.0U | 185U | 0.79 | 5.6 |
| | 12/22/99 | 67.7 | DT | 0.577U | 12,838 | 3.0U | 0U | 0.43 | 0.89 |
| | 01/12/00 | 99.4 | DT | 0U | 4,869 | 3.0U | 0U | 30.90 | 0.23 |

*Depth is below water table.

DT = sampled during drilling using temporary pump/screen and packer assembly.

DT/B = bailed during drilling.

S = sample collected by pumping from 4.5 m (15 ft) screened interval.

U = analytical result is not detected.

Table C.16. Hydrochemical Parameters at SX Tank Farm Wells

| Well | Hydrochemical Parameters | | | | | | | | |
|------------|--------------------------|---|--|---|----------------------------------|----------------------------------|----------------------------------|----------------------------------|-------|
| | pH | Conductivity ($\mu\text{S}/\text{cm}$) | Alkalinity ($\mu\text{g}/\text{L}$) | SO ₄ ($\mu\text{g}/\text{L}$) | Cl ($\mu\text{g}/\text{L}$) | Na ($\mu\text{g}/\text{L}$) | Ca ($\mu\text{g}/\text{L}$) | Mg ($\mu\text{g}/\text{L}$) | Na/Ca |
| 299-W22-48 | 7.97 | 263 | 74,000 | 21,300 | 6,910 | 26,300 | 19,400 | 5,070 | 1.36 |
| | 8.59 | 295 | --- | 19,200 | 5,900 | 27,000 | 22,200 | 6,910 | 1.22 |
| 299-W22-49 | 8.94 | 245 | 90,000 | 13,900 | 5,330 | 25,600 | 16,200 | 5,070 | 1.58 |
| | 9.09 | 240 | --- | 11,900 | 2,800 | 23,300 | 17,600 | 5,960 | 1.32 |
| | 8.1 | 244 | 86,000 | 15,400 | 3,660 | 26,000 | 16,400 | 5,320 | 1.59 |
| 299-W22-50 | --- | --- | 100,000 | 14,200 | 4,800 | 28,200 | 23,200 | 7,300 | 1.22 |
| | 8.14 | 278 | --- | 13,400 | 3,100 | 23,900 | 22,600 | 7,100 | 1.06 |
| | 8.1 | 235 | 101,000 | 12,500 | 2,500 | 20,400 | 17,800 | 6,020 | 1.15 |
| | 8.2* | 228 | 106,000 | 14,400 | 3,100 | 11,600 | 26,300 | 9,250 | 0.44 |
| | 7.9* | 242 | 114,000 | 14,400 | 4,400 | 12,700 | 28,700 | 10,200 | 0.44 |
| | 7.9* | 307 | 126,000 | 16,100 | 15,200 | 14,300 | 33,400 | 12,400 | 0.43 |
| | 7.7* | 323 | 115,000 | 19,300 | 10,000 | 15,500 | 33,000 | 12,500 | 0.47 |
| | 8.5* | 234 | 96,000 | 18,900 | 5,800 | 16,600 | 20,200 | 8,010 | 0.82 |

*Laboratory result.

Figure C.25. Technetium-99/Nitrate Ratios for Waste Management Area S-SX Network Wells

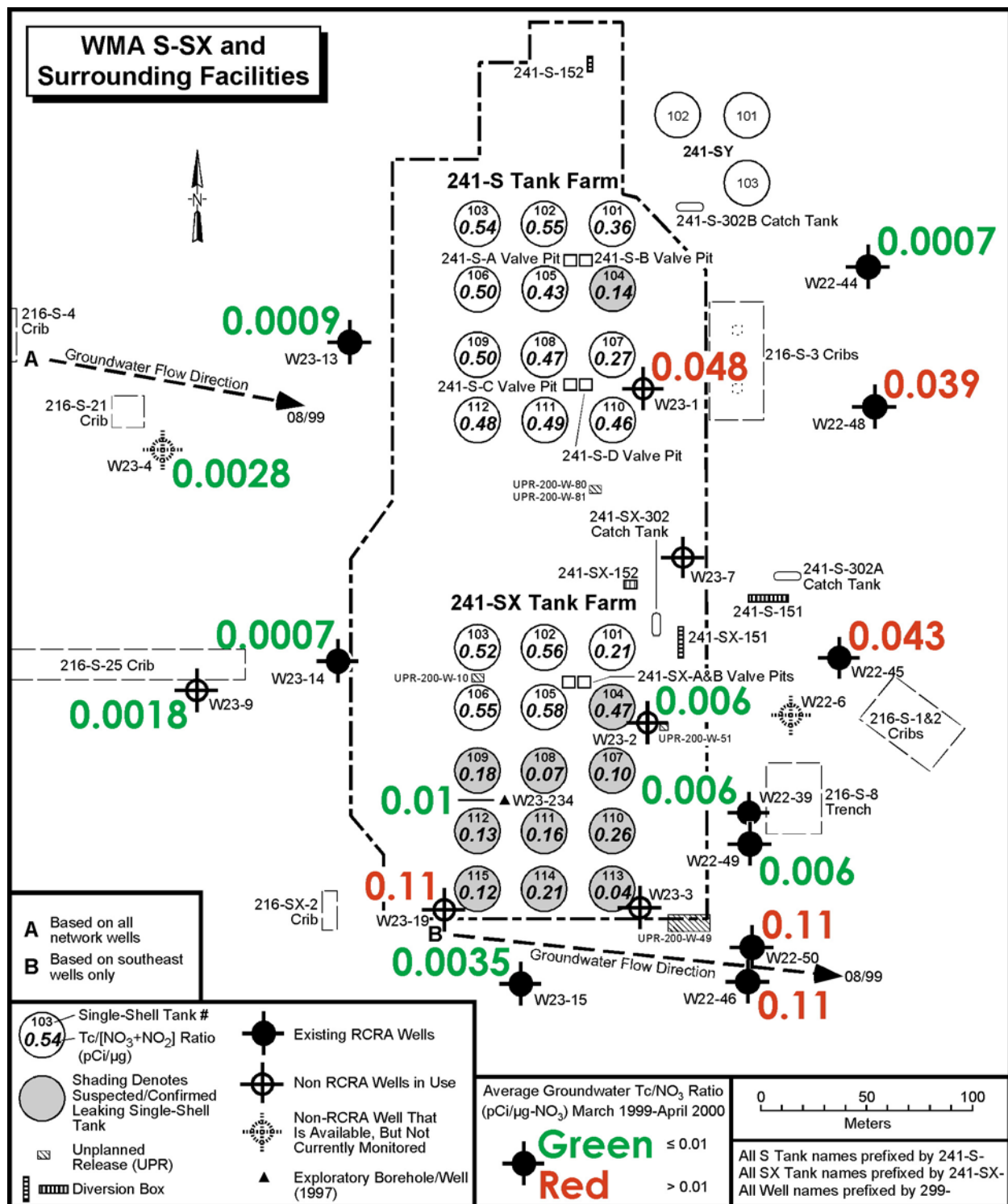
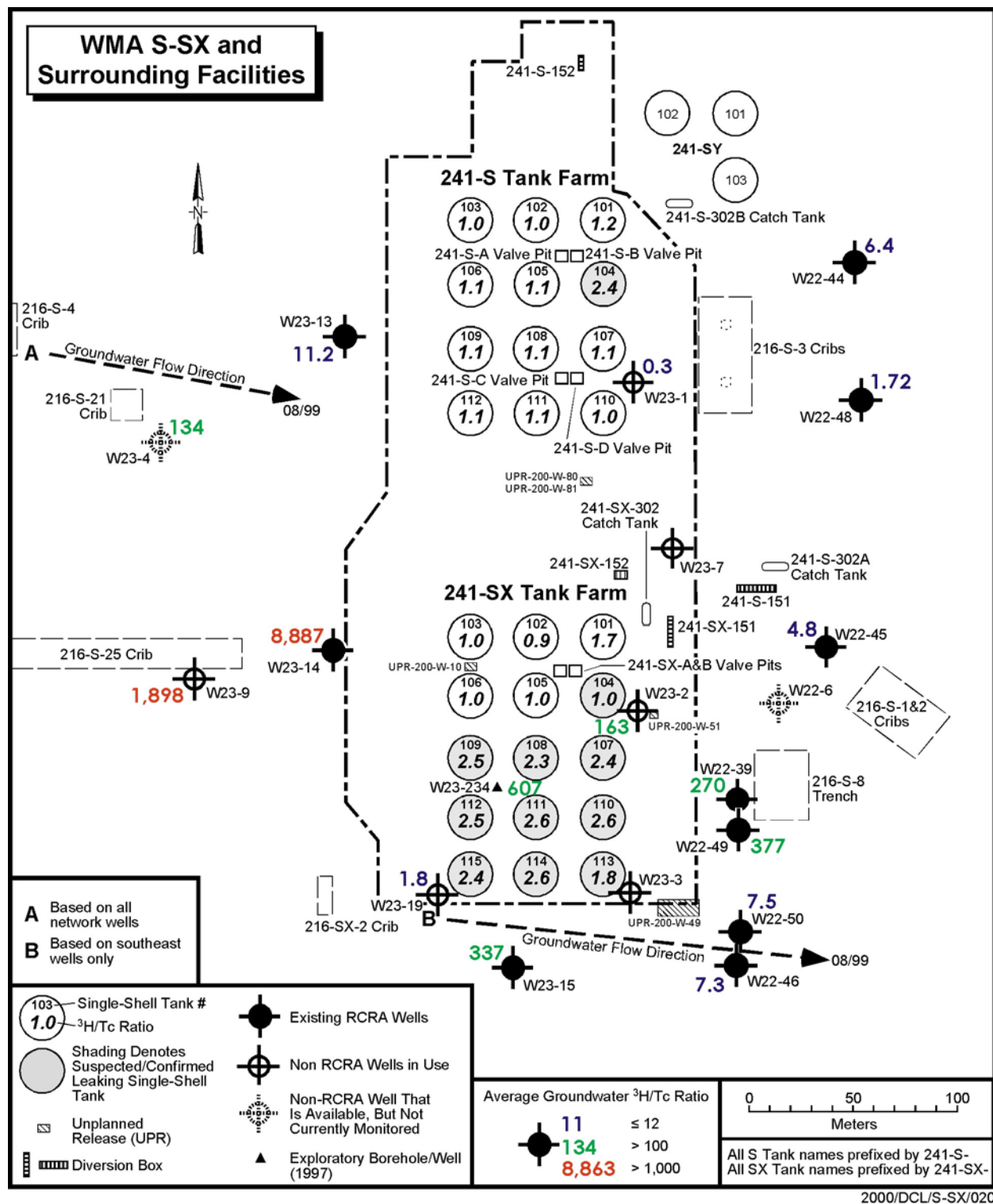


Figure C.26. Tritium/Technetium-99 Ratios for Waste Management Area S-SX Network Wells



Given the well distribution showing relatively high technetium-99 concentrations, it appears that more than one tank waste source may be contributing to groundwater contamination. The largest technetium-99 concentrations (Table C.17) that have been recorded since 1997 occur at the southern end of the SX tank farm. This contamination is attributed to the tank SX-115 leak. A plausible plume distribution is shown in Figure C.27. The characteristics of this distribution are a 10-year plume narrowly constrained to the east-southeast whose source is in the vadose zone at or southwest of tank SX-115. The wells most clearly associated with this postulated plume are 299-W23-19, 299-W22-50, and 299-W22-46. All show identical technetium-99/nitrate ratios (Figure C.25) and show good fit with relative concentrations. There is some indication that this plume has rotated slightly over time to a more easterly direction because technetium-99/nitrate ratios and technetium-99 concentrations were high in well 299-W23-15. The technetium-99 plume has since moved away from this location (Figure C.27).

Other wells suggesting the occurrence of tank waste contaminants include 299-W23-1, 299-W22-48, and 299-W22-45 towards the north of WMA S-SX. The technetium-99/nitrate values in these wells are elevated relative to crib associated values west of WMA S-SX, but not as high as those at the south end of the SX tank farm. This suggests some vadose zone source under the S tank farm upgradient of these wells. Historical knowledge identifies only the tank S-104 leak as a source of relatively high technetium-99 content. Because the technetium-99 concentrations may still be rising in wells 299-W22-48, 299-W22-44, and 299-W22-45 (Figure C.28), future changes in contamination levels are uncertain here.

Figure C.27. Theoretical Groundwater Plume Dispersion Pattern from a Tank Leak Source in the SX Tank Farm Monitoring Efficiency Model

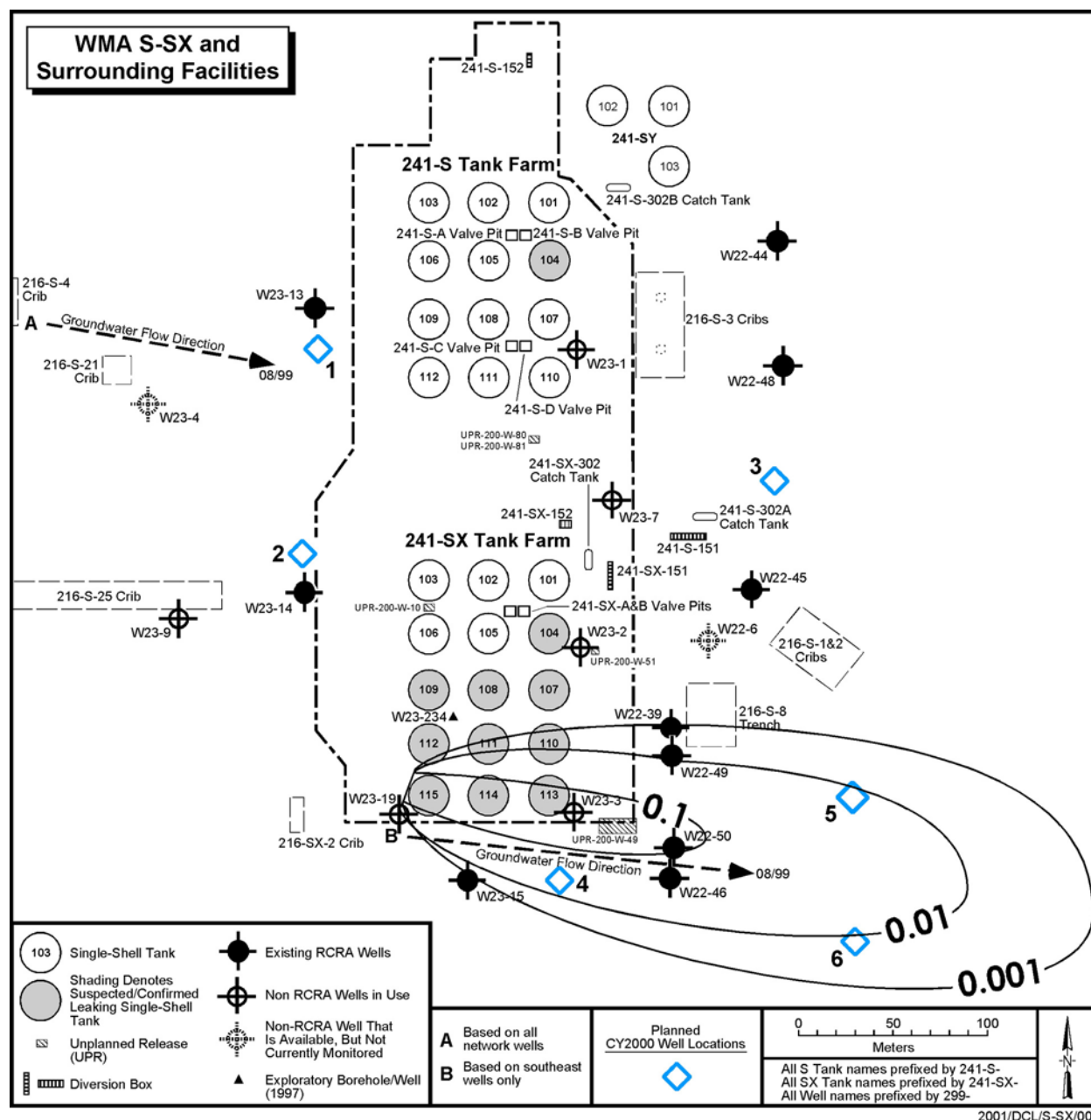


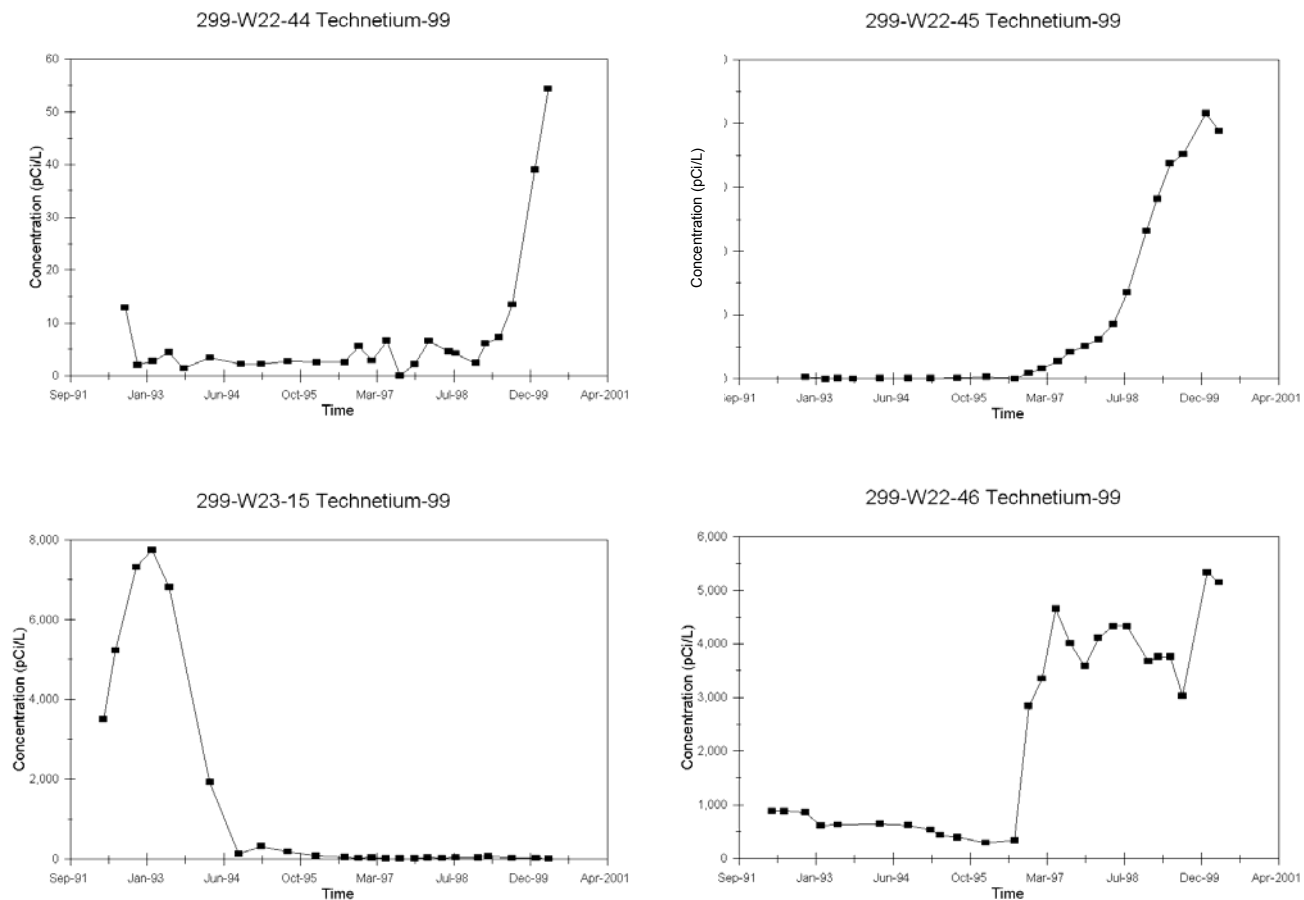
Figure C.28. Technetium-99 for Waste Management Area S-SX Network Wells

Table C.17. Maximum Contaminant Concentrations for Groundwater Samples Collected from Waste Management Area S-SX Network Wells (November 1997 to April 2000)

| Analyte | MCL | W22-39 | W22-44 | W22-45 | W22-46 | W22-48 | W22-49 | W22-50 | W23-1 | W23-2 |
|--------------------------------------|------------|--------------|--------------------|---------------------|--------------|--------------|---------------------|---------------------|--------------|--------------|
| Chromium ^(a) (µg/L) | 100 | 16.3 | 5 ^(b) | 27.4 ^(b) | 26 | 7.1 | 4.6U | 10.4 | 29 | 6.1 |
| ⁹⁹ Tc (pCi/L) | 900 | 120 | 56 | 2,080 | 5,330 | 720 | 58.3 | 4,240 | 2,890 | 75.6 |
| Nitrate (as NO ₃) (µg/L) | 45,000 | 16,822 | 37,628 | 47,367 | 49,580 | 18,593 | 13,546 | 57,991 | 50,023 | 11,952 |
| Uranium (µg/L) | 20 | 4.81 | 6.48 | 7.97 | 5.91 | 3.23 | 3.27 | 30.9 | 8.06 | 6.57 |
| Gross alpha (pCi/L) | 15 | 3.56 | 4.81 | 6.36 | 4.36 | 1.21 | 2.24 | 20.9 | 5.68 | 4.65 |
| Gross beta (pCi/L) | 50 | 37.5 | 20.7 | 768 | 1,836 | 223 | 22 | 1,420 | 1,090 | 29.3 |
| Tritium (pCi/L) | 20,000 | 27,100 | 238U | 18,800 | 58,700 | 249U | 22,000 | 31,400 | 1,010 | 12,700 |
| ⁹⁰ Sr (pCi/L) | 8 | 0.261U | 0.295U | 1.4U | 4.92U | 0U | 0U | 1.03U | 7.54 | 0.205U |
| ¹³⁷ Cs (pCi/L) | 200 | 1.82U | 2.42U | 2.78U | 4.59U | 0U | 1.7U | 0U | 1.82U | 0U |
| Iron ^(a) (µg/L) | 300 | 118 | 146 ^(b) | 65.9 | 122 | 54.9 | 85.8 ^(b) | 95.5 ^(b) | 59 | 39.5 |
| Manganese ^(a) (µg/L) | 50 | 7.7 | 8.1 ^(b) | 3.8 | 4.3 | 306 | 244 | 167 | 7 | 11.8 |
| Carbon tetrachloride (µg/L) | 5 | 3.8 | 6.2 | 12 | 30 | 4 | 6 | 19 | -- | -- |
| Fluoride (µg/L) | 4,000 | 473 | 400 | 480 | 440 | 490 | 550 | 730 | 458 | 424 |
| Aluminum ^(a) (µg/L) | 50 | 51 | 58.3U | 41.8U | 45.7 | 41.8U | 64.6 | 93.2 | 31.3U | 20.6U |
| pH | [6.5, 8.5] | [7.93, 8.48] | [7.92, 8.25] | [8.07, 8.35] | [7.89, 8.33] | [7.97, 8.59] | [8.1, 9.09] | [8.1, 8.14] | [7.33, 8.19] | [8.11, 8.26] |

| Analyte | W23-4 ^c | W23-9 ^c | W23-13 ^c | W23-14 ^c | W23-15 | W23-19 ^c | W23-234 | Max ^d | Max/MCL |
|--------------------------------------|--------------------|--------------------|---------------------|---------------------|--------------------|---------------------|---------|------------------|---------|
| Chromium ^a (µg/L) | 4.6U | 8.5 | 33.9 | 12.5 | 8.1 ^(b) | 89.8 | 7.5 | 89.8 | 0.9 |
| ⁹⁹ Tc (pCi/L) | 21.1 | 408 | 10.6U | 218 | 72.1 | 52,300 | 80.4 | 52,300 | 58.1 |
| Nitrate (as NO ₃) (µg/L) | 4,869 | 165,562 | 7,698 | 134,575 | 14,697 | 562,204 | 19,080 | 562,204 | 12.5 |
| Uranium (µg/L) | 24.4 | 25.8 | 16.5 | 18 | 14.6 | 17.6 | 3.4 | 30.9 | 1.5 |
| Gross alpha (pCi/L) | 14.5 | 17.3 | 11.7 | 9.82 | 10.8 | 21.9 | -- | 21.9 | NA |
| Gross beta (pCi/L) | 15 | 56.6 | 11.4 | 19.7 | 27.8 | 23,000 | -- | 23,000 | NA |
| Tritium (pCi/L) | 1,540 | 502,000 | 215U | 382,000 | 22,200 | 95,800 | 138,000 | 502,000 | 25.1 |
| ⁹⁰ Sr (pCi/L) | 0.222U | 0.481U | 0.189U | 0.425U | 0.36U | 9.63U | 0.2U | 7.54 | 0.94 |
| ¹³⁷ Cs (pCi/L) | 3.96U | 0U | 1.33U | 1.71U | 2.31U | 1.63U | 1.3U | Not detected | NA |
| Iron ^a (µg/L) | 81.5 | 83.3 | 154 | 110 | 938 | 46 | 48.2 | 938 | 3.1 |
| Manganese ^a (µg/L) | 2.4 | 30.3 | 10.2 | 12.7 | 20.1 | 203 | 5.7 | 306 | 6.1 |
| Carbon tetrachloride (µg/L) | 100 | 2 | 11 | 0.51 | 140 | 22 | -- | 140 | 28 |
| Fluoride (µg/L) | 340 | 319 | 390 | 350 | 490 | 340 | 497 | 730 | 0.2 |
| Aluminum ^a (µg/L) | 41.8U | 41.8U | 41.8U | 33.5U | 83.2 | 41.8U | 33.5U | 93.2 | 1.9 |
| pH | [8.0, 8.09] | [7.72, 8.1] | [7.72, 8.58] | [7.78, 8.52] | [7.74, 8.12] | 8.05 | 8.54 | [7.33, 9.09] | NA |

Note: All well numbers prefixed by 299-. U denotes analytical result is not detected. **Bold** indicates well with maximum.

^aFiltered sample results.

^bOutliers removed.

^cUpgradient wells.

^dMaximum across all network wells.

^eSubsequent groundwater sample analyses show increases in chromium and technetium-99 concentrations (138 µg/L and 81,500 pCi/L, respectively) as of March 2001.

C.8.0 REFERENCES

- Agnew S. F., 1997, *Hanford Tank Chemical and Radionuclide Inventories: HDW Model Rev. 4*, LA-UR-96-3860, Los Alamos National Laboratory, Los Alamos, New Mexico.
- Agnew, S. F., and R. A. Corbin, 1998, *Analysis of SX Farm Leak Histories—Historical Leak Model (HLM)*, LA-UR-96-3537, Los Alamos National Laboratory, Los Alamos, New Mexico.
- Baker, V. R., B. N. Bjornstad, A. J. Busacca, K. R. Fecht, E. P. Kiver, U. L. Moody, J. G. Rigby, D. F. Stradling, and A. M. Tallman, 1991, “Quaternary Geology of the Columbia Plateau,” in R. B. Morrison, ed., *Quaternary Nonglacial Geology, Conterminous U.S.*, Boulder, Colorado, Geological Society of America, The Geology of North America, v. K-2.
- Barney, G. S., 1976, *Vapor Liquid Phase Equilibria of Radioactive Sodium Salt Wastes at Hanford*, ARH-ST-133, Atlantic Richfield Company, Richland, Washington.
- Bjornstad, B. N., 1984, *Suprabasalt Stratigraphy With and Adjacent to the Reference Repository Location*, SD-BWI-DP-039, Rockwell Hanford Operations, Richland, Washington.
- Bjornstad, B. N., 1990, *Geohydrology of the 218-W-5 Burial Ground, 200 West Area, Hanford Site*, PNL-7336, Pacific Northwest Laboratory, Richland, Washington.
- Brown, D. J., 1959, *Subsurface Geology of the Hanford Separations Areas*, HW-61780, General Electric Company, Richland, Washington.
- Brown, D. J., 1960, *An Eolian Deposit Beneath 200-West Area*, HW-67549, General Electric Company, Richland, Washington.
- Corbin, R. A., B. C. Simpson, and S. F. Agnew, 2001, *Hanford Soil Inventory Model*, BHI-01496, Rev. 0, Bechtel Hanford, Inc., Richland, Washington.
- DOE, 1996, *Vadose Zone Characterization Project at the Hanford Tank Farms, SX Tank Farm Report*, GJPO-HAN-4, Final Draft, U.S. Department of Energy, Richland Operations Office, Richland, Washington.
- DOE, 1988, *Consultation Draft Site Characterization Plan*, DOE/RW-0164, 9 volumes, U.S. Department of Energy, Richland Operations Office, Richland, Washington.
- DOE-GJO, 2000, *Addendum to S Tank Farm Report*, GJO-97-31-TARA, U.S. Department of Energy, Albuquerque Operations Office and Grand Junction Projects Office, Grand Junction Colorado.
- DOE-GJPO, 2000, *Addendum to the SX Tank Farm Report SX Supplement*, GJPO-HAN-4, U.S. Department of Energy, Albuquerque Operations Office, Grand Junction Projects Office, Grand Junction, Colorado.

- DOE-RL, 1993, *200 West Groundwater Aggregate Area Management Study Report*, DOE/RL-92-16, Rev. 0, U.S. Department of Energy, Richland Operations Office, Richland, Washington.
- Fecht, K. R., K. A. Lindsey, D. G. Horton, G. V. Last, and S. P. Reidel, 1999, *An Atlas of Clastic Injection Dikes of the Pasco Basin and Vicinity*, BHI-01103, Rev. 0, Bechtel Hanford, Inc., Richland, Washington.
- GE, 1951, *REDOX Technical Manual*, HW-18700, General Electric Company, Richland, Washington.
- Gee, G. W., M. J. Fayer, M. L. Rockhold, and M. D. Campbell, 1992, "Variations in Recharge at the Hanford Site," *Northwest Science*, 66:237-250.
- Godfrey, W. L., 1971, *Inventory of Rhodium, Palladium, and Technetium Stored in Hanford Tanks*, ARH-1979, Atlantic Richfield Hanford Company, Richland, Washington.
- Goodman, D., 2000, *Estimation of SX-Farm Vadose Zone Cs-137 Inventories From Geostatistical Analysis of Drywell and Soil Core Data*, HNF-5782, Rev. 0, Montana State University, Bozeman, Montana.
- H-2-37985, 1974, *Civil North Section Contoured Elevation 241-SX Tank Farm*, Rev. 0, Atlantic Richfield Hanford Corporation, Richland, Washington.
- Hanlon, B. M., 2001, *Waste Tank Summary Report for Month Ending March 31, 2001*, HNF-EP-0182, Rev. 156, CH2M HILL Hanford Group, Inc., Richland, Washington.
- Harmon, M. K., 1949, *Neutralization of REDOX Aqueous Waste Streams*, HW-12566, General Electric Company, Richland, Washington.
- Henderson, J. C., 1999, *Preliminary Site-Specific Work Plan Addendum for WMA S-SX*, HNF-4380, Rev. 1, Lockheed Martin Hanford Corporation, Richland, Washington.
- Horton, D. G., and V. G. Johnson, 2000, *Borehole Data Package for Wells 299-W22-48, 299-W22-49, and 299-W22-50 at Single-Shell Tank Waste Management Area S-SX*, PNNL-13200, Pacific Northwest National Laboratory, Richland, Washington.
- Johnson, V., and C. J. Chou, 1998, *Results of Phase I Groundwater Quality Assessment for Single-Shell Tank Waste Management Areas S-SX at the Hanford Site*, PNNL-11810, Pacific Northwest National Laboratory, Richland, Washington.
- Johnson, V., and C. J. Chou, 1999, *Addendum to the RCRA Assessment Report for Single-Shell Tank Waste Management Areas S-SX at the Hanford Site*, PNNL-11810 ADD. 1., Pacific Northwest National Laboratory, Richland, Washington.
- Johnson, V. L., and C. J. Chou, 2001, *RCRA Groundwater Quality Assessment Report for Waste Management Area S-SX (November 1997 through April 2000)*, PNNL-13441, Pacific Northwest National Laboratory, Richland, Washington.

- Johnson, V. G., T. E. Jones, S. P. Reidel, and M. I. Wood, 1999, *Subsurface Conditions Description For the S-SX Waste Management Area*, HNF-4936, Rev. 0, Lockheed Martin Hanford Corporation, Richland, Washington.
- Jones, T. E., R. Khaleel, D. A. Myers, J. W. Shade, and M. I. Wood, 1998, *A Summary and Evaluation of Hanford Site Tank Farm Subsurface Contamination*, HNF-2603, Rev. 0, Lockheed Martin Hanford Corporation, Richland, Washington.
- Jones, T. E., R. A. Watrous, and G. T. Maclean, 2000a, *Inventory Estimates for Single-Shell Tank Leaks in S and SX Tank Farms*, RPP-6285, Rev. 0, CH2M HILL Hanford Group, Inc., Richland, Washington.
- Khaleel, R., T. E. Jones, A. J. Knepp, F. M. Mann, D. A. Myers, P. M. Rogers, R. J. Serne, and M. I. Wood, 2000, *Modeling Data Package for S-SX Field Investigation Report (FIR)*, RPP-6296, Rev. 0, CH2M HILL Hanford Group, Inc., Richland, Washington.
- Kovach, J. L., 1998, *TWRS Technetium Workshop*, Letter Report prepared by an Independent Review Plan for the U.S. Department of Energy, Richland Operations Office, Richland, Washington.
- Kupfer, M. J., A. L. Boldt, K. M. Hodgson, L. W. Shelton, B. C. Simpson, R. A. Watrous, M. D. LeClair, G. L. Borsheim, R. T. Winward, B. A. Higley, R. M. Orme, N. G. Colton, S. L. Lambert, D. E. Place, and W. W. Schulz, 1998, *Standard Inventories of Chemicals and Radionuclides in Hanford Site Tank Wastes*, HNF-SD-WM-TI-740, Rev. 8, prepared by Lockheed Martin Hanford Corporation for Fluor Daniel Hanford, Inc., Richland, Washington.
- Last, G. V., B. N. Bjornstad, M. P. Bergeron, D. W. Wallace, D. R. Newcomer, J. A. Schramke, M. A. Chamness, C. S. Cline, S. P. Airhart, and J. S. Wilbur, 1989, *Hydrogeology of the 200 Areas Low-Level Burial Grounds - An Interim Report*, PNL-6820, 2 volumes, Pacific Northwest Laboratory, Richland, Washington.
- Lindsey, K. A., 1996, *The Miocene to Pliocene Ringold Formation and Associated Deposits of the Ancestral Columbia River System, South-Central Washington and North-Central Oregon*, Open-File Report 96-8, Washington Division of Geology and Earth Resources, Olympia, Washington.
- Lindsey, K. A., S. P. Reidel, K. R. Fecht, J. L. Slate, A. G. Law, and A. M. Tallman, 1994, "Geohydrologic Setting of the Hanford Site, South-Central Washington", in D.A. Swanson and R. A. Hagerud, eds., *Geologic Field Trips in the Pacific Northwest: 1994 Geological Society of America Meeting*, Chapter 1C, Geological Society of America, Boulder, Colorado, p. 1C-1 to 1C-16.
- Lindsey, K. A., S. E. Kos, and K. D. Reynolds, 2000, *Vadose Zone Geology of Boreholes 299-W22-50 and 299-W23-19 S-SX Waste Management Area Hanford Site, South-Central Washington*, RPP-6149, Rev. 0, Daniel B. Stephens & Associates, Richland, Washington.

- MacLean, G. T., and K. M. Eager, 1998, *Evaluation of the Environmental Simulation Program (ESP) as a Computer Simulator of Nuclear Waste Processing*, HNF-3257, Rev. 0, Numatec Hanford Company, Richland, Washington.
- Myers, C. W. and S. M. Price, 1979, *Geologic Studies of the Columbia Plateau -- A Status Report*, RHO-BWI-ST-4, Rockwell Hanford Operations, Richland, Washington.
- Myers, D. A., 1997, *Activity Plan: Extension of Borehole 41-09-39, SX Tank Farm*, HNF-SD-WM-AP-044, Rev. 0, Lockheed Martin Hanford Corporation, Richland, Washington.
- Myers, D. A., D. L. Parker, G. Gee, V. G. Johnson, G. V. Last, R. J. Serne, and D. J. Moak, 1998, *Findings of the Extension of Borehole 41-09-39, 241-SX Tank Farm*, HNF-2855, Lockheed Martin Hanford Corporation, Richland, Washington.
- Myers, D. A., 2000, *Moisture Content in the S-SX Tank Farm*, RPP-7613, CH2M HILL Hanford Group, Inc., Richland, Washington.
- Price, W. H., and K. R. Fecht, 1976a, *Geology of the 241-SX Tank Farm*, ARH-LD-134, Atlantic Richfield Hanford Company, Richland, Washington.
- Price, W. H., and K. R. Fecht, 1976b, *Generalized Geology of the 241-SY Tank Farm*, ARH-LD-139, Atlantic Richfield Hanford Company, Richland, Washington.
- Raymond, J. R., and E. G. Shdo, 1966, *Characterization of Subsurface Contamination in the SX Tank Farm*, BNWL-CC-701, Pacific National Laboratory, Richland, Washington.
- Resource Conservation and Recovery Act of 1976*, Public Law 94-580, 90 Stat. 2795, 42 USC 901 et seq.
- Reidel, S. P., 1997, "Geologic Setting" in *Hanford Site Groundwater Monitoring for Fiscal Year 1996*, Pacific Northwest National Laboratory, Richland, Washington.
- Rogers, P. M., and A. J. Knepp, 2000, *Site-Specific SST Phase I RFI/CMS Work Plan Addendum for WMA S-SX*, HNF-5085, Rev. 1, CH2M HILL Hanford Group, Inc., Richland, Washington.
- Serne, R. J., H. T. Schaef, B. N. Bjornstad, B. A. Williams, D. C. Lanigan, D. G. Horton, R. E. Clayton, V. L. LeGore, M. J. O'Hara, C. F. Brown, K. E. Parker, I. V. Kutnyakov, J. N. Serne, A. V. Mitroshkov, G. V. Last, S. C. Smith, C. W. Lindenmeier, J. M. Zachara, and D. B. Burke, 2001a, *Characterization of Uncontaminated Sediments from the Hanford Reservation-RCRA Borehole Core and Composite Samples*, PNNL-2001-1, Pacific Northwest National Laboratory, Richland, Washington.

- Serne, R. J., G. V. Last, G. W. Gee, H. T. Schaef, D. C. Lanigan, C. W. Lindenmeier, R. E. Clayton, V. L. LeGore, R. D. Orr, M. J. O'Hara, C. F. Brown, D. B. Burke, A. T. Owen, I. V. Kutnyakov, T. C. Wilson, and D. A. Myers, 2001b, *Geologic and Geochemical Data Collected from Vadose Zone Sediments from Borehole SX 41-09-39 in the S/SX Waste Management Area and Preliminary Interpretations*, PNNL-2001-2, Pacific Northwest National Laboratory, Richland, Washington.
- Serne, R. J., H. T. Schaef, B. N. Bjornstad, D. C. Lanigan, G. W. Gee, C. W. Lindenmeier, R.E. Clayton, V. L. LeGrove, R. D. Orr, M. J. O'Hara, C. F. Last, I. V. Kutnyakov, D.B. Burke, T. C. Wilson, and B. A. Williams, 2001c, *Geologic and Geochemical Data Collected from Vadose Zone Sediments from Borehole 299-W23-19 [SX-115] in the S/SX Waste Management Area and Preliminary Interpretations*, PNNL-2001-3, Pacific Northwest National Laboratory, Richland, Washington.
- Siddall III, T. H., 1959, *Behavior of Technetium in the PUREX Process*, DP-634, E. I. du Pont & Co., Aiken, South Carolina.
- Slate, J. L., 1996, "Buried Carbonate Paleosols Developed in Pliocene-Pleistocene Deposits of the Pasco Basin, South-Central Washington, USA," *Quaternary International*, Vol. 34-36, pp. 191-196.
- Slate, J. L., 2000, *Nature and Variability of the Plio-Pleistocene Unit in the 200 West Area of the Hanford Site*, BHI-01203, Rev. 0, Bechtel Hanford, Inc., Richland, Washington.
- Sobczyk, S. M., 2000, *Subsurface Interpretation of the SX Tank Farm Hanford Site, Washington Based on Gamma-Ray Logging*, Nez Perce Tribe Environmental Restoration Waste Management Program, Ladwai, Idaho.
- Sterner, S. M.; J. R. Rustad; and A. R. Felmy, 1996, *The Hanford Thermochemical Databank: v 1.00 with Parameters for the ESP and Pitzer Models*, Pacific National Laboratory, Richland, Washington.
- Sterner, S. M.; A. R. Felmy; J. R. Rustad; and K. S. Pitzer, 1997, *Thermodynamic Analysis of Aqueous Solutions Using INSIGHT*, PNWD-SA-4436, Pacific National Laboratory, Richland, Washington.
- Sterner, S. M., J. R. Rustad, and A. R. Felmy, 1996, *The Hanford Thermochemical Databank: v 1.00 with Parameters for the ESP and Pitzer Models*, Pacific Northwest National Laboratory, Richland, Washington.
- Sullivan, P., M. P. Connelly, and T. E. Jones, 2001, *Geostatistical Analysis of Gamma-Emitting Radionuclides in the SX Tank Farm Vadose Zone*, RPP-8209, Rev. 0, CH2M Hill Hanford Group, Inc., Richland, Washington.
- Tallman, A. M., K. R. Fecht, M.C. Marratt, and G. V. Last, 1979, *Geology of the Separations Areas, Hanford Site, South-Central Washington*, RHO-ST-23, Rockwell Hanford Operations, Richland, Washington.

- Tomlinson, R. E., 1963, *Waste Management Program Chemical Processing Department*, HW 76352, General Electric Company, Richland, Washington.
- Waite, J. L., 1991, *Tank Wastes Discharged Directly to the Soil at the Hanford Site*, WHC-MR-0227, Westinghouse Hanford Company, Richland, Washington.
- WHC, 1992a, *Tank 241-SX-108 Leak Assessment*, WHC-MR-0300, Westinghouse Hanford Company, Richland, Washington.
- WHC, 1992b, *Tank 241-SX-109 Leak Assessment*, WHC-MR-0301, Westinghouse Hanford Company, Richland, Washington.
- WHC, 1992c, *Tank 241-SX-115 Leak Assessment*, WHC-MR-0302, Westinghouse Hanford Company, Richland, Washington.
- Wood, M. I., T. E. Jones, R. Schalla, B. N. Bjornstad, and F. N. Hodges, 2001, *Subsurface Conditions Description of the T-TX-TY Waste Management Area*, RPP-7123, Rev. 0, CH2M HILL Hanford Group, Inc., Richland, Washington.